Optimization and analysis of structure-based prion vaccines in transgenic mouse models

by

Madeleine Fleming

A thesis submitted in partial fulfillment of the requirements for the degree of

Master of Science

Department of Biochemistry
University of Alberta

Abstract

Prion diseases are rare and fatal neurodegenerative disorders caused by the misfolding of the cellular prion protein (PrP^{C}) to its infectious form (PrP^{Sc}). Until recently, the structure of PrP^{Sc} was a subject of much debate as there is evidence to support both the 4-rung β-solenoid model and published parallel in-register β-sheet (PIRIBS) cryo-EM structures. Prion diseases can be genetic, sporadic, or acquired. The most common genetic variants are genetic Creutzfeldt-Jakob Disease (gCJD), Gerstmann-Sträussler-Scheinker syndrome (GSS) and Fatal Familial Insomnia (FFI).

14R1, a protein previously constructed in the Wille lab, has shown potential as a structure-based prion vaccine. This protein mimics the proposed 4-rung β-solenoid structure modified from an innocuous fungal protein, HET-s. This antigen has shown promising results as a safe and effective vaccine in transgenic mouse lines with mutations corresponding to GSS. This project aims to optimize and analyze the efficacy of 14R1 in transgenic mouse models for gCJD, GSS, and FFI. For all vaccine trials, antigen was expressed, purified, and verified by quality control measures of SDS-PAGE and TEM. The vaccine and selected adjuvant were then co-administered to young mice on a prime-

boost schedule. Serum was collected at the pre-immune stage and following each immunization. We then measured the antibody titre in the serum using an ELISA.

Following comparison to other immunopotentiators, alum proved to be the best adjuvant in the GSS mouse line. Although immunization with 14R1 significantly delayed symptom onset and increased survival, GSS mice eventually succumb to prion disease. However, continued vaccination following the initial prime-boost schedule did not improve efficacy. Comparison of the immune response to 14R1 between mouse lines warranted investigation into immunological shortcomings and biases of each transgenic mouse model. gCJD and FFI mice, on a C57BL/6J background, had a much lower antibody titre following vaccination than the GSS mice, on an FVB background. However, the vaccine still showed efficacy in the FFI mice. gCJD mice were found to have a deficiency in a protease, cathepsin E, responsible for antigen processing. In response to the knowledge of a helper T-cell bias in gCJD mice, it was found that QS21 adjuvant was the better immunopotentiator for these mice as it significantly improved the immune response compared to alum adjuvant.

Considering 14R1 as a proof of concept for rationally designed structure-based prion vaccines, new PIRIBS-based prion vaccines were designed and developed in response to emerging PrP^{Sc} cryo-EM structures. Following rational design, purification, and quality control, four vaccine constructs (P1, P2, P3a, and P4) were administered to FVB mice to

assess the immune response. All PIRIBS vaccine candidates produced a large immune response, comparable to 14R1. A bridge ELISA determined that all animals immunized with P1, P2, and P3a produced antibodies which recognize PrP^{Sc} in RML-infected brain homogenate, while all animals immunized with P4 did not.

Considering both 14R1 and the new PIRIBS vaccine candidates show potential PrP^{Sc} recognition, structural changes associated with prion disease becomes much more complex. Overall, these findings are an important step towards development of a prion disease vaccine for use in large animals and at-risk humans.

Preface

All in-text citations, headings, tables, and figures are linked. Clicking a link will take you to the page it is located.

This project received animal research ethics approval from the University of Alberta Animal Care and Use Committee according to guidelines from the Canadian Council on Animal Care. The research protocols of these results were approved under AUP00002852, titled "Vaccines for neurodegenerative diseases".

Portions of this work were accomplished with the help of many collaborators and lab members. HET-2s and 14R1 were designed by Dr. Andrew Fang (section 1.11.2 & 1.11.3). The purification method for HET-s-based vaccine candidates was optimized by Dr. Andrew Fang (section 2.1). The electron micrographs were collected with the help of Dr. Andrew Fang, Dr. Razieh Kamali Jamil, and Dr. Yongliang Wang. Specifically, the micrograph of HET-2s was provided by Dr. Andrew Fang (Figure 3.3). The HET-2s and 14R1 efficacy trials with Freund's adjuvant in P101L mice were performed by Dr. Andrew Fang (Figure 3.5 & Figure 3.6). Models of 14R1, PrP^{C}, and PrP^{Sc} were created by Dr. Holger Wille (Figure 1.4 & Figure 1.5). The spleen extraction and lymphocyte isolation were completed with the help of Dr. Xinli Tang. The immunoblotting was performed with

the help of Dr. Xinli Tang. Immunization, serum collection, and rotarod experiments of the FFI mouse line were performed by Dr. Roberto Chiesa and his lab members at the Mario Negri Institute for Pharmacological Research in Milan, Italy. Maintenance and monitoring of mice was conducted by the animal staff technicians. Genotyping of the P101L mice was performed by Brian Tancowny. Undergraduate student, Cynthia Yuen, assisted with purification and quality control of the PIRIBS vaccine candidates under my direct supervision. The remainder of results and figures presented in this thesis are my own original work.

To mom, for everything.

The Brain—is wider than the Sky—
For—put them side by side—
The one the other will contain
With ease—and You—beside—

The Brain is deeper than the sea—
For—hold them—Blue to Blue—
The one the other will absorb—
As Sponges—Buckets—do—

Emily Dickinson, 1863

Acknowledgements

Firstly, thank you to my supervisor, Dr. Holger Wille. Your guidance and support throughout my undergraduate and graduate studies are so appreciated. Thank you for your continuous encouragement and for fostering an environment which promotes both independence and fellowship. It has truly been a pleasure to be a part of your team. Thank you for every opportunity to improve my research and communication skills.

Thank you to my committee members, Dr. Olivier Julien and Dr. Valerie Sim. Your insight and advisement were always positive and encouraging. I left each committee meeting excited to apply what I had learned and ponder your helpful comments.

I would also like to thank my fellow members of the Wille lab for being such great coworkers and friends. To Dr. Andrew Fang, thank you for mentoring me throughout my BIOCH 499. I am beyond grateful to you for imparting your research techniques and for answering each of my many questions. Thank you for teaching me how to “work smart”.

Thank you to the Alberta Prion Research Institute and the CJD Foundation for your generous monetary support of this project. It is a privilege to be entrusted with both government and personal funds for such an important cause.

I am grateful for the worldwide collaboration which allowed us to conduct research with multiple mouse lines. Thank you to Dr. Glenn Telling, Dr. Roberto Chiesa, and Dr. Ruth Gabizon for the use of the GSS, FFI, and CJD mouse line, respectively.

I'd like to thank my family and friends for all their love and support throughout the years. A special thank you to my grandparents and to my stepfather for their encouragement and support as I decided what to do with my life. Lastly, thank you to my fiancé, Derek, for lifting me up on the tough days and celebrating with me on the good days.

Table of Contents

List of Tables

List of Figures

List of Acronyms and Abbreviations

4RβS	four-rung β-solenoid
Ab	antibody
AD	Alzheimer's disease
ADE	antibody-dependent enhancement
Aβ	amyloid-β
ASO	antisense oligonucleotide
BBB	blood-brain barrier
BH	brain homogenate
bp	base pair
BSE	bovine spongiform encephalopathy
CFA	complete Freund's adjuvant
CJD	Creutzfeldt-Jakob disease
CNS	central-nervous system
Cryo-EM	cyogenic electron microscopy
CSF	cerebral spinal fluid
CWD	chronic wasting disease
DC	dendritic cell
DNA	deoxyribonucleic acid
ds	double stranded
DSE	disease-specific epitope
DW-MRI	diffusion-weighted MRI
E. coli	*Escherichia coli*
EEG	electroencephalogram
ELISA	enzyme-linked immunosorbent assay
FA	Freund's adjuvant
fCJD	familial Creutzfeldt-Jakob disease
FFI	fatal familial insomnia
FT	flexible tail
gCJD	genetic Creutzfeldt-Jakob disease
GD	globular domain
GPI	glycosylphosphatidyl inositol
GSS	Gerstmann-Sträussler-Scheinker disease
HE	hematoxylin and eosin

hGH	human growth hormone
hDM	human dura matter
HR	hydrophobic region of PrP
HRP	horseradish peroxidase
IC	intracerebral
iCJD	iatrogenic Creutzfeldt-Jakob disease
ICV	intracerebroventricular
ID	intradermal
IFA	incomplete Freund's adjuvant
IgA	immunoglobulin A
IgG	immunoglobulin G
IgM	immunoglobulin M
IM	intramuscular
IN	intranasal
IP	intraperitoneal
IV	intravenous
kDa	kilodalton
mAb	monoclonal antibody
MRI	magnetic resonance imaging
mRNA	messenger RNA
MW	molecular weight
N/A	not applicable
NMR	nuclear magnetic resonance spectroscopy
OD	optical density
OD_{450nm}	optical density at 450 nm
OR	octapeptide repeat region of PrP
ORF	open reading frame
P. anserina	*Podospora anserina*
P1	PIRIBS 1
P2	PIRIBS 2
P2V	PIRIBS 2V
P3a	PIRIBS 3a
P3b	PIRIBS 3b
P4	PIRIBS 4
pAb	polyclonal antibody
PCR	polymerase chain reaction
PD	Parkinson's disease
PDB	Protein Data Bank

PE	phosphatidylethanolamine
PERK	protein kinase RNA-like endoplasmic reticulum kinase
PFD	prion-forming domain
PIRIBS	parallel-in-register intermolecular β-sheet
PK	proteinase K
PMCA	protein misfolding cyclic amplification
PMSF	phenylmethylsulfonyl fluoride
PNS	peripheral nervous system
PRNP	human prion protein gene
Prnp	animal prion gene
Prnp$^{-/-}$	PrP knockout
PrP	major prion protein
PrP^{C}	cellular prion protein
PrP^{Sc}	infectious prion protein
PrP^{res}	protease-resistant prion protein
[*PSI*$^{+}$]	prion form of Sup35
PSPr	protease-sensitive prionopathy
PTM	post-translational modification
PVDF	polyvinylidene fluoride
Q. Saponaria	*Quillaja Saponaria*
recPrP	recombinant PrP
REM	rapid eye movement
RIPA	radioimmunoprecipitation assay
RML	Rocky Mountain Laboratory
RNA	ribonucleic acid
RNAi	RNA interference
RPM	revolutions per minute
RT	room temperature
RT-QuIC	real-time quaking-induced conversion
S. cerevisiae	*Saccharonmyces cerevisiae*
SC	subcutaneous
scFV	single-chain variable fragment
sCJD	sporadic Creutzfeldt-Jakob disease
SDS-PAGE	sodium dodecyl sulfate-polyacrylamide gel electrophoresis
sFI	sporadic familial insomnia
SHa	Syrian hamster
shRNA	short hairpin RNA
siRNA	small interfering RNA

SOD1	superoxide dismutase 1
ss	single-stranded
ssNMR	solid-state NMR
SynPep	synthetic peptides
TEM	transmission electron microscopy
Th1	T-helper type 1 cells
Th2	T-helper type 2 cells
TSE	transmissible spongiform encephalopathy
UK	United Kingdom
UPR	unfolded protein response
UPS	ubiquitin-proteasome system
[*URE3*]	prion form of Ure2
v/v	volume/volume
vCJD	variant Creutzfeldt-Jakob disease
VPSPr	variably protease-sensitive prionopathy
w/v	weight/volume
WT	wild type
WTD	white-tailed deer

List of Chemicals and Reagents

AAHS	aluminum hydroxyphosphate sulfate
BCA	bicinchoninic acid
BME	β-mercaptoethanol
BSA	bovine serum albumin
DAB	3,3'-diaminobenzidine
ddH2O	double distilled water
DMEM	Dulbecco's Modified Eagle Medium
DOC	deoxycholic acid
EDTA	ethylenediaminetetraacetic acid
EtBr	ethidium bromide
Gdn	guanidinium
H_2SO_4	sulphuric acid
HCl	hydrochloride
LDS	lithium dodecyl sulfate
MgCl2	magnesium chloride
NaCl	sodium chloride
NaOAc	sodium acetate
NBF	neutral buffered formalin
Ni-NTA	nickel-nitrilotriacetic acid
PBS	phosphate-buffered saline
PMSF	phenylmethylsulfonyl fluoride
SDS	sodium dodecyl sulfate
TBS	Tris-buffered saline
TBST	TBS 0.1% Tween-20
TMB	3,3',5,5'-tetramethylbenzidine
THAM	tris(hydroxymethyl)aminomethane

Standard Amino Acid Codes

Alanine	Ala	A
Arginine	Arg	R
Asparagine	Asn	N
Aspartate	Asp	D
Cysteine	Cys	C
Glutamate	Glu	E
Glutamine	Gln	Q
Glycine	Gly	G
Histidine	His	H
Isoleucine	Iso	I
Leucine	Leu	L
Lysine	Lys	K
Methionine	Met	M
Phenylalanine	Phe	F
Proline	Pro	P
Serine	Ser	S
Threonine	Thr	T
Tryptophan	Trp	W
Tyrosine	Tyr	Y
Valine	Val	V

1 Introduction

1.1 Protein folding

Protein folding is a stochastic mechanism in which a primary amino acid structure adopts the most thermodynamically stable conformation (Dobson, 2003). Protein folding is determined both by the intrinsic properties of the amino acid sequence and by the influence of the complex cellular environment (Dobson, 2003). Properly folded proteins are imperative to the function and regulation of many cellular mechanisms. As such, there are mechanisms established to ensure misfolded and dysfunctional proteins are repaired or removed (Hartl, 2017). Reparation of misfolded proteins is carried out by chaperone proteins. However, there are proteins that can evade chaperones. These proteins have a propensity to misfold into an alternative, yet stable, fibril conformation which are likely to aggregate and cause cell loss and dysfunction (Soto & Estrada, 2008).

1.2 Amyloids

Amyloids are insoluble, filamentous proteins with a common cross-β architecture that arise from normally-folded, soluble monomeric proteins (Cremades & Dobson, 2018). Amyloids consist of β-sheet rich protofilaments and are stabilized by both side chain interactions and backbone hydrogen bonds (Michaels et al., 2018). Amyloids can be stained with amyloid dyes. When stained with Congo red, amyloids will display birefringence under polarized illumination and when stained with Thioflavin T, amyloids will fluoresce. Amyloid fibrils can aggregate and accumulate to form plaques in the brain (Cremades & Dobson, 2018). Amyloids can be associated with many neurological disorders as they often result in both a loss of normal function and a gain of toxic function of the misfolded protein (Soto & Estrada, 2008).

1.3 Protein misfolding

The mechanism of protein misfolding is yet to be fully understood. However, the amyloidogenic process is characterized by an initial, slow nucleation event in which monomeric proteins spontaneously misfold to a β-sheet rich intermediate species. The accumulation of β-structured oligomers occurs due to a self-replication pathway in which

misfolded intermediates act as a template for further nucleation events. Fragmentation of both mature fibrils and oligomeric species produces pathogenic seeds that promote misfolding of like proteins. This autocatalysis results in an exponential growth phase of fibrils and is associated with the onset and progression of protein misfolding diseases (figure 1.1.1) (Jucker & Walker, 2013; Michaels et al., 2018).

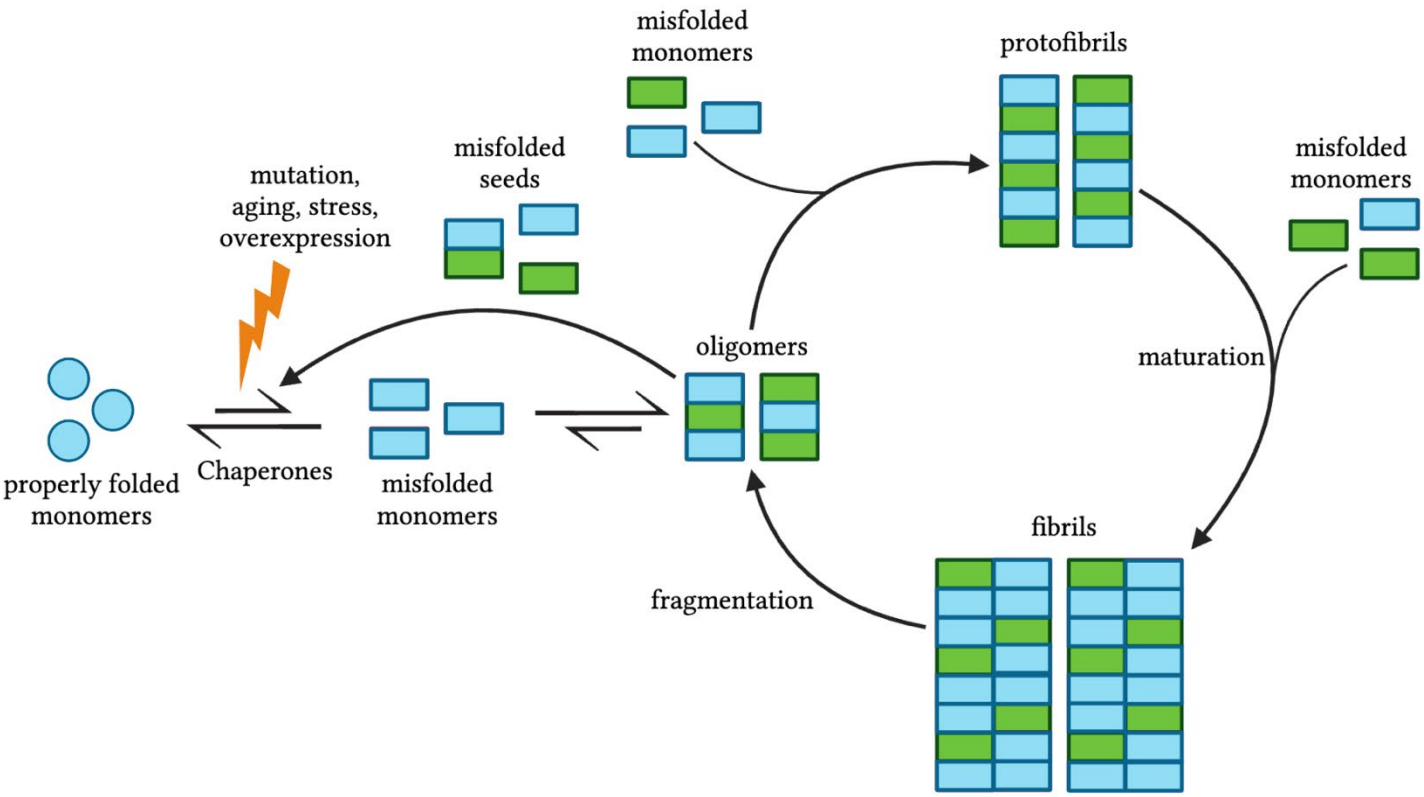

Figure 1.1.1: **Protein misfolding mechanism**. Initial misfolding of monomeric proteins, although thermodynamically unstable, can occur with aging, mutation, stress, and overexpression. Misfolded oligomers can fragment to form pathogenic seeds which induce monomeric misfolding. Addition of misfolded monomers to oligomers and protofibrils results in mature fibrils which can self-replicate by fragmentation. Figure was created with Biorender.

1.4 Protein misfolding diseases

Protein misfolding diseases are characterized by amyloid deposition in tissues. Amyloid deposition in tissues outside the central nervous system (CNS) results in non-neuropathological diseases such as type II diabetes and cataracts. Amyloids present in the central nervous system are associated with neurodegenerative diseases such as Alzheimer's, Parkinson's, Huntington's, and prion diseases. A list of protein misfolding diseases and their associated proteins is provided below (table 1.1).

Approximately one third of human neuropathological diseases are genetic. These arise from autosomal dominant mutations and normally result in an early onset of diseases. Hereditary neurodegenerative disorders are the result of mutations in the gene of the misfolding protein or the gene of a protein which processes the misfolding protein associated with the disease. Around half of all neurodegenerative diseases are sporadic. These diseases have a later age of onset suggesting accumulation of misfolded protein as well as aging play a role in disease phenotypes. Around one sixth of protein misfolding diseases are transmissible (Chiti & Dobson, 2017). This can occur iatrogenically, via direct or indirect contact with tissues and fluids, or upon ingestion of infected tissue.

Table 1.1: List of protein misfolding diseases

Protein misfolding disease	Associated protein	Reference
Alzheimer's disease	Amyloid β (Aβ) & Tau	(Bloom, 2014)
Parkinson's disease	α-synuclein	(Mehra et al., 2019)
Prion disease	Prion protein (PrP)	(Prusiner, 1998)
Huntington's disease	Huntingtin (poly Q)	(Shacham et al., 2019)
Amyotrophic lateral sclerosis	TDP43 & SOD1	(Paré et al., 2018)
Type II diabetes	Amylin	(Pillay & Govender, 2013)
Cataracts	Crystallins	(Moreau & King, 2012)
Spinocerebellar ataxia 3	Ataxin-3	(Paulson, 2012)
Familial amyloidosis	Transthyretin	(João Saraiva et al., 2004)
Spinal muscular atrophy	Androgen receptor	(Cicardi et al., 2019)
Lewy body dementia	α-synuclein	(Cummings, 2004)
Multiple Myeloma	Immunoglobulin (IgG)	(Aronson & Davies, 2012)
Nephrogenic diabetes insipidus	Vasopressin 2 receptor	(Bichet, 2008)
Sickle cell anemia	Hemoglobin	(Valastyan & Lindquist, 2014)
Retinal dystrophies	Rhodopsin	(Lin & Lavail, 2010)
Fabry disease	α-galactosidase	(Yam et al., 2005)

1.5 PrP^C structure and function

The cellular prion protein, PrP^C, is a constitutively expressed protein bound to the plasma membrane by a GPI-anchor (Stahl et al., 1987; Zhu & Aguzzi, 2021). PrP^C is expressed throughout the body with its highest levels in the central nervous system (CNS), mainly the neurons and astrocytes. It is also expressed in the peripheral nervous system (PNS) and in lymphoid tissues. PrP^C is highly conserved throughout many vertebrates (Watts et al., 2018). Figure 1.1.2b shows the structure of the globular domain of PrP^C, as solved by NMR spectroscopy. The folded domain of PrP^C is composed of two anti-parallel β-strands and three α-helices. The second and third helices are stabilized by a single disulphide bond which form a twisted V-shape that anchors the short α-helix and the two-rung β-sheet (Riek et al., 1996).

The N-terminus of the prion protein is unfolded. It is characterized by a polybasic region rich with positively-charged residues and an octapeptide repeat (OR) region followed by another polybasic region ending with a chain of hydrophobic residues (HR) (figure 1.1.2a) (Hara & Sakaguchi, 2020).

a.

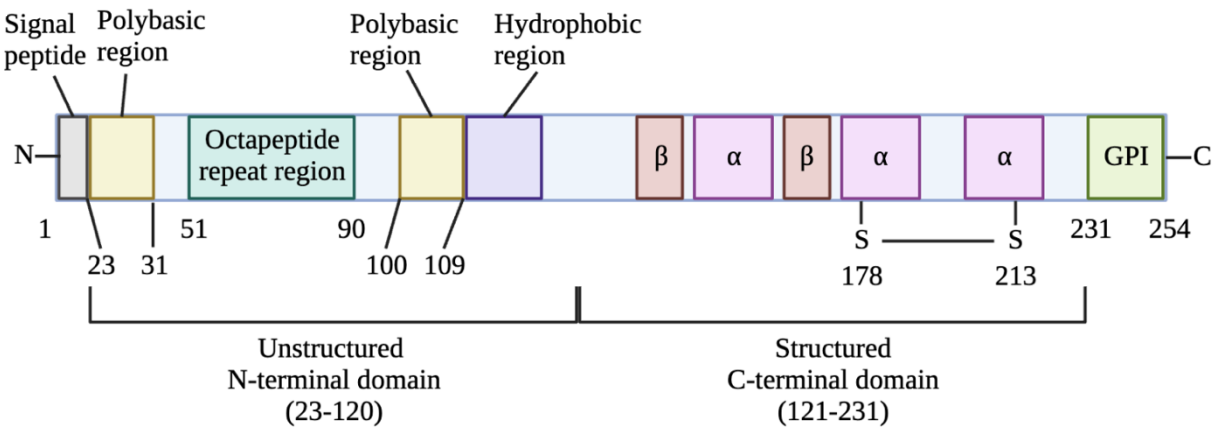

b.

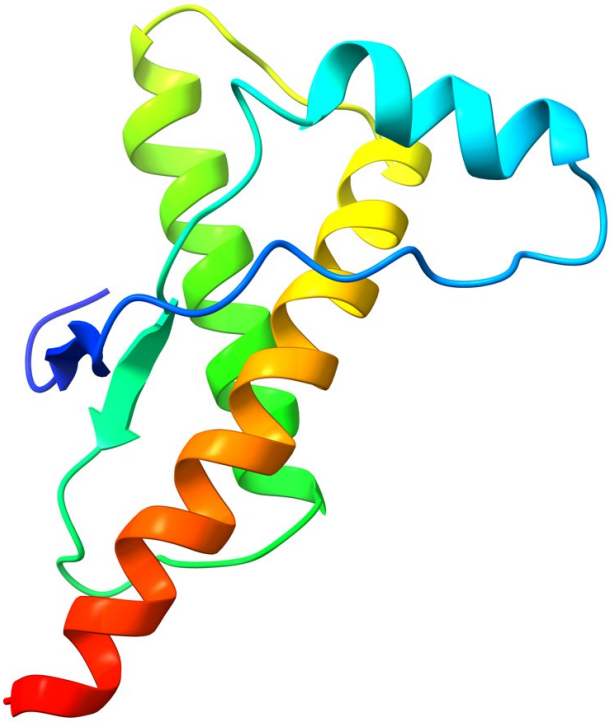

Figure 1.1.2: Structure of the human cellular prion protein (PrP^C). a. PrP^C is a 254 amino acid protein composed of an unstructured N-terminal domain and a globular folded C-terminal domain. b. The folded domain of PrP^C contains three alpha helices and two antiparallel β-strands. Coloured backbone transforms from red (N-terminal) to indigo (C-terminal). Figure was visualized and illustrated with UCSF ChimeraX. PDB: 1QLX from (Zahn et al., 2000).

The function of PrP^C has been studied extensively as it is the essential substrate for prion disease and therefore a potential therapeutic target. Through knockout studies, molecular evolutionary studies, and protein-protein interactions, PrP^C has been linked to many functions (Castle & Gill, 2017; Watts et al., 2018). Most notably, the cellular prion protein has been evidenced to play a role in stress neuroprotection (Bounhar et al., 2001; Castle & Gill, 2017; Guillot-Sestier et al., 2009; Yu et al., 2012), neuronal growth signalling pathways (Llorens et al., 2013; Loubet et al., 2012), cell adhesion and differentiation (Lee & Baskakov, 2014), and proliferation (Corsaro et al., 2016). PrP^C has also been linked to neuronal excitability (del Río & Gavín, 2016; Striebel et al., 2013), myelination (Bremer et al., 2010; Küffer et al., 2016), and circadian rhythm (Cagampang et al., 1999; Strom et al., 2011; Tobler et al., 1996). Recently, PrP^C has shown a potential role in protection against Alzheimer's disease by inhibiting Aβ accumulation (Parkin et al., 2007; Whitehouse et al., 2013) and downregulating tau transcription (Chen et al., 2013). Although evidence exists for a wide variety of PrP^C functions, there is much debate as many conflicting studies have been published on the subject (Castle & Gill, 2017).

1.6 PrP^{Sc} structure and mechanism

The most significant attribute of PrP^{C} is its ability to misfold and aggregate. The soluble and globular PrP^{C} undergoes a conformational change to form the insoluble and β-sheet rich PrP^{Sc}. PrP^{Sc} is the causative, infectious agent in prion diseases. It was first described by Stanley Prusiner in 1982 as a "proteinaceous infectious particle" free of nucleic acids (Prusiner, 1982). Since then, PrP^{Sc} structure, mechanism, and significance has been studied extensively.

The structure of PrP^{Sc} has been widely debated for decades. The structure of PrP^{Sc} has been elusive due to its insolubility and propensity to aggregate. Requena and Wille outlined and examined experimental data to support a number of PrP^{Sc} models (Jesús R. Requena & Holger Wille, 2014). Many models have been proposed with two standouts: the four-rung β-solenoid (4RβS) and the parallel in-register β-sheet (PIRIBS).

Evidence for the 4-rung β-solenoid model includes low resolution cryo-electron microscopy (cryo-EM) (Vázquez-Fernández et al., 2016) and x-ray fiber diffraction studies (Wille et al., 2009), circular dichroism and Fourier-transform infrared spectroscopy (J. R. Requena & H. Wille, 2014), mass spectrometry (Welker et al., 2002) and proteinase K

digestion mapping (Vázquez-Fernández et al., 2012), and glycan accommodation (Baskakov & Katorcha, 2016). The proposed four-rung β-solenoid structure is composed of two protofilaments, each with repeating monomers of 4 anti-parallel β-strands to form a super helix with a triangular hydrophobic core (Spagnolli et al., 2019). The distance between two residues in the same position of stacked β-strands is 19.2 Å, whereas the distance between the same residue in two stacked monomers is 38.4 Å (Spagnolli et al., 2019).

Alternatively, the PIRIBS model has been evidenced by electron paramagnetic resonance (Cobb et al., 2007), solid-state nuclear magnetic resonance spectroscopy (ss-NMR) (Groveman et al., 2014; Jones et al., 2011; Tycko et al., 2010), H/D exchange mass spectrometry (Smirnovas et al., 2011), and FTIR (Baron et al., 2011). Most notably, recent brain-derived, high-resolution cryo-electron microscopy (cryo-EM) structures of PrP^{Sc} adopt a PIRIBS conformation (figure 1.3) (Hallinan et al., 2022; Hoyt et al., 2022; Kraus et al., 2021; Manka et al., 2022). The PIRIBS structure is characterized by a single, asymmetric, protofilament in which individual monomers are stacked to form each rung of the fibrils. In the PIRIBS structure, each residue of a rung is separated by 4.9 Å from the same residue of the next rung.

a. 263K

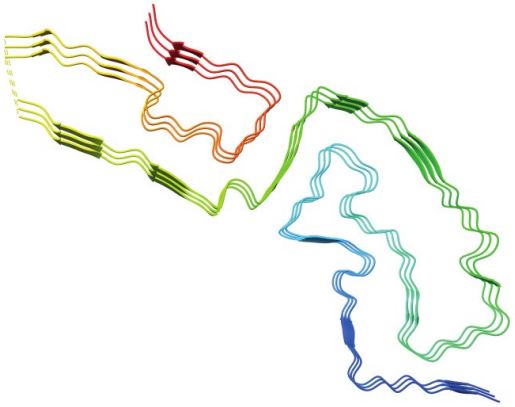

b. aRML

c. RML

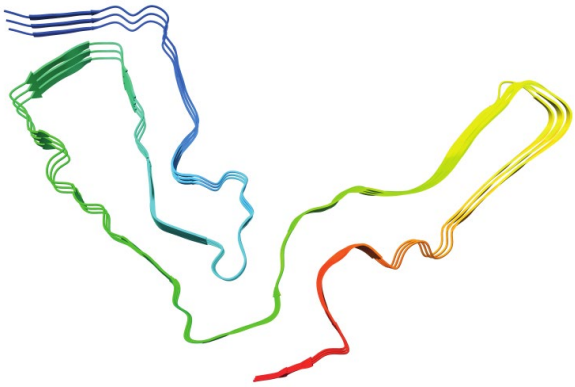

d. GSS type I

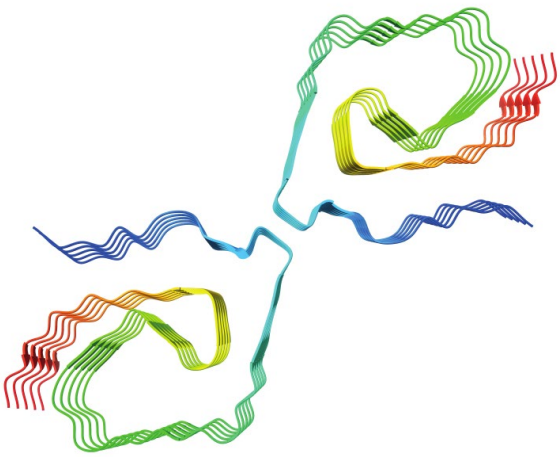

e. GSS type II

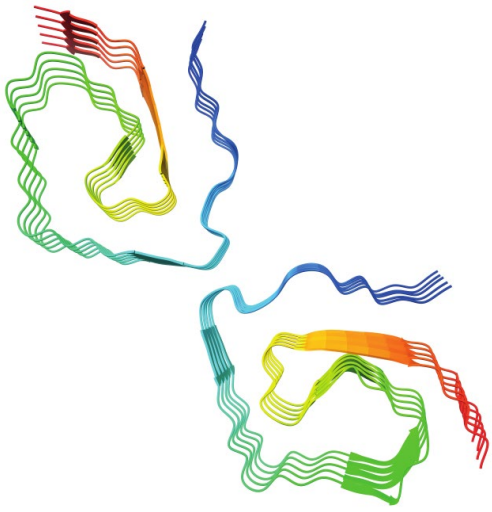

Figure 1.3: High resolution structures of brain-derived PrP^{Sc} solved by cryo-EM. All structures demonstrate a PIRIBS conformation with 4.9 Å spacing between monomers. a. 263K hamster prion structure. PDB: 7LNA (Kraus et al., 2021). b. anchorless RML mouse prion structure. PDB: 7TD6 (Hoyt et al., 2022). c. GPI-anchored RML mouse prion structure. PDB: 7QIG (Manka et al., 2022). d. human GSS type I structure. PDB: 7UMQ (Hallinan et al., 2022). e. human GSS type II structure. PDB: 7UN5 (Hallinan et al., 2022). Coloured backbone transforms from red (N-terminal) to indigo (C-terminal). Figures were visualized and illustrated with UCSF ChimeraX.

Cryo-EM structures and low-resolution models of PrP^{Sc} structure have helped to reveal potential mechanisms for the templated misfolding of PrP^{C} and the aggregation of PrP^{Sc}. Most researchers support the idea of unfolding of PrP^{C} followed by formation of an intermediate species prior to formation of the misfolded monomeric PrP^{Sc} (Kraus et al., 2021). The structure, infectivity, and toxicity of a potential intermediate is yet to be determined. Even with the recent publications of cryo-EM structures of PrP^{Sc}, many questions remain surrounding the mechanism of misfolding and the significance of these structures in prion disease.

1.7 History of prion disease

Prion diseases are transmissible neurodegenerative disorders associated with the misfolding of the prion protein. In 1920, neurologists Creutzfeldt and Jakob first described a human neurological disorder that would come to be known as Creutzfeldt-Jakob disease (CJD) (Creutzfeldt, 1920; Jakob, 1921). In 1957, another human neurodegenerative disease affecting the Fore people of Papua New Guinea, kuru, was described by Gajdusek and Zigas (Gajdusek & Zigas, 1959). Kuru was later linked to ritualistic funerary cannibalism (Mathews et al., 1968). In 1959, Hadlow proposed a link between kuru and the transmissible disease affecting sheep, scrapie (Hadlow, 1959). However, Hadlow supported the theory, proposed by Sigurdsson in 1954, that a "slow-virus" was the causative agent of the diseases (Sigurdsson, 1954). Following Hadlow's recommendation, Gajdusek, Gibbs, and Alpers established transmissibility of the disease by intracerebrally inoculating chimpanzees with brain material from humans that died of kuru (Gajdusek et al., 1966). Shortly after, this experiment was repeated using brain material from humans that died of CJD (Gibbs et al., 1968). For his work connecting CJD, kuru, and scrapie as distinct forms of the same neuropathy, Gajdusek was awarded the Nobel Prize in Medicine in 1976. It wasn't until 1967, that Griffith defined the "protein-only hypothesis" which explained the self-propagation of an infectious agent free of nucleic acids (Griffith, 1967),

contradicting both the central dogma of biology, outlined by Crick (Crick, 1958), and the "slow virus" hypothesis of Sigurdsson (Sigurdsson, 1954). This hypothesis later became widely accepted following Stanley Prusiner's purification of this protein-only infectious agent, PrP^{Sc}, in 1982 for which he was awarded the Nobel Prize in Medicine in 1997 (Prusiner, 1982). Since then, many prion diseases in many mammals have been studied extensively (Heppner & Aguzzi, 2003; Zabel & Reid, 2015).

1.8 Animal prion diseases

1.8.1 Scrapie

Scrapie, the prion disease affecting sheep and goats was first officially reported in 17^{th} century Europe (Lisle, 1757; Ness et al., 2023). Cuillé and Chelle described scrapie as a transmissible disease which is unique in its long incubation period and resistance to sterilization techniques (Cuillé & Chelle, 1938). Scrapie was the first prion disease evidenced to be both infectious and transmissible (Cuillé & Chelle, 1936). Once considered an endemic worldwide, scrapie is now prevented with selective breeding (Goldmann, 2008). Several *Prnp* codons that confer the susceptibility of disease in sheep have been identified. For example, codon 171, if which contains homozygous glutamine (QQ) residues, animals are susceptible whereas if the codon has homozygous arginine (RR)

residues, animals are resistant to scrapie (Goldmann et al., 1994). Scrapie transmission occurs via the gut-associated lymphoid tissues and transfers to the CNS via the PNS (Mathiason, 2017). With decades of conflicting evidence, the zoonotic potential of scrapie has been studied rather extensively but there is yet to be a clear risk to public health (Requena et al., 2016).

1.8.2 Bovine spongiform encephalopathy

Bovine spongiform encephalopathy (BSE) or mad-cow disease affecting cattle was discovered in 1986 and is thought to have originated due to consumption of bone and tissue from either a spontaneous case of BSE-infected cattle (Capobianco et al., 2007) or scrapie-infected sheep (Huor et al., 2019). The propagation of disease due to industrial cannibalism led to an epizootic in Great Britain. The transmissibility of BSE to humans proved catastrophic as cases of variant CJD (vCJD) emerged as a result of consumption of contaminated beef products (Weissmann & Aguzzi, 1997).

1.8.3 Chronic wasting disease

More recently, chronic wasting disease (CWD), affecting cervids, has been spreading rapidly throughout North America, South Korea, and Scandinavia. CWD was first described in captive mule deer in 1967 by researchers in Fort Collins, Colorado (Williams, 2005). CWD was later classified as a prion disease due to spongiform patterns in the brain (Williams & Young, 1980), prion protein aggregation (Spraker et al., 2002), and transmissibility (Browning et al., 2004). CWD has now been detected in white-tail deer, black-tail deer, moose, elk, and reindeer populations. CWD is the only prion disease known to affect both free-range and farmed animal populations as it is highly contagious, spreading indirectly through the environment (Otero et al., 2021). A possible explanation for the effective transmission of CWD prions can be attributed to the structure of PrP^C. The loop which connects the β-sheet strand to the alpha-helices is quite rigid in cervids and has been evidenced to influence PrP^C misfolding. Most concerning, the zoonotic potential of CWD is unknown. Many studies examining interspecies transmission of CWD have provided no clear evidence of a risk to humans (Kurt et al., 2015; Marsh et al., 2005; Mawhinney et al., 2006; Race et al., 2009; Race et al., 2018; Raymond et al., 2000; Waddell et al., 2018). Although, a recent study by Hannaoui et al. evidenced transmission of CWD prions to mice expressing human PrP (Hannaoui et al., 2022). The spread of CWD

remains a threat to ecosystems and agriculture and therefore requires further investigation and therapeutic intervention.

1.9 Human prion diseases

Human prion diseases are rare, however, particularly devastating due to their rapid progression of neurodegeneration following symptom onset and their invariable fatality. Prion diseases affecting humans can be sporadic (sCJD), acquired (kuru, vCJD, and iCJD), or familial (gCJD, FFI, and GSS). Human prion diseases usually have a long incubation period/non-clinical phase (decades) with a short clinical duration (months). Symptoms of prion diseases vary based with type of disease but often include cognitive impairment, dementia, ataxia, myoclonus, and speech impairment. Prion diseases are diagnosed definitively by post-mortem autopsy to analyze brain tissue by immunohistochemistry. Currently, a definitive prion disease diagnosis requires a patient to present with a neurological disorder in addition to positive real-time quaking-induced conversion (RT-QuIC) seeding in cerebral spinal fluid (CSF). Probable cases can also be determined by clinical symptoms, EEG signals, 14-3-3 CSF assay, and high signal of diffusion-weighted MRI (Zerr et al., 2009). Currently, there are no therapeutics or cure for prion disease.

1.9.1 Sporadic prion diseases

Sporadic CJD (sCJD) is the most common, however least understood, of the prion diseases affecting humans (Parchi et al., 2011). Molecular and phenotypic subtypes of sCJD are classified by PRNP polymorphisms at codon 129 and MW of unglycosylated PrP^{Sc}. A polymorphism for either a methionine (M) or valine (V) residue at codon 129 of the PRNP gene determines susceptibility to sCJD. Methionine homozygotes are more susceptible to sCJD than heterozygotes or valine homozygotes (Palmer et al., 1991; Parchi et al., 1999). Another variability of sCJD is difference in MW of the unglycosylated PK-resistant PrP fragments. Type 1 have a MW of 21 kDa whereas type 2 have a MW of 19 kDa (Parchi et al., 1996). Therefore, sCJD cases are classified as either MM/MV 1, VV 2, MV 2K, MM/MV 2C, MM 2T, VV 1. CJD cases are phenotypically distinguished by their symptoms (onset and duration), diffusion-weighted MRI (DW-MRI) signals, periodic sharp-wave complexes of EEG, and spongiform patterns in regions of the brain (Parchi et al., 2011). The most common genotype associated with sCJD is MM/MV 1, present in 40% of all sCJD cases. This genotype has an average symptom onset of 70 years with a 4-month clinical duration. Initial symptoms are variable but normally include cognitive decline, ataxia, speech disruptions, and myoclonus. VV2 sCJD cases are the next most common genotype, present in 15% of cases, with an average clinical onset of 65 years and

a clinical duration of 6 months. Diseases phenotype is characterized by severe ataxia followed by dementia. MV 2-kuru sCJD cases, present in 8% of cases have a clinical onset of 65 years with a 16-month clinical duration. The distinct feature of this phenotype is the kuru plaques visible with hematoxylin and eosin (HE) staining. The sCJD phenotype, MM/MV 2-cortical, present in 1% of cases, has a symptom onset of 68 years with a disease duration of 20 months. This phenotype differs from others in that there is an absence of myoclonus but extensive vacuolation throughout the cortex. MM 2-thalamic sCJD cases, also observed at a 1% occurrence, are very similar to the genetic prion disease, FFI (section 1.9.3.2). This phenotype is characterized by notable decay of the thalamus. Finally VV 1 type sCJD, contributing 1% of cases, has the youngest clinical onset of 39 years with a 15-month duration (Parchi et al., 2011). As well, there can be mixed phenotypes of sCJD, the most common of which is MM/MV 1 + 2C, present in 43% of all MM cases and presenting with varying symptoms of the two protein types (Collins et al., 2006; Parchi et al., 2009).

Another sporadic prion disease, discovered in 2008, is clinically indistinct from sCJD but is characterized by abnormal PrP aggregates sensitive to protease digestion (Gambetti et al., 2008). Variable protease-sensitive prionopathy (VPSPr) accounts for 2%

of all sporadic prion disease cases, 65% of which are homozygous for valine at codon 129 (Notari et al., 2018).

1.9.2 Acquired prion diseases

1.9.2.1 Kuru

Kuru is a transmissible spongiform encephalopathy found exclusively among the Fore people and neighbouring tribes in the Eastern highlands of Papua New Guinea (Alpers, 2008). When first recorded in the late 1950's, Kuru affected the people at epidemic levels with one thousand deaths in the first five years (Gajdusek & Zigas, 1957). By the late 1960's Kuru had been attributed to ceremonial consumption of deceased tribe members (Alpers, 1968). Once funerary cannibalism was banned, occurrence of the disease began to decline and has since been eradicated with the last case reported in 2005 (Collinge et al., 2008). Cases of kuru were distributed mainly among the women and children of the tribe as they were the main participants in endocannibalism. Kuru presents as progressive ataxia with associated neuropathology including neuronal loss, vacuolation, and spongiform appearance throughout the brain and spinal cord. Amyloid or "Kuru" plaques are most pronounced in the cerebellum. Kuru can have a prolonged incubation period extending up to 50 years with a mean clinical duration of one year. Study of the

cause, transmission, and histopathology of kuru have contributed greatly to the understanding of human prion disease.

1.9.2.2 vCJD

Variant CJD (vCJD) was first described in 1996 following 10 cases of atypical neurodegeneration with a much earlier onset (29 years) and longer disease duration (14 months) than sCJD (Will et al., 1996). Following epidemiological studies, experimental mouse models, and PrP^{Sc} biochemical phenotype, it was determined that vCJD resulted from exposure to BSE. The biophysical properties of PrP^{Sc} in vCJD cases are distinct from other human prion diseases but closely resemble the phenotype observed following transmission of BSE to animal models (Collinge et al., 1996). vCJD was most prevalent in the UK with 178 confirmed cases (232 worldwide), peaking in the year 2000. All but one of the confirmed cases possessed a homozygous methionine polymorphism in PRNP codon 129. Secondary transmission of vCJD via blood transfusion from presymptomatic individuals has been confirmed following 3 cases identified in the UK (Hewitt et al., 2006; Llewelyn et al., 2004; Wroe et al., 2006). New cases of variant CJD have been largely eradicated due to control measures established to prevent BSE in cattle and to prevent secondary transmission by those exposed to BSE (Ritchie et al., 2021).

1.9.2.3 iCJD

Iatrogenic CJD (iCJD) occurs as a result of medical treatment contaminated with sCJD brain material. This can include infected transplant tissues, brain electrodes, and surgical tools (Douet et al., 2021). The first reported case of iCJD in 1974 presented in a recipient of a corneal graft from a donor who died of sCJD (Duffy et al., 1974). Other causes of iCJD have been attributed to contaminated neurosurgical instruments, human pituitary-derived growth hormone (hGH), and lyophilised human dura mater (hDM) (Douet et al., 2021). hGH treatment was popular and successful in the 1950's but has since been replaced with biosynthetic growth hormone since the first case of iCJD was linked to the therapy in 1985 (Brown et al., 2012). The risk of developing iCJD and the length of incubation period following hGH therapy depend on both the age of the recipient (Swerdlow et al., 2003) and the polymorphism at codon 129 in the PRNP gene (Peckeu et al., 2020).

1.9.3 Genetic prion diseases

Genetic prion diseases occur as a result of mutations in the PRNP gene on the short arm of chromosome 20 (Brown & Mastrianni, 2010). Single codon mutations, STOP

codon mutations, or insertions or deletions of octa-peptide repeats have been associated with a variety of hereditary prion diseases (Schmitz et al., 2017). All identified mutations are autosomal dominant with variable penetrance and expression. Genetic mutations occur in around 10-15% of prion disease patients and often have an earlier onset than those which are sporadic or variant (Gambetti et al., 2003). As with sporadic prion disease, polymorphisms on codon 129 have been linked to phenotype determination (Puoti et al., 2000).

1.9.3.1 gCJD

Genetic CJD can be caused by a variety of mutations with the most common being at position 200, 178, and 210 (Schmitz et al., 2017). The E200K mutation, discovered in 1991 (Goldfarb et al., 1991), is the most prevalent cause of gCJD. The E200K phenotype is similar to that of sCJD with an average symptom onset of 50-70 years and a clinical duration of 6 months (Gambetti et al., 2003). However, the disease penetrance increases with age, reaching nearly 100% beyond age 80 (Spudich et al., 1995). E200K carriers show histopathology indistinguishable from sCJD patients (Jarius et al., 2003). As well, E200K gCJD presents symptoms similar to sCJD including cognitive impairment, myoclonus, and ataxia (Gambetti et al., 2003). Although the global prevalence of CJD is one in one

million annual cases, there are geographical regions with much higher rates of gCJD. Most notably, prevalence of the E200K mutation among Libyan Jews is one in ten thousand (Colombo, 2000).

1.9.3.2 GSS

Gerstmann-Sträussler-Scheinker (GSS) syndrome was first described by neurologists of the same name in 1936 as a slow progressive cerebellar ataxia with cognitive impairment affecting members of a large Austrian family (Gerstmann, 1928; Gerstmann, 1936). The PRNP mutation responsible for the disease was discovered to be P102L (Hsiao et al., 1989). Other mutations responsible for GSS include, F198S and A117V (Doh-ura et al., 1989; Goldgaber et al., 1989). Symptom onset normally occurs between age 50 and 60 but can vary by decades. Clinical duration can also vary from a few months to over a decade with a mean of around 5 years (Collins et al., 2001; Masters et al., 1981). Neuropathological distinctions exist between CJD and GSS. GSS is characterized by widespread PrP amyloid plaque deposition, often absent in CJD cases. As well, CJD patients show extensive spongiform degeneration while that of GSS patients is variable (DeArmond & Prusiner, 1995).

1.9.3.3 FFI

Fatal familial insomnia (FFI) was first reported in five members of a large Italian family in 1986 (Lugaresi et al., 1986) and was subsequently labelled as a distinct, genetic prion disease in 1992 (Medori et al., 1992). D178N is the mutation in PRNP associated with FFI. However, FFI is unique in that the disease phenotype occurs only with a methionine polymorphism at codon 129. If a D178N mutation occurs with a valine at codon 129, genetic CJD will be the result (Goldfarb et al., 1992). The neuropathology of FFI differs from other genetic prion diseases in that neurodegeneration is most prominent in the thalamus (Manetto et al., 1992). As the name suggests, a characteristic of FFI is lack of sleep, including occasional near complete absence of rapid eye movement (REM) phases (Reder et al., 1995). As with other genetic prion diseases, clinical onset and duration are highly variable but average 50 years and 14 months respectively (Zerr et al., 1998). Fatal insomnia has a sporadic form, a phenocopy of FFI termed sporadic fatal insomnia (sFI). sFI and FFI share clinical symptoms and neuropathy, however sFI is even more rare than FFI (Cracco et al., 2018).

1.10 Prion Disease Therapeutics

To date, there is no treatment or cure available for any prion disease, human or animal. Despite the rarity, there is a great need for prion disease therapeutics to aid families afflicted and to prevent further economic and agricultural consequences. As well, solving the mystery of prion diseases may guide therapeutic approaches for other neurodegenerative disorders such as Alzheimer's and Parkinson's disease. Recently, there have been some attempts to treat or prevent prion diseases including small molecules, antisense oligonucleotides, and active and passive immunotherapy. Current approaches to prion disease therapeutics include inhibition of PrP misfolding, substrate (PrP^C) reduction, and clearance of misfolded PrP (ubiquitination and autophagy).

1.10.1 Small Molecules

Anti-prion small molecules have been discovered through both high-throughput screening and rational design. Small molecules have been both discovered and developed to interfere with prion conversion and reduce PrP^C expression. A summary of trials and outcomes of small molecules targeting prion disease can be found in table 1.2. Compounds that bind amyloids in general, such as polythiophenes (Doh-ura et al., 2004; Honda et al.,

2012) and Congo red (Ingrosso et al., 1995; Poli et al., 2004), have been proposed as anti-prion therapeutics due to their ability to hyper-stabilize PrP^{Sc}. However, both have difficulty permeating the blood brain barrier (BBB) and potential toxicity due to non-specific binding. Other small molecules which can easily cross the BBB, such as quinacrine, have other pharmacological issues resulting in unreliable efficacy and toxicity (Collinge et al., 2009; Geschwind et al., 2013). Many of the anti-prion small molecule hopefuls fail to show efficacy *in vivo* due to poor pharmacokinetics and toxicity. Molecules which enhance clearance pathways, including rapamycin (Cortes et al., 2012) and astemizole (Karapetyan et al., 2013), display potential, however, only in mouse models thus far. Protein kinase inhibitors which target and prevent sustained activation of the unfolded protein response (PERKi) prevented clinical onset of prion disease in the Rocky Mountain Laboratory (RML) mouse model (Moreno et al., 2013). Nevertheless, human trials with PERKi have not been attempted due to potential toxicity.

Table 1.2: Trials and outcomes of small molecules against prion disease.

Reference	Host	Prion	Inoculation Route	Compound	Delivery route	Outcome
(Terzano et al., 1983)	Humans	CJD	N/A	Amantadine	Oral	No difference in survival
(Pocchiari et al., 1987)	Golden SHas	263K	IC or IP	Amphotericin B	IP	Increased incubation period
(Ingrosso et al., 1995)	Golden SHas	263K, 139H	IC and/or IP	Congo red	IP	Slight increase in incubation period
(Adjou et al., 2000)	Golden SHas	263K	IC	Amphotericin B derivative	IP	Delayed neuropathology
(Doh-ura et al., 2004)	Mice	263K, RML, Fukuoka-1	IC	Pentosan polysulfates	ICV	Increased incubation period
(Otto et al., 2004)	Humans	sCJD, fCJD	N/A	Flupirtine	Oral	Decreased progressive dementia, no difference in survival
(Poli et al., 2004)	Golden SHas	263K	IC or IP	Congo red and derivatives	SC or IC	Slightly prolonged survival time
(Solassol et al., 2004)	C57BL/6 mice	Scrapie	IP	Dendrimers	IP	Reduced infectivity in mice spleens
(Kocisko et al., 2006)	Tg7 mice	263K	IP	Porphyrins	IP	Significant increase in survival time
(Collinge et al., 2009)	Humans	All CJD	N/A	Quinacrine	Oral	No benefit
(Ghaemmaghami et al., 2009)	Mice	RML	IC	Quinacrine	Oral liquid	No benefit
(Cortes et al., 2012)	TgA116V mice	GSS	N/A	Rapamycin	IP	Delayed disease onset
(Honda et al., 2012)	Humans	iCJD, sCJD, GSS	N/A	Pentosan polysulfates	ICV	No benefit
(Geschwind et al., 2013)	Humans	sCJD	N/A	Quinacrine	Oral	No benefit
(Karapetyan et al., 2013)	C57BL/6 mice	RML	IC	Astemizole	IP	Slight increase in survival time
(Moreno et al., 2013)	Tg37 mice	RML	IC	PERKi	Oral liquid	Abrogated development of prion disease
(Haïk et al., 2014)	Humans	All CJD	N/A	doxycycline	Oral	No difference in survival or neuropathy
(Giles et al., 2015)	Mice	RML, ME7, 22L	IC	2-aminothiazoles	Oral liquid	No benefit in Tg chimeric human mice
(Herrmann et al., 2015)	Mice	RML6 or 263K	IC	polythiophenes	ICV	Increase in survival time

1.10.2 Oligonucleotides

One therapeutic strategy targeting prion diseases is to reduce PrP^C in order to prevent prion conversion, propagation, and neurotoxicity. There is considerable evidence to support that reduction of PrP^C at the genetic level is a viable therapeutic option. Animal models show that reduction of neuronal PrP^C prevents disease progression and reverses neuropathology (Mallucci et al., 2003). Notably, PrPKO mouse models are healthy and behave normally (Büeler et al., 1992). PrPKO mice are also resistant to prion infection (Büeler et al., 1993). Several methods to decrease PrP^C at the genomic, transcriptional, and translational level have been considered. RNA interference (RNAi) is the process of sequence-specific, post-transcriptional gene silencing. Small interfering RNAs (siRNAs) are 21 nucleotide duplexes which can specifically suppress expression of a target gene (Elbashir et al., 2001). siRNAs have been shown to specifically inhibit expression of the prion protein (Daude et al., 2003). As well, short hairpin RNAs (shRNAs), consisting of complementary strands (19-22 bp) of ribonucleic acid (RNA) connected by a short loop (4-11 nt), are processed into siRNA duplexes to bind target mRNA and inhibit expression of the target gene (Moore et al., 2010). shRNA delivered with a viral vector to RML-infected mice were able to decrease levels of PrP but not at a sufficient level to increase survival (Ahn et al., 2014). Effective RNAi treatment for prion

diseases is impeded by practical delivery to the brain (Vallabh et al., 2020). With recent advancements in antisense oligonucleotides (ASOs), reducing neuronal PrP^C in the human brain is now an attainable goal. ASOs are single-stranded, short (17-20 base) oligonucleotides which specifically bind and target RNA sequences for degradation (Vallabh et al., 2020). ASO clinical trials for other neurodegenerative disorders such as spinal muscular atrophy (Finkel et al., 2017) and Huntington's disease (Tabrizi et al., 2019) have had promising results. In a recent study, ASO-mediated suppression of PrP significantly delayed prion disease onset and extended survival time in mice following infection of multiple prion strains (Minikel et al., 2020).

1.10.3 Passive Immunotherapy

Passive immunotherapy involves delivery of exogenous antibodies targeting toxic species to the patient. Passive immunotherapy was first achieved in the 1890s to target diphtheria and tetanus (Kossel, 1893). Considering the rarity of human prion diseases, a benefit of passive immunotherapy is that treatment begins following symptom onset. Passive immunotherapy can utilize polyclonal (pAbs) or monoclonal antibodies (mAbs), each with their own benefits and drawbacks. The main advantage of using polyclonal antibodies is multiple epitope specificity whereas monoclonal antibodies can only target

one epitope. However, monoclonal antibodies are much more specific and consistent than polyclonal antibodies (Slifka & Amanna, 2018). A disadvantage of antibody treatment is the cost and potential dose-dependent toxicity, as seen with ICSM18 (Reimann et al., 2016) and POM1 (Herrmann et al., 2015).

1.10.3.1 Anti-PrP^C antibodies

Passive immunotherapy to treat prion diseases involves antibodies targeting PrP^C which, in turn, reduces the amount of PrP^{Sc} by eliminating the substrate required for conversion (Frontzek & Aguzzi, 2020). Antibodies targeting PrP^C were first shown to decrease prion titre in 1988 (Gabizon et al., 1988). Since then, many antibodies have been developed and tested in pre-clinical mouse models (Table 1.3). Recently, a study with a fully humanized anti-PrP^C antibody, PRN100, was tested in six human patients presenting probable CJD (Mead et al., 2022). PRN100 was well-tolerated, non-neurotoxic, and reached promising CSF and brain tissue concentrations. However, all treated patients presented progressive neurodegeneration. Anti-PrP^C antibodies target either the globular domain (GD) or the flexible tail (FT) region of PrP^C (Frontzek & Aguzzi, 2020). Anti-PrP^C-FT compounds have illustrated neuroprotection whereas anti-PrP^C-GD compounds have been shown to be neurotoxic (Sonati et al., 2013). The mechanism responsible for

the negative effects of anti-PrP^{C}-GD treatment can be attributed to autoimmune encephalitis (Lancaster & Dalmau, 2012). Anti-PrP^{C}-FT treatment reduces accumulation of PrP^{Sc} by inhibiting PrP^{C} misfolding by preventing participation of the flexible tail in prion conversion.

Table 1.3: Summary of passive immunotherapeutics targeting prion disease; in vivo trials and outcomes

Authors	Host	Prion	Inoculation Route	Antibody	Delivery Route	Outcome
(White et al., 2003)	FVB/N mice	RML	IP	ICSM 18/35	IP	Extended survival in Ab-treated mice
(Sigurdsson et al., 2003)	CD-1 mice	139A	IP	8B4/8H4/8F9	IP	Significant delay in disease onset
(Lefebvre-Roque et al., 2007)	Tg20 mice	BSE	IP	4H11	ICV	No extension in survival, behavioural defects, neuronal loss
(Song et al., 2008)	ICR mice	Obijiro/Chandler	ICV	31C6	ICV	Extended survival when administered following inoculation
(Moda et al., 2012)	Mice	RML	IP	scFvD18	Stereotaxic AAV9	Delayed disease onset in AAV9-inoculated animals
(Ohsawa et al., 2013)	ICR mice	Chandler	IC	31C6	IV	Extended survival
(Mead et al., 2022)	Human	Probable CJD	N/A	PRN100	IV	Well-tolerated, target CSF and brain concentration

1.10.4 Active Immunotherapy

Active immunotherapy relies on endogenous innate and adaptive immune effector mechanisms to induce a potent immune response. This is most often accomplished by administration of vaccines which resemble a portion of the pathogen (Lotze et al., 2013). The first successful vaccine was created by Dr. Edward Jenner in 1796 when he demonstrated that cowpox infection provided immunity to smallpox. Jenner inoculated a child with material collected from the cowpox sore of a milkmaid. After two months, he inoculated the child with matter from a human smallpox sore, and the child remained healthy (Jenner, 1799). Since then, vaccines have been used to treat a variety of human and animal diseases. Not until 200 years later, was active immunotherapy first considered for neurodegenerative diseases when Schenk et al. illustrated that immunizing an Alzheimer's disease mouse model with aggregated Aβ reduced cerebral plaque formation (Schenk et al., 1999).

1.10.5 Adjuvants

Active immunotherapy relies on adjuvants. Adjuvants are immunopotentiators which when co-immunized with an antigen produce a stronger immune response than

antigen alone (Ramon, 1924). There are many compounds which can act as adjuvants including microbials, emulsions, and saponins (Guy, 2007). Although adjuvants have been used in human and animal vaccines for nearly 100 years, the mechanism of action is not well characterized. Adjuvants have been proposed to play many roles in stimulating an immune response including deposition and slow release of the antigen, cytokine and chemokine secretion, immune cell recruitment, antigen uptake, immune cell maturation, antigen processing, lymph node drainage, and immunomodulation (Awate et al., 2013).

1.10.5.1 Freund's Adjuvant

Freund's adjuvant (FA) is composed of heat-killed *Mycobacterium tuberculosis* in mineral oil with surfactant (Freund & McDermott, 1942). Freund's adjuvant is a potent stimulator of cell-mediated immunity. Complete Freund's adjuvant (CFA) contains the inactivated mycobacterium whereas incomplete Freund's adjuvant (IFA) does not (Dvorak & Dvorak, 1974). Use of FA is highly regulated in animals and is prohibited in humans due to pain at injection site and potential serious side effects. Risks of use are mitigated by using CFA for the initial dose and IFA for the subsequent boosts (Dubé et al., 2020).

1.10.5.2 Alum Adjuvant

Aluminum salts were first used as adjuvants in 1926 when Alexander Glenny discovered that antigen precipitated with aluminum potassium sulfate (alum) initiated a stronger immune response than antigen alone (Glenny, 1926). Since then, alum adjuvants have had various compositions including amorphous aluminum hydroxyphosphate sulfate (AAHS), aluminum hydroxide, and aluminum phosphate. Aluminum adjuvants are the most commonly used immunopotentiators and are mainly used in childhood vaccines. Alum adjuvants not only stimulate a strong innate immune response (primary, general defence) but also result in a robust adaptive immune response (long-lasting, specific protection) (Kool et al., 2012). Alum potentiates a T-helper cell type 2 (Th2) response (Sellers, 2017).

1.10.5.3 QS21

Saponin-based compounds obtained from the bark of the South American tree, *Quillaja saponaria Molina*, have illustrated adjuvant potential (Dalsgaard, 1974; Kensil et al., 1991). *Quillaja saponaria Molina*: fraction 21 (QS21) is composed of a quillaic acid triterpene core bound by complex oligosaccharides. QS21 initiates a strong T-helper cell

type 1 (Th1) response with moderate reactogenicity (Isaacs et al., 2021). QS21 has been tested with potential vaccines targeting neurodegenerative disease, including the first and unsuccessful Alzheimer's vaccine, AN1792, and subsequent ACC-001 trial (Bayer et al., 2005; Pasquier et al., 2016).

1.10.6 Prion vaccination

There have been many attempts at vaccination to prevent prion disease, most of which rely on PrP. Prion disease vaccines are designed to target PrP^{Sc} clearance prophylactically. The main issue with PrP vaccination is the extensive expression of PrP^{C}. Effective vaccination with PrP is impeded by self-tolerance resulting in insufficient affinity to prevent disease (Bade & Frey, 2007). Strategies to avoid self-tolerance include PrP modification (Bachy et al., 2010), dimerization (Abdelaziz et al., 2018), cross-linking (Magri et al., 2005), and use of heterologous prions (Ishibashi et al., 2007). As well, adjuvants alone, such as CpG-oligodeoxynucleotides, have shown moderate success as immunotherapies (Sethi et al., 2002). Other immunogenic compounds tested include an attenuated *Salmonella typhimurium* vaccine strain (LVR01) expressing mouse PrP cDNA to induce a gut immunoglobulin (IgA) response via mucosal vaccination (Goñi et al., 2005). Recently, immunization of elk with a disease specific epitope (DSE) resulted in

accelerated onset of CWD (Wood et al., 2018), perhaps due to antibody-dependent enhancement. This occurs when antibodies generated following immunization recognize and bind a pathogen but exploit and infiltrate cells rather than clear or block the pathogen, exacerbating disease (Lee et al., 2020). Table 1.4 provides an overview of prion vaccination trials and outcomes thus far. Overall, active immunotherapeutics targeting prion disease have yet to result in total prevention of disease. In fact, many are only marginal increases in survival time or incubation period.

Table 1.4: Prion vaccine trials and outcomes

Authors	Host	Prion	Inoculation Route	Vaccine	Adjuvant	Delivery route	Outcome
(Sethi et al., 2002)	Mice	RML	IP	Adjuvant	CpG-1826	IP	38% increase in survival time
(Sigurdsson et al., 2002)	CD-1 mice	139A	IP	recPrP	FAs	SC	Delayed onset
(White et al., 2003)	FVB/N mice	RML	IC or IP	mAbs	None	IP	Significant increase in survival (>500 days)
(Schwarz et al., 2003)	NMRI mice	139A	oral	SynPep + recPrP	IMS-1313	IP	Slight increase in survival time
(Pollera et al., 2004)	Golden SHas	263K	IC or IP	SynPep	KLH	Unknown	Early death of IC infected immunized animals
(Polymenidou et al., 2004)	C57BL/6 mice	RML	IP	recPrP	FAs	SC	Insignificant delay in disease onset
(Goñi et al., 2005)	CD-1 mice	139A	oral	Attenuated bacteria	Alum	Oral	Prolonged survival time in 30% of mice (>500 days)
(Magri et al., 2005)	Golden SHas	263K	IP	SynPep	FAs	IM, Sc+ID	Slight increase in survival
(Müller et al., 2005)	TgBov mice	BSE	oral	DNA	None	SC+IM	Prolonged incubation period
(Bade et al., 2006)	BALB/c mice	139A	oral	recPrP	Cholera toxin	IN	Slight increase in survival time
(Fernandez-Borges et al., 2006)	129/ola mice	BSE	IC	DNA	None	IM	Delayed onset of prion disease
(Ishibashi et al., 2007)	BALB/c mice	Fukuoka-1	IP	recPrP	FAs	IP	Increase in survival
(Nitschke et al., 2007)	C57BL/6 mice	RML	IP	DNA + recPrP	CpG-1668	ID+SC	No difference in survival
(Pilon et al., 2007)	C57BL/6 mice	RML	IP	SynPep	AdjuVac	IM	Slight increase in survival
(Goñi et al., 2008)	CD-1 mice	139A	oral	Attenuated bacteria	Alum	Oral	High IgG+IgA mice had 100% survival (>400 days)
(Sacquin et al., 2008)	C57BL/6 mice	139A	IP	SynPep	CpG-1826 +FAs	SC	Very slight increase in survival
(Bachy et al., 2010)	C57BL/6 mice	139A	IP	SynPep +DC	None	IP	No difference in disease duration
(Ishibashi et al., 2011)	BALB/c mice	Fukuoka-1	IP	recPro	FAs	IP	Increase in survival
(Xanthopoulos et al., 2013)	C57BL/6 mice	RML	IP	Aggregated recPrP	FAs	SC	Elongation of survival interval
(Pilon et al., 2013)	Mule deer	CWD	Natural	SynPep	AdjuVAc	IM	No difference in infection rate
(Goñi et al., 2015)	WT deer	CWD	oral	Attenuated bacteria	Alum	Oral	Significant increase in survival
(Abdelaziz et al., 2018)	TgElk mice	CWD	IP	recPrP mers	CpG-b	SC	Very slight increase in survival
(Wood et al., 2018)	Elk	CWD	oral	DSE fusion	Emulsigen-D	IM	Accelerated onset of CWD
(Eiden et al., 2021)	C57BL/6 mice	RML	IP	VLPs	None	SC	Prolonged incubation time

1.11 Structure-based prion vaccine

1.11.1 Fungal Prions

First proposed by Wicker in 1994, fungal prions are naturally occurring proteins which can alter their conformation to an amyloid state. Fungal prions are transmissible and self-propagating (Wickner, 1994). Criteria for fungal proteins to be labelled prions includes that mutations in the gene can result in the prion-like state, overexpression of the protein can increase the amount of prion-like protein, and expression of the protein is essential to maintain the prion-like state. Other criteria include that aggregates are resistant to SDS degradation, amyloids can be formed *in vitro* by incubation with fungal amyloid seeds, and this protein can template transformation of the protein to the prion-like state (Wickner, 1994) (Staniforth & Tuite, 2012).

1.11.1.1 Yeast Prions

The first fungal prions identified were the budding yeast *Saccharomyces cerevisiae* proteins, Ure2 and Sup35. Ure2 is encoded by the gene URE2 and plays a role in the regulating the transcription of nitrogen utilization genes. Ure2 can also form the prion state [Ure3]. Sup35 is encoded by SUP35 gene and functions to arbitrate translation

termination. Sup35 can also form the prion state [PSI$^+$] (Cox, 1994). The study of fungal prions is beneficial to the field of prion research. Yeast prions have been used to study prion propagation without the risk of laboratory-acquired infection. Yeast prions have been used for high-throughput screening of chemical compounds which may interrupt prion propagation or enhance aggregate clearance (Staniforth & Tuite, 2012).

1.11.1.2 HET-s

Another fungal prion protein identified so far is HET-s, a heterokaryon incompatibility determinant of *Podospora anserina*. This 289 amino acid protein forms a filamentous structure which regulates vegetative incompatibility, a process in which contact between genetically different fungal strains fuse and cause heterokaryon death (Saupe, 2000). Vegetative incompatibility is a function gained only when HET-s is in its prion form. HET-s prion interaction with the genetically distinct and soluble HET-S protein results in cell death via destabilization of the cell membrane (Seuring et al., 2012).

The structure of the prion domain of HET-s (figure 1.4), solved by nuclear magnetic resonance (NMR) spectroscopy, was the first high-resolution prion structure to be elucidated. The proteinase K-resistant core of HET-s spans the C-terminal residues 218-

289. HET-s (218-289) forms a two-rung, left-handed β-solenoid structure with a triangular hydrophobic core (Wasmer et al., 2008).

1.11.2 HET-2s: A fungal prion vaccine scaffold

HET-s shares no sequence homology with any vertebrate protein and forms a structure similar to the 4-rung β-solenoid model proposed for PrP^{Sc} (Gendoo & Harrison, 2011). These factors allow HET-s to act as a scaffold for a structure-based prion vaccine. The main difference between HET-s and the proposed PrP^{Sc} structure is that HET-s is composed of two rungs whereas x-ray fiber diffraction evidence of PrP^{Sc} suggests four rungs. For this reason, a four-rung β-solenoid structure, HET-2s, was created by dimerization of HET-s via the addition of a 14 amino acid linker composed of mainly glycine residues (GGGGGGGAAGGGGG) (figure 1.4). HET-2s spontaneously forms fibrils similar to HET-s following purification.

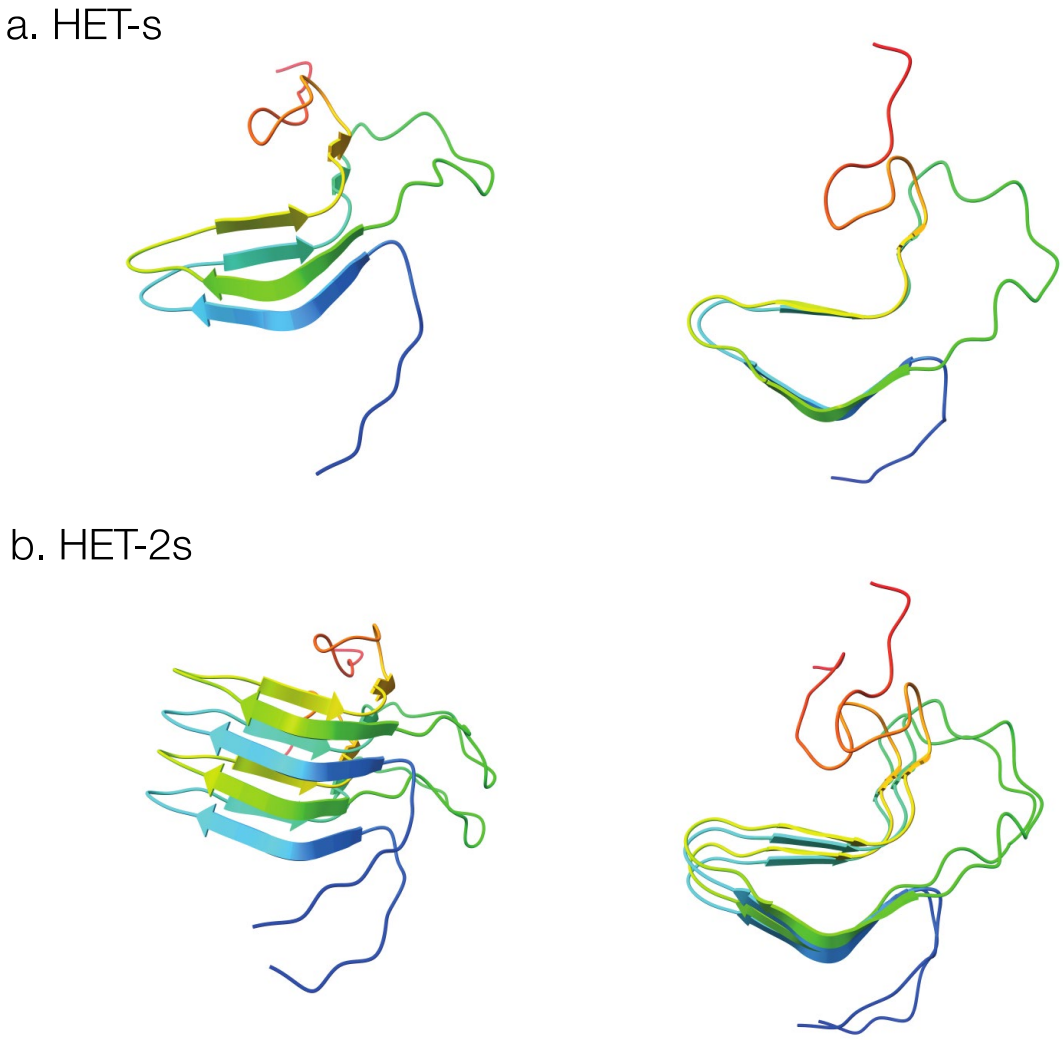

Figure 1.4: Structure of fungal prion, HET-s, and derivative, HET-2s. Structure and model of HET-s (a.) and HET-2s (b.), respectively. Two-rung HET-s (218-289) and four-rung HET-2s adapted from PDB: 2RNM (Wasmer et al., 2008). Andrew Fang created HET-2s by connecting two HET-s monomers with a glycine linker. Coloured backbone transforms from red (N-terminal) to indigo (C-terminal). Figure was visualized and illustrated with UCSF ChimeraX.

1.11.3 14R1: a structure-based prion vaccine

In order to create a vaccine antigen which produces antibodies that specifically recognize PrP^{Sc}, both the shape and exposed epitope must be relevant. In order to design the vaccine candidate, residues of HET-2s were replaced with those predicted to be exposed on the surface of the 4-rung β-solenoid model of PrP^{Sc}. Dr. Fang created many vaccine candidates but only one demonstrated potential as a vaccine against prion disease. The vaccine candidate, 14R1, contains a discontinuous epitope of 7 polar or charged amino acids which are in proximity in the PrP^{Sc} model but greatly separated in PrP^{C} (figure 1.5). The replacements, in order, are lysine (K), asparagine (N), lysine (K), histidine (H), aspartate (D), glutamate (E), and aspartate (D). As the vaccine was initially designed to target CWD, residue replacements correspond to the deer PrP residues 109, 111, 113, 114, 147, 149, and 150. Residues 109-114 were placed on rung II and residues 147-150 were placed on rung I. Epitope mapping illustrates the amino acids essential for antibody recognition are D114 and H150 residues in the β-arc region. 14R1 has a MW of 17 kDa and spontaneously forms insoluble fibrils similar to HET-2s following purification under denaturing conditions. Serum collected from FVB mice immunized with 14R1 produced antibodies which specifically recognize antigen present in prion infected brain homogenate but not in uninfected brain homogenate, most likely PrP^{Sc}. When co-immunized with

Freund's adjuvant in FVB TgP101L mice, 14R1 produces an immune response sufficient to delay symptom onset by ~150% and increase survival time by ~130% compared to unimmunized controls.

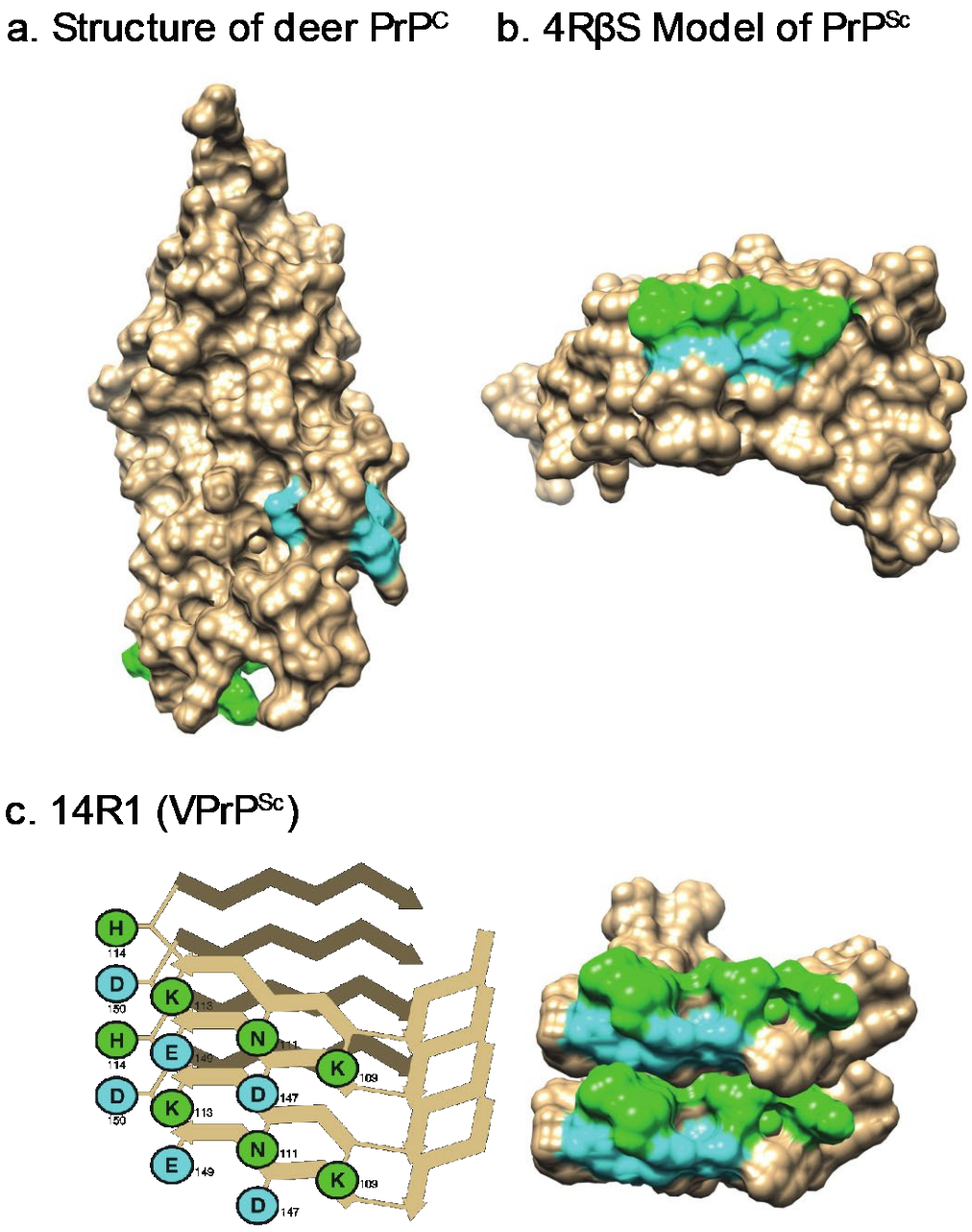

Figure 1.5: Structure-based prion vaccine design. a. Space-filling model of the globular structure of deer PrP^{C}. PDB: 4YXH (Baral et al., 2015). b. Space-filling model of a 4-rung β-solenoid PrP^{Sc}. c. Model of the prion vaccine candidate, 14R1 ($VPrP^{Sc}$). Residue replacements on the surface of the 4RβS scaffold are shown in cyan (rung I) and green

(rung II). Vaccine epitope (green and cyan) in space filling model of 14R1 (c), mimics the surface of the 4RβS model of PrP^{Sc} (b) but is not present on the surface of PrP^{C} (a). Figure adapted from Holger Wille and Andrew Fang.

1.12 Transgenic prion disease mouse models

Transgenic prion disease mouse models are useful tools which recapitulate human or large animal disease to study transmission, examine neuropathology, compare strain characteristics, and evaluate potential therapeutics. Transgenic mouse models include knockout mice, created by preventing gene expression of a target protein. Transgenic mouse models containing a protein of a different species, potentially with a disease-specific mutation are created in two ways: insertion of a transgene or knock-in. Creating transgenic mice involves implantation of fertilized embryos with a deoxyribonucleic acid (DNA) cassette encoding the mutant protein resulting in overexpression of the transgene. Knock-in mouse models are generated by replacing the endogenous protein with the protein of interest via homologous recombination in embryonic stem cells. Knock-in mice express the mutant protein at normal levels and therefore have longer pre-clinical periods than transgenic mice which overexpress PrP (Marín-Moreno et al., 2020) (Wadsworth et

al., 2010). However, overexpression of PrP can lead to non-prion related pathogenesis in the CNS (Westaway et al., 1994).

1.12.1 PrPKO mice

The first PrP knock-out (PrPKO) mouse line, Zurich I, was developed in 1992 by abolishing expression of the prion protein by disrupting the coding sequence of PRNP via homologous recombination (Büeler et al., 1992). PrPKO mice were created in order to study the function of PrP^{C} by observing the phenotype in the absence of the protein. PrPKO mice are relatively normal in their growth and development.

1.12.2 TgP101L mice

The first transgenic mice modelling a human genetic prion disease overexpressed the disease-associated mutant of PrP resulting in spontaneous onset of GSS (Hsiao et al., 1990). Transgenic mice expressing the P101L mutant have a clinical onset of ~165 days old. Symptoms include truncal ataxia, hind-limb paralysis, and tail rigidity (Nazor et al., 2005). TgP101L mice are on an FVB background. Clinical symptoms coincide with neurological degeneration including vacuolation and gliosis (Hsiao et al., 1990).

1.12.3 TgFFI mice

TgFFI mice express PrP carrying the D178N/M128 mutation associated with fatal familial insomnia. TgFFI mice are on a C57BL/6J background. These mice have a clinical onset of ~262 days old. Symptoms presented in this mouse line include motor issues, memory dysfunction, and sleep disruption. Motor issues in mice are evident by measuring the latency to fall in a rotarod experiment. TgFFI mice show a greater latency to fall beginning at ~110 days (Bouybayoune et al., 2015). TgFFI mice have a phenotype distinct from TgCJD mice D178N/V128 mutation, consistent with differences in human disease (Dossena et al., 2008).

1.12.4 TgMHu2ME199K

TgMHu2ME199K mice express chimeric mouse/human PrP with the E199K mutation associated with genetic CJD. These mice develop clinical signs of prion disease including hind limb ataxia and kyphosis at approximately 6 months of age. CJD mice exhibit progressive neurodegeneration, including neuronal loss, memory impairment, and

PrP^{Sc} aggregation in the CNS (Friedman-Levi et al., 2011) (Fainstein et al., 2016). These mice are on a C57BL/6J background.

1.13 Research objectives and hypothesis

The objective of this thesis is to both optimize and analyze the safety and efficacy of a rationally designed, structure-based prion vaccine in three human genetic prion disease mouse models. The vaccine candidate explored, 14R1, has previously shown efficacy in TgP101L mice with the toxic Freund's adjuvant. Throughout my thesis, I demonstrate that the strength of the immune response to 14R1 varies between immunized mouse lines. Investigation into the mouse background can aid in optimizing the vaccine to result in a greater immune response. This research compares the delivery of 14R1 with different adjuvants and immunization schedules to produce an immune response sufficient to delay prion disease onset and increase survival. Optimizing vaccination in transgenic mouse models expressing human genetic prion diseases is an essential step prior to human trials.

Considering the efficacy of 14R1 as a prophylactic and the PrP^{Sc}-specific antibodies generated from immunization with 14R1, the involvement of a 4RβS structure in prion

disease appears likely. However, recently published high-resolution structures of brain-derived PrP^{Sc} adopting a PIRIBS fold, rather than a 4RβS, complicates the story. In order to further understand the structural changes in PrP and their role in prion infectivity and toxicity, I have generated new vaccine constructs based on the PIRIBS structures. The PIRIBS constructs, created using the same method as 14R1, show potential as vaccine antigens. These results illustrate the versatility of structure-optimized vaccines for protein misfolding diseases.

2 Materials and Methods

2.1 Recombinant Protein Production

2.1.1 Protein Expression

Sequence-verified HET-s, and HET-2s, and 14R1 plasmid DNA was supplied by Andrew Fang. Plasmid DNA was transformed into One Shot BL21 (DE3) chemically competent *Escherichia coli (E. coli)* cells (Thermo Scientific™) and grown in the presence of 100 µg/mL ampicillin overnight at 37°C. DNA sequence was verified by Sanger Sequencing prior to transformation.

One colony from a LB-amp plate was seeded and grown for 24 hours in 350 mL Studier ZYM-5052 autoinduction media (Teknova™) at 37°C at 250 rpm with 200 µg/mL ampicillin in a baffled 2.8 L Fernbach flask.

2.1.2 Inclusion Body Purification

Cells were pelleted by centrifugation at 5,000 x g for 15 minutes and resuspended in resuspension buffer (50 mM Tris-HCl pH 8.0, 100 mM NaCl, 5 mM EDTA) at 3 mL/g

of pellet, with 0.1 mM phenylmethylsulphonyl fluoride (PMSF) and 100 µL/g of pellet recombinant human lysozyme (InVitria Lysobac). Suspension was placed on rotator for 40 minutes at room temperature. The suspension was then sonicated using 5 mm tapered microtip on a Sonifier 250 (Branson Ultrasonics, Danbury, USA) on ice at maximum power for 5 minutes total at 5 second intervals followed by centrifugation at 6,000 x g for 15 minutes at 4°C. Pellet was then resuspended in wash buffer (50 mM Tris-HCl pH 8.0, 100 mM NaCl, 0.5% Triton-X-100) at 3 mL/g of pellet with 0.1 mM PMSF. Sonication was then repeated and 2 mM $MgCl_2$, 0.5 µL/g of pellet Benzonase® nuclease, and 100 µL/g of pellet hen egg white lysozyme (Roche) were added to the suspension. Suspension was digested at room temperature for 40 minutes on rotator, and then centrifuged at 6,000 x g for 15 min. The pellet was then resuspended in resuspension buffer at 3 mL/g of pellet with 0.1 mM PMSF and centrifuged at 6,000 x g for 15 min. Resuspension and centrifugation step were repeated three times before being resuspended in pelleting buffer (100 mM Tris-HCl pH 8.0, 100 mM NaCl) at 3 mL/g of pellet. Inclusion bodies were stored overnight at -20°C prior to further purification.

2.1.3 Affinity Chromatography Purification

Inclusion bodies were resuspended in denaturation buffer (20 mM Tris-HCl pH 8.0, 6 M Gdn-HCl) at 3 mL/g of pellet and stirred on rotator at room temperature for 45 min. Resuspension was clarified via ultracentrifugation at 50,000 x g for 45 minutes at 4°C. Supernatant was then combined with Qiagen nickel-nitrilotriacetic acid (Ni-NTA) agarose resin in a 10 mL column and placed on rotator for 1 hour at room temperature. Flowthrough was collected and loaded onto column once more. Sample was washed by loading 3 x 5 mL denaturation buffer (20 mM Tris-HCl pH 8.0, 6 M Gdn-HCl) onto column. Sample was then eluted from column by loading 3 x 1 mL elution buffer (50 mM citric acid pH 2.0, 6 M Gdn-HCl).

2.1.4 Protein Desalting

Sample was desalted using 10 mL Zeba spin desalting columns (Thermo Scientific™) with a 7 kDa molecular weight cut-off. Desalted sample was split into 500 µL aliquots and titrated to pH 7.5 with 3 M Tris (Hydroxymethyl) Aminomethane (THAM). 1 mM sodium azide was added to each purified sample.

2.2 Protein Quality Control

2.2.1 SDS-PAGE

Guanidine was removed from samples collected during purification by addition of methanol and chloroform as outlined by Wessel and Flügge (Wessel & Flügge, 1984). SDS samples and Precision Plus Protein™ Dual Xtra prestained protein standards (Bio-Rad) were loaded into 12% Bis-Tris gel (Invitrogen) and a two-step electrophoresis (70 V for 30 minutes followed by 130 V for 90 min) was performed. Gel was rinsed on shaker 3 x 5 minutes with water and then stained with Coomassie Blue Brilliant G250 (Bio-Rad) for 1 hour on shaker. The gel was then destained with water overnight. The gel was then visualized with the ProteinSimple FluorChem M gel imaging system.

2.2.2 Transmission Electron Microscopy

Carbon film, 400 mesh copper grids were prepared by a 1-minute glow discharge at 15 mA and 0.39 mBar (PELCO easiGlow™). 5 µL sample was absorbed to grid for 1 minute and then rinsed three times with 50 µL of 100 mM ammonium acetate, 10 mM ammonium acetate, and then stained with filtered 1% uranyl acetate twice. Grids were

then visualized at either 14k, 19k, or 25k magnification by transmission electron microscopy using a FEI Tecnai TF20 operating at 200 kV acceleration.

2.3 Vaccine Preparation

2.3.1 Buffer Exchange

Purified protein was centrifuged at 21,000 x g for 20 minutes and supernatant containing Tris and sodium azide was removed. The pellet containing pure protein was then resuspended in 1X PBS for use in animals and immunoassays. Total protein concentration was determined using a Pierce™ BCA Protein Assay Kit (Thermo Scientific™).

2.3.2 Protein Sonication

In order to disperse fibrils, buffer exchanged protein was sonicated with a 3 mm double stepped microtip at minimum amplitude on a Sonifier 250 (Branson Ultrasonics, Danbury, USA) in 1 mL of sample volume for 30 seconds at minimum power.

2.3.3 Adjuvant Addition

Three different adjuvants were used for the animal immunizations. Immunizations with Freund's adjuvant (FA) were carried out by Andrew Fang. Both Freund's complete adjuvant (FCA) and Freund's incomplete adjuvant (FIA) were used. As well, Alhydrogel adjuvant 2% "alum" (InvivoGen, San Diego, USA), and a *Quillaja saponaria* (*Q. saponaria*) saponin "QS-21" (Desert King International, San Diego, USA).

FA was added to buffer-exchanged antigen (section 2. 3. 1) at 1:1 volume/volume (v/v) ratio of antigen:adjuvant and vortexed until a single emulsion droplet no longer dissipated when placed on water(Dvorak & Dvorak, 1974).

The alum-containing vaccine was prepared by mixing Alhydrogel® adjuvant 2% (InvivoGen) and protein antigen in a 1:1 antigen:adjuvant ratio and vortexing for 5 minutes. QS-21 was resuspended in PBS at 1 mg/mL final concentration and stirred for 1 hour until solution was fully clarified. The QS21-containing vaccine was prepared in a 1:10 antigen:adjuvant ratio by mixing 10 µg QS-21 (Desert King International) and 100 µg antigen.

2.4 Mouse Work

2.4.1 Ethics Statement

All experiments were performed in accordance with the ethics guidelines from the University of Alberta Animal Care and Use Committee and those from the Canadian Council on Animal Care. The research protocols of these results were approved under AUP00002852, titled “Vaccines for neurodegenerative diseases”.

2.4.2 Animal Maintenance

Animals were fed irradiated “LabDiet 5053” chow (Lab Supply, Fort Worth, USA) and maintained in green line ventilated racks (Techniplast, Buguggiate, Italy) on a 12-hour light and 12-hour dark cycle. Cage environment enrichment included “Nestlets” nesting material (Ancare, Bellmore, USA). Animal health were monitored daily by animal staff technicians. Cage contents including food, water, and bedding were changed bi-weekly or earlier as needed.

2.4.3 Animal Handling and Euthanasia

Animal handling was executed following comprehensive training and certification from the Health Sciences Laboratory Animal Services. Mice under serious health condition were anesthetized via isoflurane inhalation and euthanized via cervical dislocation.

2.4.4 Tg P101L Mouse Genotyping

Each TgP101L mouse was genotyped to verify the presence of a P101L mutation. Genomic DNA extraction was performed by adding tail buffer (50 mM Tris-HCl pH 8.0, 100 mM NaCl, 1% SDS, 25 mM EDTA pH 8.0) and 20 mg/mL Proteinase K to a 2-5 mm tail snip and incubating overnight at 55°C. 500 µL of buffer saturated phenol was then added and sample vortexed and centrifuged for 10 minutes at 21,500 x g. Upper layer (no phenol) was transferred to tube containing 1 mL 95% ethanol and inverted. Sample was centrifuged again at 21,500 x g for 10 minutes and 1 mL of 70% ethanol was added to pellet. Sample was centrifuged again at 21,500 x g for 10 minutes and 1 mL of 100% ethanol was added to the pellet. The sample was then centrifuged at 21,500 x g for 2 minutes, supernatant discarded, and centrifuged again for 30 seconds. Pellet was dried at

room temperature for 2 hours and then 50 µL of TE (10 mM Tris-HCl pH 8.0, 1 mM EDTA pH 8.0) was added for storage at 4°C.

Tail-derived genomic DNA was amplified using primers: PrPFwd (5'-ATGGCGAACCTTGGCTACTGGCTGCTG) and PrPRev (5'-TCATCCCACGATCAGGA AGATGAGGAAGGAGATGAGG). A two-step touchdown polymerase chain reaction (PCR) protocol was performed as follows: 1) 98°C for 30 seconds, 2) 98°C for 10 seconds, 3) 82°C for 20 seconds, reducing the temperature by 1°C per cycle, 4) 72°C for 30 seconds, 5) 10 cycles of steps 2-4, 6) 98°C for 10 seconds, 7) 72°C for 30 seconds, 8) 20 cycles of step 6-8, 9) 72°C for 2 minutes. PCR products were electrophoresed at 200 V for 15-18 minutes in a 1% agarose gel and visualized with ethidium bromide (EtBr) and ultraviolet light using a ProteinSimple FluorChem M gel imaging system. The presence of a band at ~762 bp indicated the presence of target amplification. The results were further confirmed by Sanger Sequencing.

2.4.5 Serum Collection

For routine serum collection during immunization trials, ~50 µL blood was sampled from lateral tail vein. Mice were warmed under a heat lamp for ~5 minutes, and then

placed in a restraining device. A small incision (2-5 mm) was made using a sterile 18 g needle, and blood was collected using "microvette" serum collection tubes (Sarstedt, Newton, USA). Collected whole blood clotted at RT for 1 hr, then centrifuged at 10,000 × g for 5 minutes. Serum was collected from the supernatant (~10 µL) and frozen at -20°C. Pre-immune sera were collected immediately prior to administration of the primary dose. Sera were also collected 2 weeks following each dose.

For serum collection from terminal mice, blood was collected via cardiac puncture. Mice were placed under surgical plane anesthesia using Isoflurane and ~1 mL blood was collected directly from the cardiac muscle using a 23 g needle and 3 mL syringe. Mice were then euthanized via cervical dislocation. Serum (~500 µL) was isolated from whole blood by centrifugation at 10,000 x g for 5 minutes and stored at -20°C.

2.4.6 Mouse Immunizations

Mice were vaccinated via intraperitoneal injection every two weeks beginning at 50-70 days old. Each animal received 100 µg antigen in 100 µL total volume. Mice were given a primary dose followed by three subsequent boosts at two-week intervals. Continuously boosted mice received additional boosts every 14 weeks to a total of 6 boosts.

Buffer-exchanged antigen (section 2.3.1) was sonicated for 10 seconds (section 2.3.2) and combined with selected adjuvant (section 2.3.3). ~50 µL of blood was collected from the lateral tail vein every two weeks prior to vaccine administration. Whole blood was centrifuged at 10,000 x g for 5 minutes and the serum (supernatant) was collected and stored at -20°C. For mice which received FA, FCA was used for the primary dose and FIA was used for the subsequent boosts

2.4.7 Tissue Collection and Fixation

Following euthanasia, whole brain was collected from each mouse. Each brain was separated at the midsagittal plane. One half of each brain was stored at -20°C for brain homogenate preparation and the other was fixed in 10% neutral buffered formalin (NBF) for histopathology.

Approximately 1 cm of sciatic nerve collected from the hind limb of each euthanized mouse, placed on cardstock paper, and fixed in a solution of 5% glutaraldehyde, 1% paraformaldehyde, and 74 mM phosphate buffer.

2.4.8 Brain homogenate preparation

10% mouse brain homogenate was prepared with radioimmunoprecipitation assay (RIPA) lysis buffer (Tris-HCl pH 7.4, 150 mM NaCl, 1% Nonidet P-40, 0.25% deoxycholic acid (DOC), 1 mM EDTA) with EDTA-free protease inhibitor cocktail to 10% weight/volume (w/v). Manual homogenization of the brain-lysis buffer mixture was achieved by continuously drawing up and dispersing the mixture with an 18 g blunt fill needle and 5 mL syringe. Brain homogenates were then aliquoted and stored frozen at -80°C.

2.4.9 Spleen cell preparation and lymphocyte isolation

Mice were euthanized via cervical dislocation prior to obtaining whole spleen. The spleen was placed in 5 mL of serum free Dulbecco's Modified Eagle Medium (DMEM) and minced with a scalpel into 0.2 cm portions. The excised spleen was then transferred to a 50 mL conical tube by pressing through a 70 µm cell strainer. 15 mL of serum free DMEM was then added to the spleen cell preparation. The cells were then washed through the cell strainer with excess medium and centrifuged at 524 x g for 5 minutes at 4ºC and the

supernatant was discarded. The cell pellet was resuspended in 5 mL of serum free DMEM at 3-4 x 10^7 cells/mL.

Lymphocytes were isolated from the spleen cell suspension using Lympholyte-M cell separation media (Cedarlane). The spleen cell suspension (5 mL) was carefully layered onto 5 mL of Lympholyte-M in a 15 mL centrifuge tube and centrifuged at room temperature for at 1,250 x g for 20 minutes. Following centrifugation, the lymphocytes at the interface of the suspension were removed carefully with a Pasteur pipette and transferred to a new centrifuge tube. The isolated cells were then diluted with PBS and centrifuged at 800 x g for 10 mins. Cells were then washed 2-3 times with PBS. The final lymphocyte cell pellet was dissolved in 50-100 uL of RIPA cell lysis buffer.

2.5 Immunoassays

2.5.1 Indirect Enzyme-linked Immunosorbent Assay

The antibody titre of each mouse following each vaccination was analyzed by an indirect enzyme-linked immunosorbent assay (ELISA) for comparison to the pre-immune serum titre. Antigen was buffer exchanged and sonicated as described (Section 2.3.1. and 2.3.2 respectively) prior to dilution in 1X PBS to 5 µg/mL. All following incubation steps

were performed on a rotator at room temperature. A 96 well, flat bottom, high binding "UltraCruz" strip plate (Santa Cruz Biotechnology, Santa Cruz, USA) was coated with 0.5 µg/well antigen and incubated overnight in a moisture chamber. Coated plates were blocked with 200 µL of 5% skim milk in TBS 0.1% Tween-20 (TBST) for 1 hour and then washed three times with 0.1% TBST with either a squirt bottle or plate washer (Bio-Rad Laboratories, Hercules, USA) and tapped firmly on benchtop to remove excess liquid. Anti-serum/1° antibody was serially diluted in 1X PBS (100 µL/well) and added before another 1-hour incubation, followed by three washes with 0.1% TBST. 2° goat anti-mouse HRP-conjugated antibody was added at 1:5000 in 5% skim milk TBS (100 µL/well), incubated for 30 minutes, and then washed five times with 0.1% TBST. 100 µL/well of 3,3',5,5'-tetramethylbenzidine (TMB) substrate (Surmodics, Eden Prairie, USA) was added and incubated for 30 minutes without the presence of light. 50 µL/well of 2 M sulphuric acid was added to stop the reaction followed immediately by absorbance measurement of all wells at 450 nm with a SpectraMax M5 spectrophotometer.

2.5.2 Bridge ELISA

Antibodies of each PIRIBS-immunized mouse were analyzed for recognition of PrP^{Sc} in infected brain homogenate by bridge ELISA. Antigen was sonicated for 10

seconds at minimum power and diluted in 1X PBS to 5 µg/mL. All following incubation steps were performed on a rotator at room temperature. A high binding 96-well microplate was coated with 0.5 µg/well antigen and incubated overnight at room temperature on a rotator. Coated plates were blocked with 200 µL of 5% skim milk in TBST (0.1% tween-20) for 1 hour and then washed three times with 0.1% TBST.

RML mouse brain homogenate was digested with 50 µg/mL proteinase K at 37ºC for 1 hour. The digestion reaction was stopped by addition of 5 mM PMSF and incubated for 1 hour at room temperature. The total protein concentration of brain homogenate was determined via BCA assay. All dilutions of brain homogenate and serum were done with 1X PBS. 50 µL of 1 µg/µL of either RML infected mouse brain homogenate or uninfected mouse brain homogenate was loaded into the antigen-coated and blocked 96-well microplate and incubated for 15 mins on a rotator at room temperature. 50 µL of post-immune antibody serum from immunized mice was added to the corresponding antigen-coated well containing either the RML infected mouse brain homogenate or uninfected mouse brain homogenate and incubated for 1 hour on a rotator at room temperature. Sera dilutions were titre-matched based on the ELISA results for each mouse. Sera was diluted to that which closely reached a titre of around 0.500-1.00 at OD_{450nm}.

The wells were then washed three times with 0.1% TBST. 2° goat anti-mouse HRP-conjugated antibody was added at 1:5000 in 5% skim milk TBS (100 µL/well), incubated for 30 minutes, and then washed five times with 0.1% TBST. 100 µL/well of TMB substrate was added and incubated for 30 minutes without the presence of light. 50 µL/well of 2 M sulphuric acid was added to stop the reaction followed immediately by absorbance measurement of all wells at 450 nm with an iMark microplate absorbance reader (Bio-Rad).

Data was analyzed by setting a cut-off value calculated as the sum of the average and standard deviation of the uninfected BH for each sample/animal tested in triplicate. The final value was obtained by subtracting the cut-off value from each of the experimental values.

2.5.3 Protein Immunoblotting

The Pierce™ BCA Protein Assay Kit (Thermo Scientific™) was used to determine the protein concentration of lymphocyte cell lysate. The lysate was then diluted to 2 mg/mL and 10 µg of each sample were combined with NuPAGE™ LDS Sample Buffer (4X) (Invitrogen) with 5% beta-mercaptoethanol (BME) and boiled at 70ºC for 10

minutes before being loaded into a 12% Bis-Tris gel (Invitrogen). Samples and Precision Plus Protein™ Dual Xtra prestained protein standards (Bio-Rad) were electrophoresed for 10 minutes at 100 V followed by 130 V for 90 minutes.

Protein from the gel was then transferred to a polyvinylidene difluoride (PVDF) membrane using a semi-dry transfer method. The PVDF membrane was activated with methanol for 1 minute and then rinsed with transfer buffer (25 mM Tris, 192 mM glycine, 20% methanol, pH 8.3) before layering the transfer stack. The protein was transferred for 60 minutes at 40 V.

The protein transferred membrane was blocked for 1 hour at room temperature in 5% milk in TBS. The membrane was then incubated with 4 ug/mL rat anti-mouse cathepsin E monoclonal antibody (R&D Systems, MAB1130) in milk for 1 hour at room temperature. Following primary antibody incubation, the membrane was washed 3 x 5 minutes in 0.1% TBST. The membrane was then incubated with HRP-conjugated rabbit anti-rat IgG (H+L) secondary antibody (R&D Systems, 61-9520) and then washed 3 x 5 minutes in 0.1% TBST.

The signal was developed by incubating the membrane in Pierce™ ECL western blotting substrate (32106) solution for 1 minute. The image was then captured by exposure in an x-ray film cassette for 5 minutes.

2.6 Digestion Analysis

2.6.1 SDS-PAGE

Cathepsin E digestion of 14R1 and HET-2s were compared using SDS-PAGE. 60 µg of either 14R1 or HET-2s was combined with recombinant human cathepsin E protein (rhCathepsin, R&D Systems, 1294-AS) in assay buffer (0.1 M NaOAc, 0.5 M NaCl, pH 3.5). rhCathepsin E was diluted to 1.0 µg/mL in assay buffer and incubated at room temperature for 30 minutes to allow full activation. rhcathepsin E was then further diluted to 0.2 µg/µL in assay buffer. 60 µg of either 14R1 or HET-2s was added to 60 µL of assay buffer and sonicated for 10 seconds. 20 µL was removed from each sample for a control prior to addition of 1 ng in 1 µL of rhcathepsin E to each sample for a final protease:protein ratio of 1:40 000. Samples were then incubated in a 37°C water bath. At each timepoint (one hour and overnight), 20 µL was removed from each reaction and added to labelled tubes containing 4X LDS sample buffer with 5% BME and heated at

70ºC for 10 minutes. 20 µL (7 µg protein/well) of each sample was then electrophoresed as described (section 2.2.1).

2.7 PIRIBS Vaccine Candidates

2.7.1 Plasmid Design

PIRIBS protein vaccine candidates were designed by replacing surface amino acids of HET-s with those on the surface of 263K- and RML-derived PrP^{Sc} (Kraus et al., 2021; Manka et al., 2022).

Nucleotide sequences were based on *E. coli* codon optimized version of the prion forming domain of the fungal prion protein HET-s (Maddelein et al., 2002), spanning residues 218-289 (Balguerie et al., 2003). Synthetic plasmid dsDNA containing the replaced codons for each PIRIBS vaccine candidate and a 6 × histidine-tag (6×His-tag) were ordered commercially (IDT, Coralville, USA). Plasmid DNA was resuspended according to manufacturer details prior to storage at -20ºC.

2.8 Statistics

The percent healthy and survival data for mouse immunization trials were plotted in Kaplan-Meier curves. Unpaired t-tests were performed to analyze significance. P-values of < 0.05 were considered significant.

3 Optimization of a 4-rung β-solenoid prion vaccine in P101L mice

3.1 Preparation and quality control of vaccine antigen

14R1 was expressed and purified as described (section 2.1). Following fibrilization, 14R1 was subjected to quality control measures to ensure sufficient purity and fibril formation. SDS-PAGE of the protein purification (figure 3.1) showed a single band at ~18 kDa in the eluted pure sample lane which matches the band present in the 14R1 control lane previously purified by Andrew Fang. The lanes which contain the flow through and washes, show that impurities were removed throughout the purification process.

Negative stain electron microscopy was used to visualize and confirm fibril formation of 14R1. TEM micrographs of 14R1 (figure 3.2) show long, bundled, and abundant fibril formation, typical of 14R1, at 19k magnification. 14R1 fibrils are similar in appearance to those of the vaccine scaffold, HET-2s (figure 3.3).

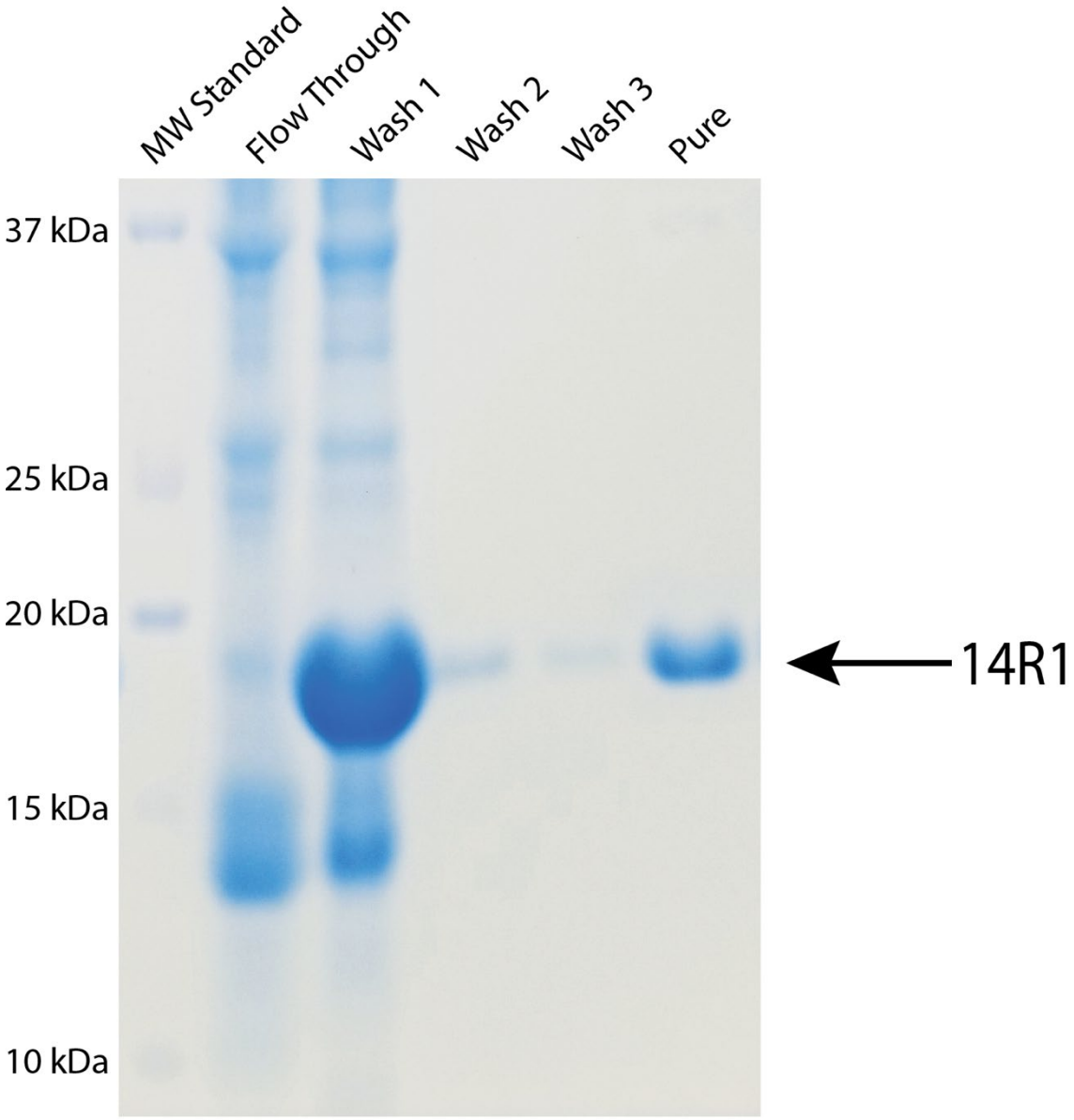

Figure 3.1: **SDS-PAGE of 14R1 purification.** A single band at ~17 kDa corresponds to 14R1 in the pure lane. Additional bands in the flow through and wash lanes show impurities removed during purification. Samples were separated by gel electrophoresis on a 12% Bis-Tris gel and stained with Coomassie Blue.

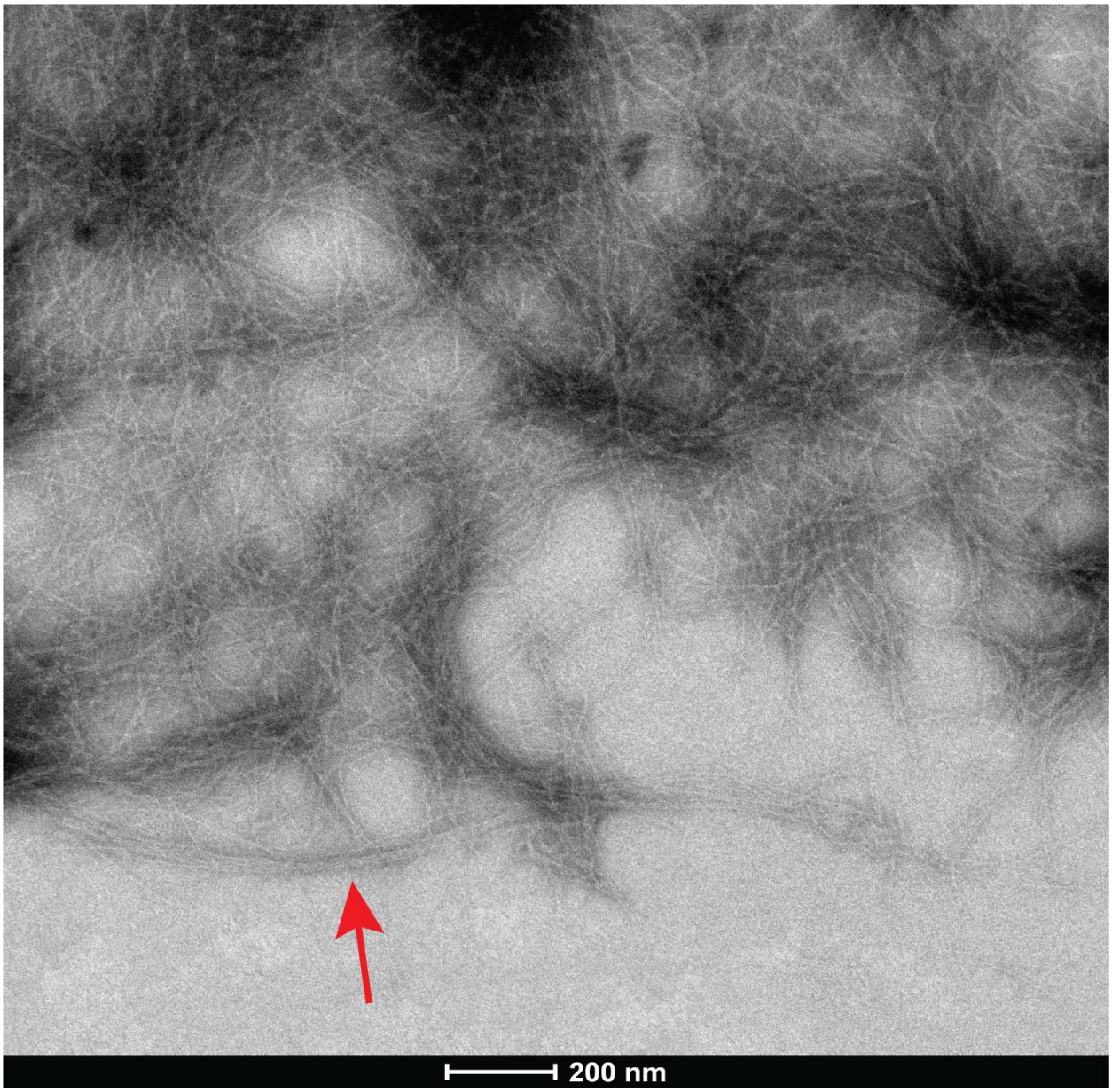

Figure 3.2: **TEM of 14R1 fibrils.** Purified 14R1 shows long bundled fibrils. Red arrow indicates typical bundled fibrils of 14R1. Fibrils were stained with 2% uranyl acetate and visualized at 19k magnification.

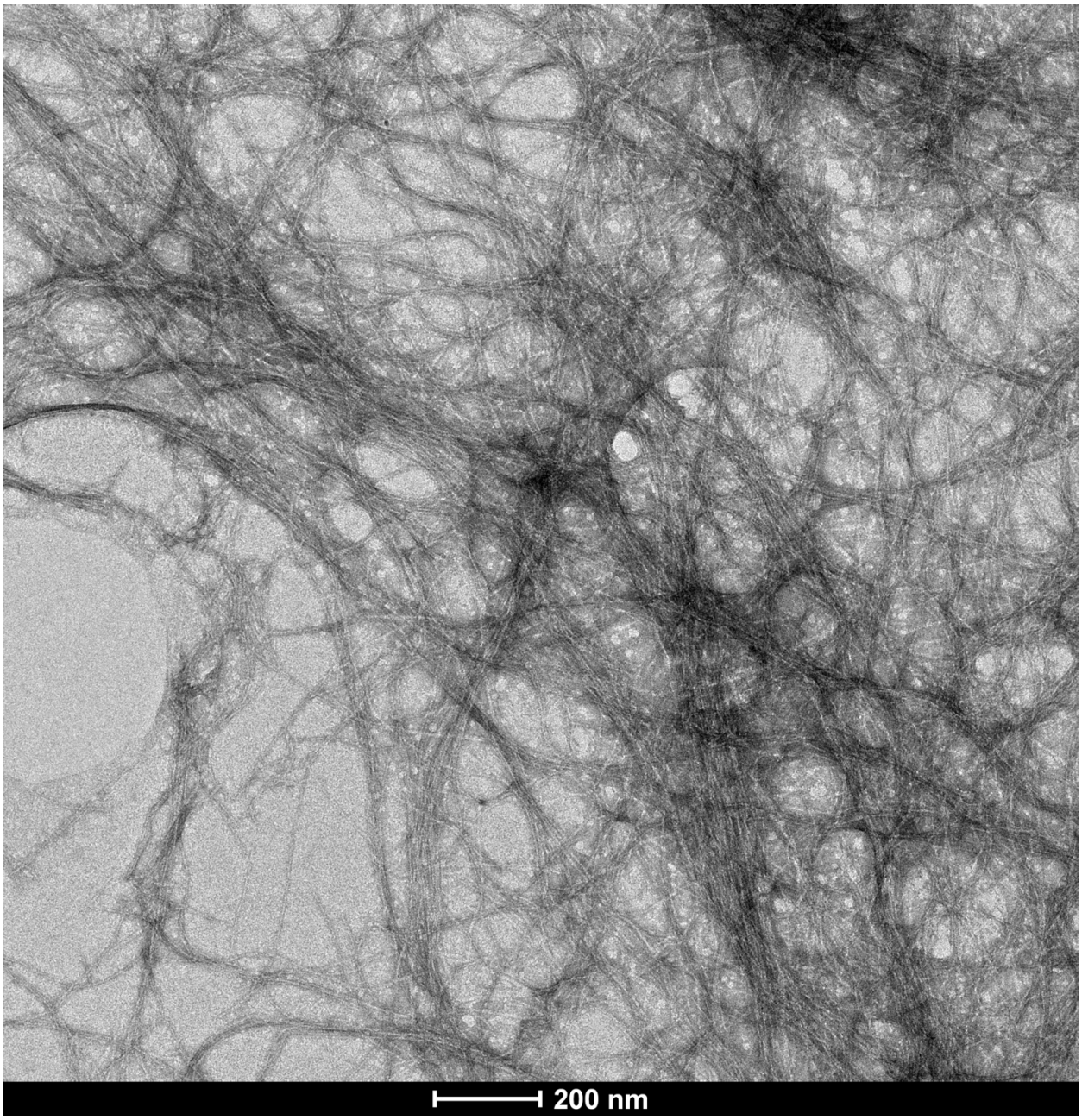

Figure 3.3: **TEM of HET-2s fibrils.** Purified HET-2s shows long bundled fibrils. Fibrils were stained with 2% uranyl acetate and visualized at 19k magnification. Image collected by Andrew Fang.

3.2 Comparison of immune response to vaccine with different adjuvants

TgP101L mice were initially immunized with 14R1 and Freund's complete adjuvant at around 8 weeks of age followed by three subsequent boosts at 2-week intervals with 14R1 and Freund's incomplete adjuvant (n=9). This antigen/adjuvant combination yielded a mean titre of 3.42 in the post-immune serum when diluted 3.33 x 10^5 fold (figure 3.4). Freund's adjuvant resulted in the fastest antibody production as evidenced by the titre reaching its maximum level following the first boost. Mice immunized with 14R1 and alum adjuvant (n=12) produced a mean titre of 3.44 in the post-immune serum (figure 3.4). Although alum proved to be slower at initiating an immune response than both Freund's and QS21, it reached the highest final titre. When immunized with 14R1 and QS21, the TgP101L mice produced a mean titre of 3.14 in the post-immune serum (n=9) (figure 3.4). Both QS21 and alum-immunized mice had a steadily increasing antibody production over the course of the three boosts. Mice immunized with only antigen and PBS (no adjuvant) (n=11) produced a mean antibody titre of 1.90 in the post-immune serum, much lower than the immune response produced with any of the three adjuvants (figure 3.4).

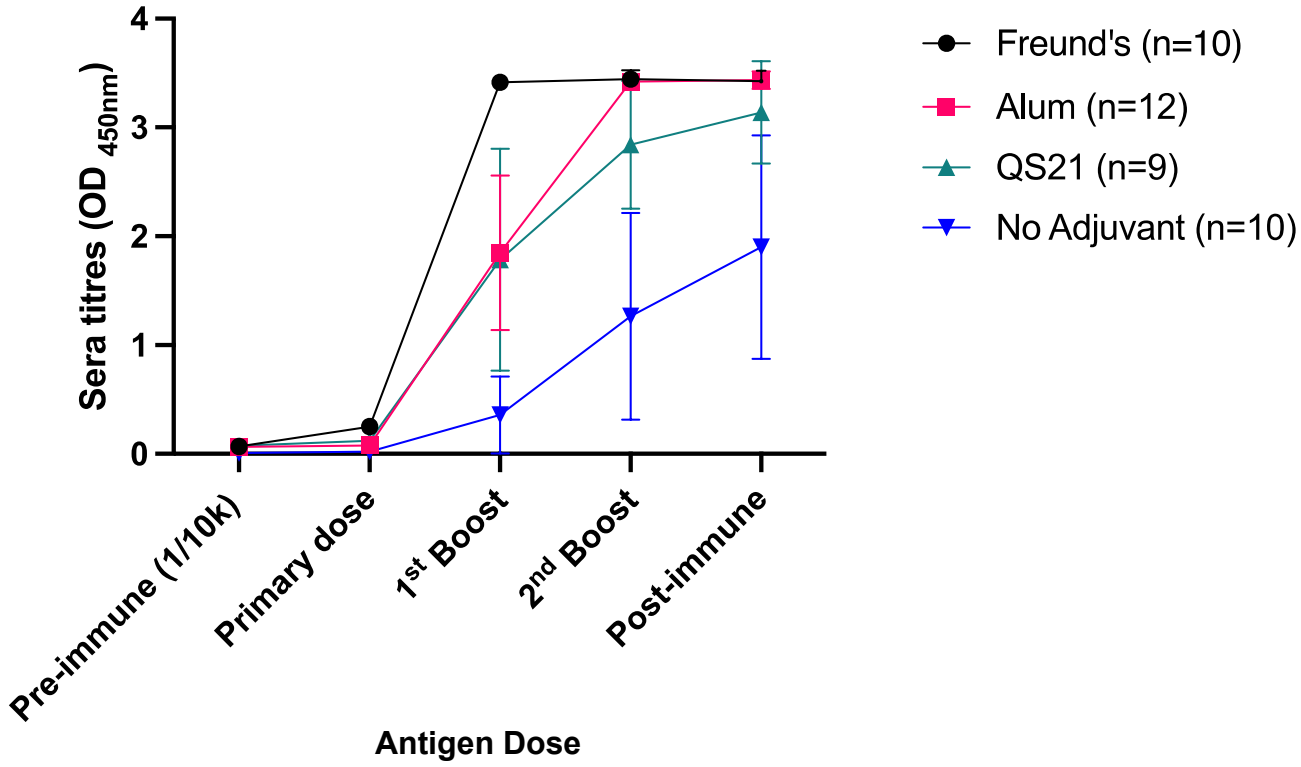

Figure 3.4: **Immune response of 14R1-immunized TgP101L mice.** Antibody titres of collected sera were determined via indirect ELISA by measurement of the OD at 450 nm. Mice immunized with adjuvant had a much higher immune response than those which received the antigen alone. Pre-immune serum has produced no immune response. The pre-immune titre was measured at a 1.00 x 10^4 fold dilution while the primary dose and subsequent boosts were measured at a 3.33 x 10^5 fold dilution.

3.3 Comparison of vaccine efficacy with different adjuvants

The Kaplan-Meier curve in figure 3.5 illustrates the efficacy of the vaccine to delay symptom onset with various adjuvants. Non-immunized TgP101L mice display prion disease symptoms including hind limb ataxia, circling, hunched posture, and tail rigidity at approximately 177 ± 17 days (n=12). It has been shown by Andrew Fang that mice immunized with the scaffold antigen, HET-2s, and Freund's adjuvant have a symptom onset of 161 ± 26 days (n=13) and that those immunized with 14R1 and Freund's adjuvant have a significantly delayed symptom onset of 444 ± 41 days (n=10).

TgP101L mice which receive 14R1 without adjuvant become symptomatic at 412 ± 88 days (n=10) whereas mice immunized with 14R1 and QS21 have a symptom onset of 479 ± 58 days (n=9). Mice immunized with 14R1 and alum adjuvant had the longest delay in disease onset with mice becoming symptomatic at 506 ± 52 days (n=12). 14R1 and alum-immunized mice had a significantly increased delay in symptom onset compared to 14R1 and Freund's-immunized mice (p-value = 0.009). Immunization with 14R1, regardless of adjuvant, results in a significant delay in the onset of prion disease symptoms compared to non-immunized TgP101L mice ($p<0.0001$).

The Kaplan-Meier survival curve in figure 3.6 illustrates the survival of each experimental and control group of TgP101L mice. Unimmunized mice survive to an average of 200 ± 22 days (n=12). Although immunization with the scaffold is not sufficient to delay symptom onset, HET-2s-immunized mice have a varied yet significant increase in survival (379 ± 148 days) compared to non-immunized controls (p-value = 0.0004). All 14R1-immunized mice, regardless of adjuvant, have a significantly increased survival time compared to unimmunized controls ($p<0.0001$). Mice immunized with 14R1 without adjuvant have a mean survival of 439 ± 29 days. Addition of adjuvants Freund's, QS21, and alum increase survival times to 460 ± 50 days, 512 ± 69 days, and 527 ± 48 days respectively compared to non-immunized controls. In this trial, addition of alum significantly improves the age of survival compared to those which receive the vaccine alone (p-value = 0.02).

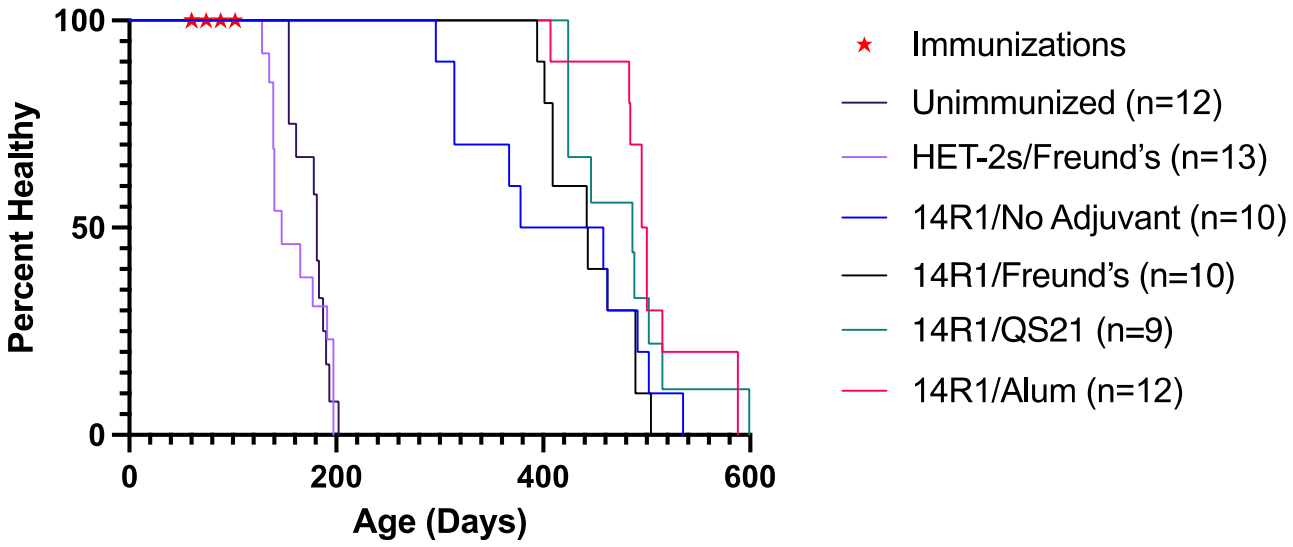

Experimental Group	Symptom Onset (Days)	P-value compared to Unimmunized
Unimmunized	177 ± 17 days	NA
HET-2s/Freund's	161 ± 26 days	0.0844
14R1/No Adjuvant	412 ± 88 days	<0.0001
14R1/Freund's	444 ± 51 days	0.009
14R1/QS21	479 ± 56 days	<0.0001
14R1/Alum	506 ± 52 days	<0.0001

Figure 3.5: **Health status of TgP101L mice.** A Kaplan-Meier curve showing the percentage of healthy mice over time. Unimmunized (dark purple) and HET-2s-immunized (light purple) mice have a similar mean age of onset. Mice receiving 14R1 with either no adjuvant (blue), Freund's (black), QS21 (teal), or alum (magenta) adjuvant have a significantly delayed symptom onset. Red stars indicate immunization time points.

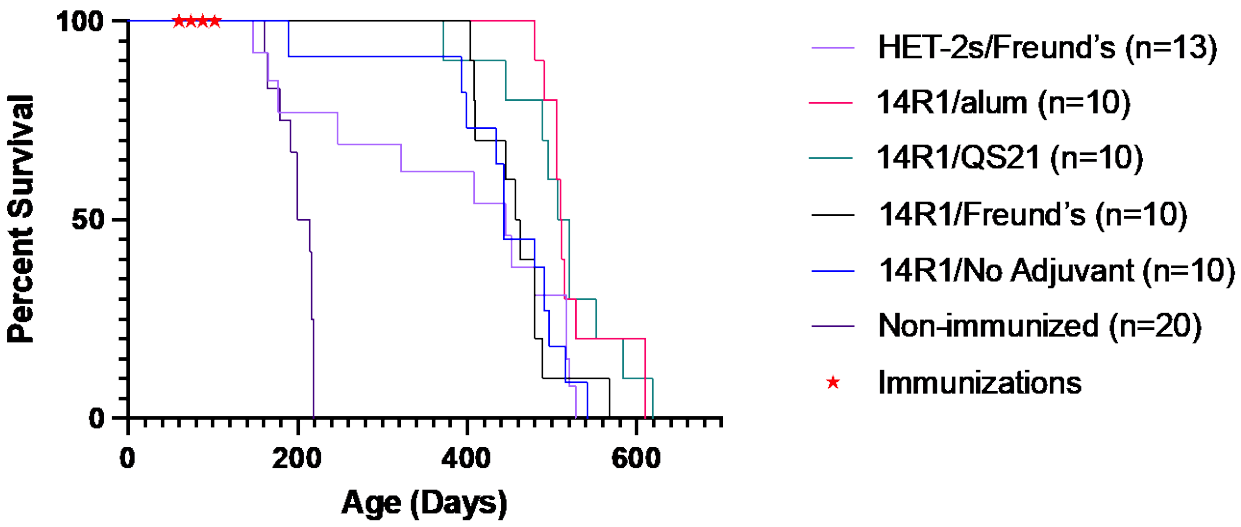

Experimental Group	Survival (Days)	P-value compared to Unimmunized
Unimmunized	200 ± 22 days	NA
HET-2s/Freund's	379 ± 148 days	0.0004
14R1/No Adjuvant	439 ± 29 days	<0.0001
14R1/Freund's	460 ± 50 days	<0.0001
14R1/QS21	512 ± 69 days	<0.0001
14R1/Alum	527 ± 46 days	<0.0001

Figure 3.6: **Survival status of TgP101L mice.** A Kaplan-Meier curve showing the survival percentage of mice over time. Unimmunized mice (dark purple) have a lower survival rate than any of the experimental groups. All immunized mice, including HET-2s (light purple) have a significantly increased survival time with 14R1/alum-immunized mice (magenta) having the greatest increase. Red stars indicate immunization time points.

3.4 Continuous boosts of 14R1 in P101L mice

Although 14R1 immunization greatly delays symptom onset and increases survival, all mice eventually succumb to prion disease. From previous work in the lab, it was known that the antibody titre falls as the mice age. Therefore, in an attempt to further increase the preclinical phase in TgP101L mice and maintain the antibody titre, I administered additional boosts of 14R1 and alum.

Figure 3.7 shows the antibody titre of continuously boosted TgP101L mice. All titres (except the pre-immune) are shown at a 1.37 x 10^7 fold dilution. Following regular prime-boost schedule of 14R1 and alum, TgP101L mice reached a maximum antibody titre of 0.19 in the 3rd boost serum (n=7). Serum collected 14 weeks following the 3rd boost had a significantly decreased antibody titre of 0.08 (p-value = 0.0008). By administering a 4th boost at 14 weeks post 3rd boost, the titre was able to increase slightly to 0.10. After 14 weeks, the titre fell again to 0.08. However, with an additional boost of 14R1, the antibody titre rose significantly to 0.14 (p-value = 0.03). 14 weeks following the 5th boost, the titre fell to its lowest at 0.04. After receiving a 6th and final boost, the antibody titre increased slightly to 0.06. Mice that remained alive 14 weeks following the 6th boost (n=4) had an antibody titre of 0.05.

Upon analysis of the health curve of the continuously boosted TgP101L mice (figure 3.8), the titre increase does not seem to result in a further delay of symptom onset. With an average symptom onset of 421 ± 110 days (n=10), the continuously boosted mice maintain a significant delay of prion disease compared to non-immunized ($p<0.0001$), but have a reduced delay compared to mice receiving the normal prime-boost schedule (p-value = 0.04). As indicated by the red stars, only 50% of the mice remained healthy at the time of the 5^{th} boost.

The Kaplan-Meier curve in figure 3.9 illustrates the survival of the continuously boosted mice compared to those which receive the regular prime-boost schedule and the non-immunized controls. TgP101L mice which receive a continuous boosting of 14R1, and alum have a mean survival of 497 ± 129 days. Despite the broader range in survival of these mice, there remains a significant improvement over non-immunized mice (p-value = 0.0001) and a significantly worse survival than mice which receive the normal prime-boost scheduled immunizations (p-value = 0.04).

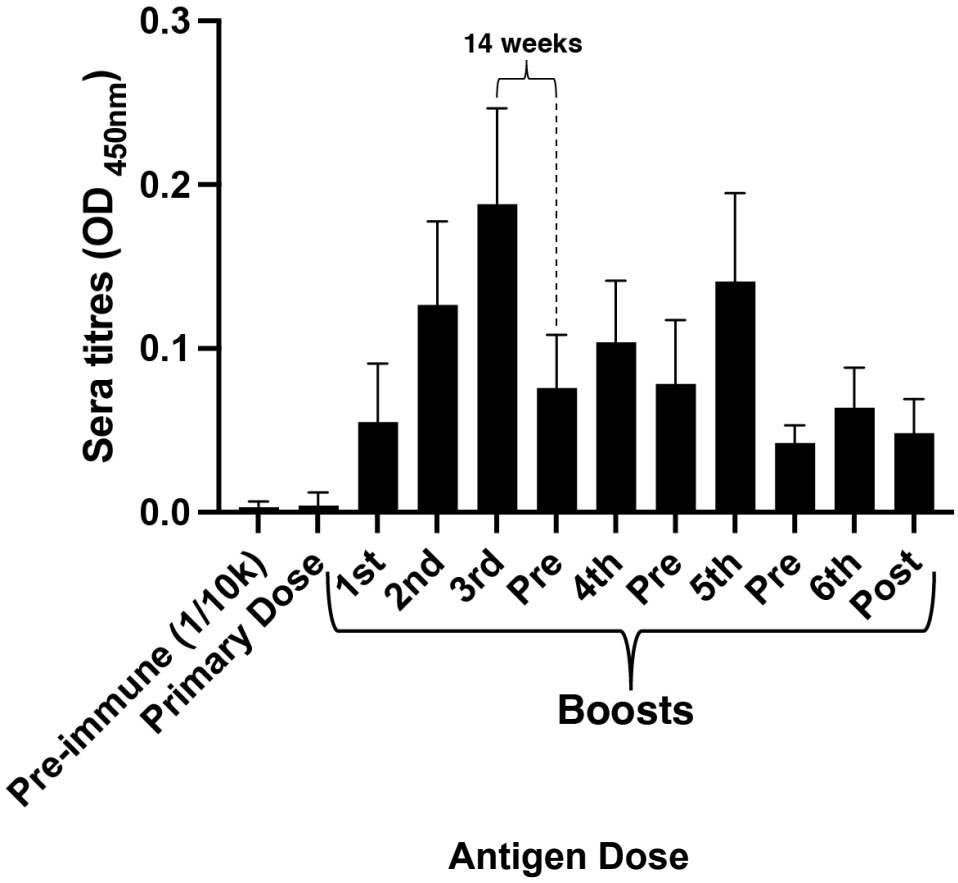

Figure 3.7: **Immune response of continuously boosted 14R1/alum-immunized TgP101L mice.** Antibody titres of collected sera were determined via indirect ELISA by measurement of the OD at 450 nm. Pre-immune serum produced no immune response. The antibody titre rises gradually from the primary dose to a maximum by the third boost. 3rd, 4th, 5th, and 6th boosts and respective following "Pre" samples are measured from serum collected 14 weeks apart. 4th, 5th, and 6th boost samples are measured from serum collected 2 weeks following the preceding "Pre". "Post" sample was measured from serum collected 14 weeks following the 6th boost. The pre-immune titre was measured at a 1.00 x 10^4 fold dilution while the primary dose and subsequent boosts were measured at a 1.37 x 10^7 fold dilution.

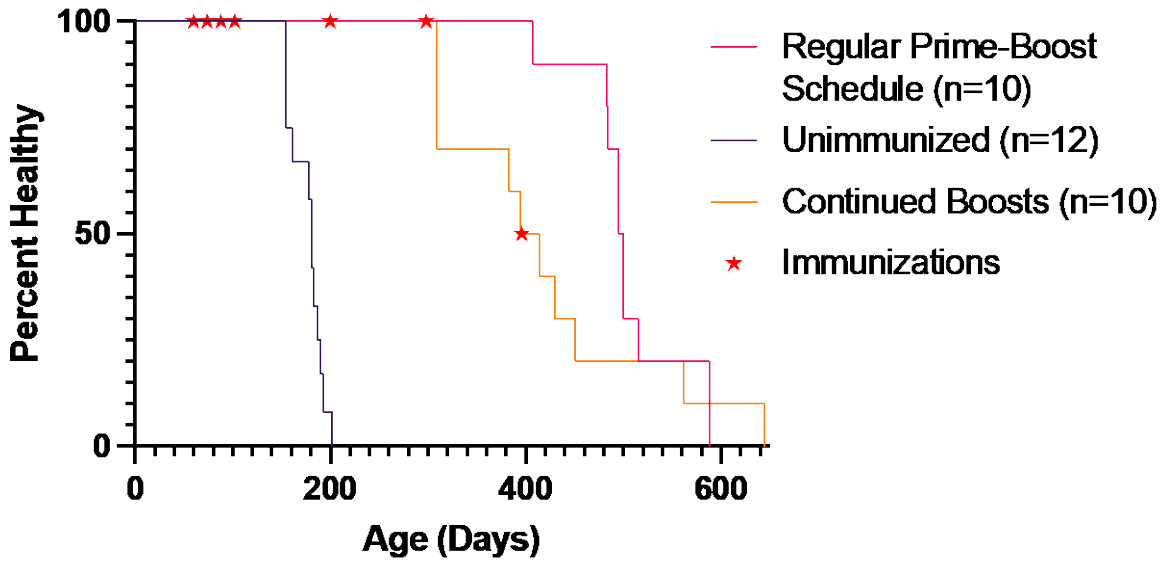

Experimental Group	Symptom Onset (Days)	P-value compared to Continued Boosts
Unimmunized	177 ± 17 days	<0.0001
Regular Prime-Boost Schedule	506 ± 52 days	NA
Continued Boosts	421 ± 110 days	0.0418

Figure 3.8: **Health status of continuously boosted 14R1/alum-immunized TgP101L mice.** A Kaplan-Meier curve showing the percentage of healthy mice over time. Regular prime-boost schedule (magenta) refers to mice which received a primary dose and three consecutive boosts at 2-week intervals. Continued boosts (orange) refers to mice which received the regular prime-boost schedule followed by an additional three boosts at 14-week intervals. Mice continuously boosted with 14R1 and alum had an earlier symptom onset than mice which received the regular prime-boost schedule but a delayed symptom onset compared to unimmunized mice (dark purple). Red stars indicate immunization time points.

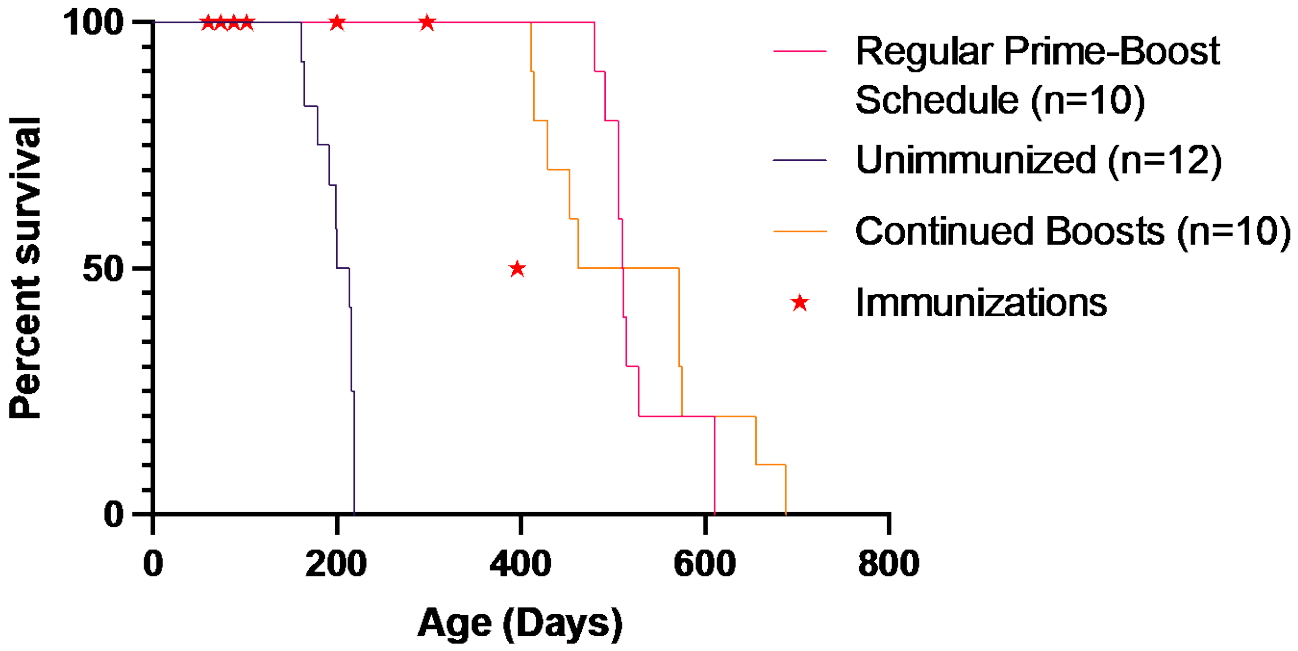

Experimental Group	Survival (Days)	P-value compared to Continued Boosts
Unimmunized	200 ± 22 days	0.0001
Regular Prime-Boost Schedule	527 ± 46 days	0.04
Continued Boosts	497 ± 129 days	NA

Figure 3.9: **Survival status of continuously boosted 14R1/alum-immunized TgP101L mice.** A Kaplan-Meier curve showing the survival percentage of mice over time. Regular prime-boost schedule (magenta) refers to mice which received a primary dose and three consecutive boosts at 2-week intervals. Continued boosts (orange) refers to mice which received the regular prime-boost schedule followed by an additional three boosts at 14-week intervals. Mice continuously boosted with 14R1 and alum had a similar survival time as mice which received the regular prime-boost schedule. Red stars indicate immunization time points

4 Analyzing the safety and efficacy of a 4-rung β-solenoid prion vaccine in TgFFI mice

4.1 Immune response to prion vaccine

TgFFI mice were immunized with 14R1 and Freund's adjuvant at around 8 weeks of age followed by three subsequent boosts at 2-week intervals (n=10). This antigen/adjuvant combination yielded a mean titre of 1.79 in the post-immune serum when diluted 1.00 x 10^4 fold (figure 4.1). A significant antibody titre compared to the pre-immune serum was detected up to a 1.23 x 10^6 fold dilution with a mean titre of 0.047 (p-value = 0.01). However, TgFFI mice immunized with HET-2s and Freund's adjuvant had a much lower antibody titre with a mean of 0.103 in the post-immune serum when diluted 1.00 x 10^4 fold (Figure 4.1). This titre is significant compared the pre-immune serum at the same dilution (p-value = 0.03).

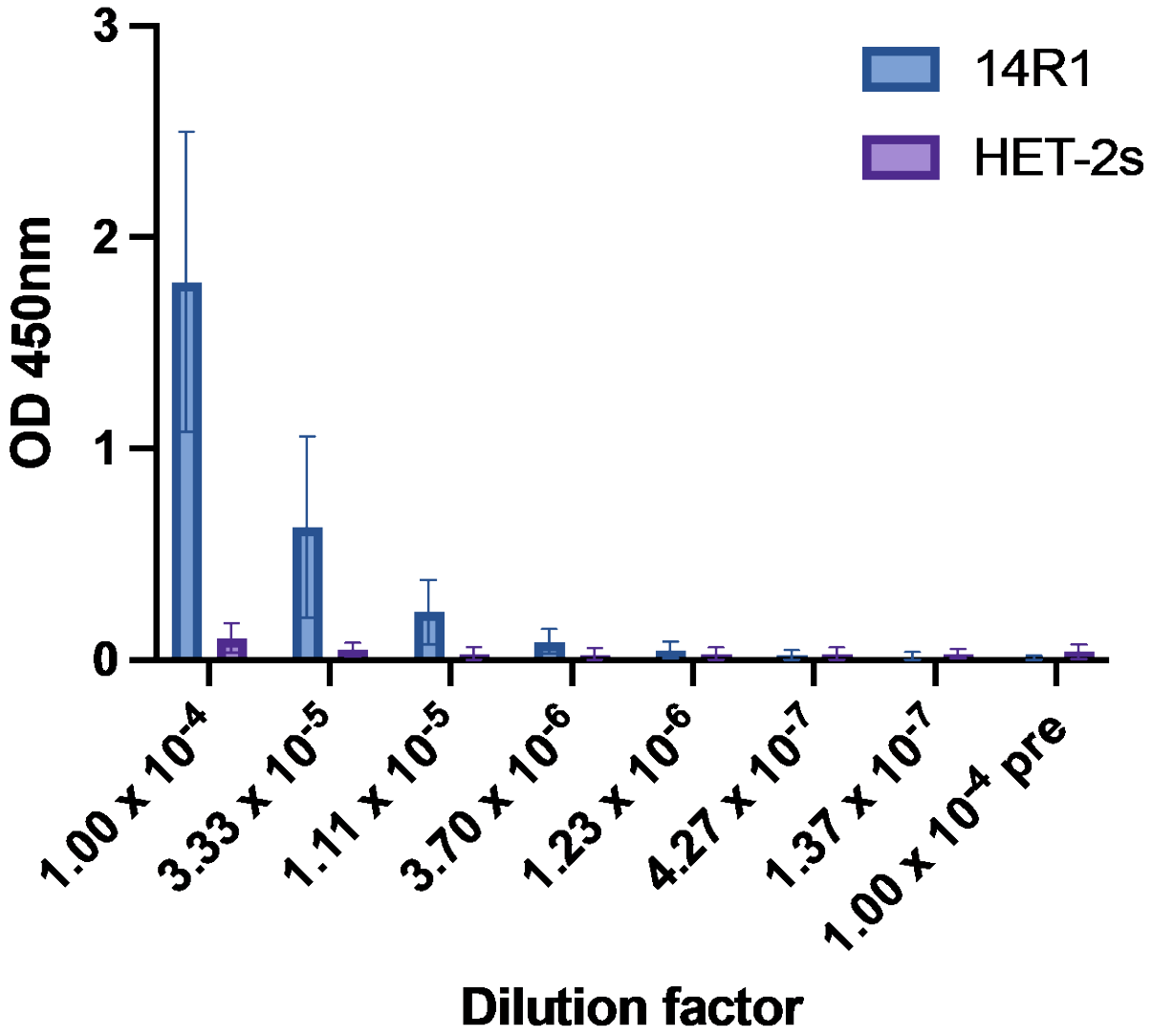

Figure 4.1: **Immune response of vaccine and scaffold immunization in TgFFI mice following prime-boost schedule.** Antibody titres of collected sera following the third and final boost of 14R1 and FA were determined via indirect ELISA by measurement of the OD at 450 nm. The pre-immune titre was measured at a 1.00 x 10^4 fold dilution while the post-immune serum was serial diluted from 1.00 x 10^4 to 1.37 x 10^7 fold.

4.2 Efficacy of 14R1 immunization in TgFFI mice

Following immunization, motor coordination of transgenic and wildtype mice was compared with by analyzing performance on a rotarod. Mice were placed on a rotating rod and time (seconds) they were able to hang on was measured. Non-transgenic mice have a decreased latency to fall with age compared to TgFFI mice. However, 14R1-immunized TgFFI (n=5) had a decreased latency to fall as they aged compared to HET-2s-immunized mice (n=5) (p-value = 0.05) (figure 4.2). 14R1-immunized TgFFI mice did not have a significantly different latency to fall compared to 14R1-immunized non-Tg mice (p-value = 0.3). These results suggest that vaccine immunization is sufficient to prevent loss of motor coordination in TgFFI mice.

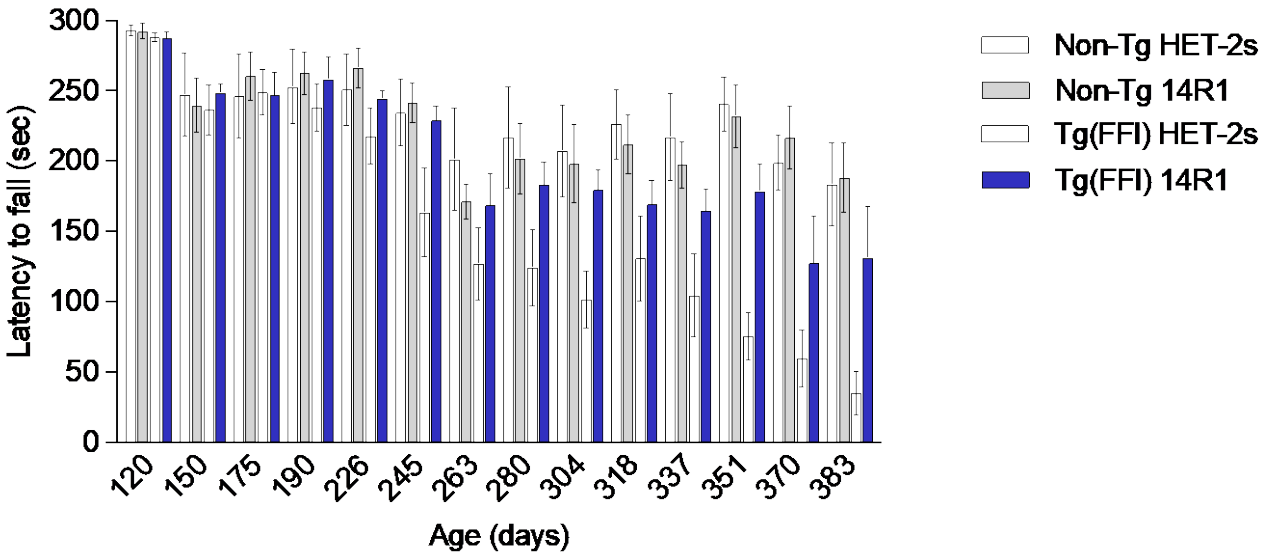

Figure 4.2: **Latency to fall from a rotarod for immunized TgFFI mice**. Latency to fall (seconds) was measured using a rotarod beginning at 120 days-old and continued every 2-4 weeks until 383 days-old. Transgenic FFI mice immunized with 14R1 and FA have a decreased latency to fall compared to HET-2s-immunized mice (p-value = 0.05).

5 Optimization of a 4-rung β-solenoid prion vaccine in E199K mice

5.1 Immune response to prion vaccine with alum adjuvant

TgMHu2ME199K mice were immunized with 14R1 and alum adjuvant at around 8 weeks of age followed by three subsequent boosts at 2-week intervals (n=12). This antigen/adjuvant combination yielded a mean titre of 1.23 in the post-immune serum when diluted 1.00 x 10^4 fold (figure 5.1). A significant antibody titre compared to the pre-immune serum was detected up to a 1.23 x 10^6 fold dilution with a mean titre of 0.058 (p-value = 0.0006).

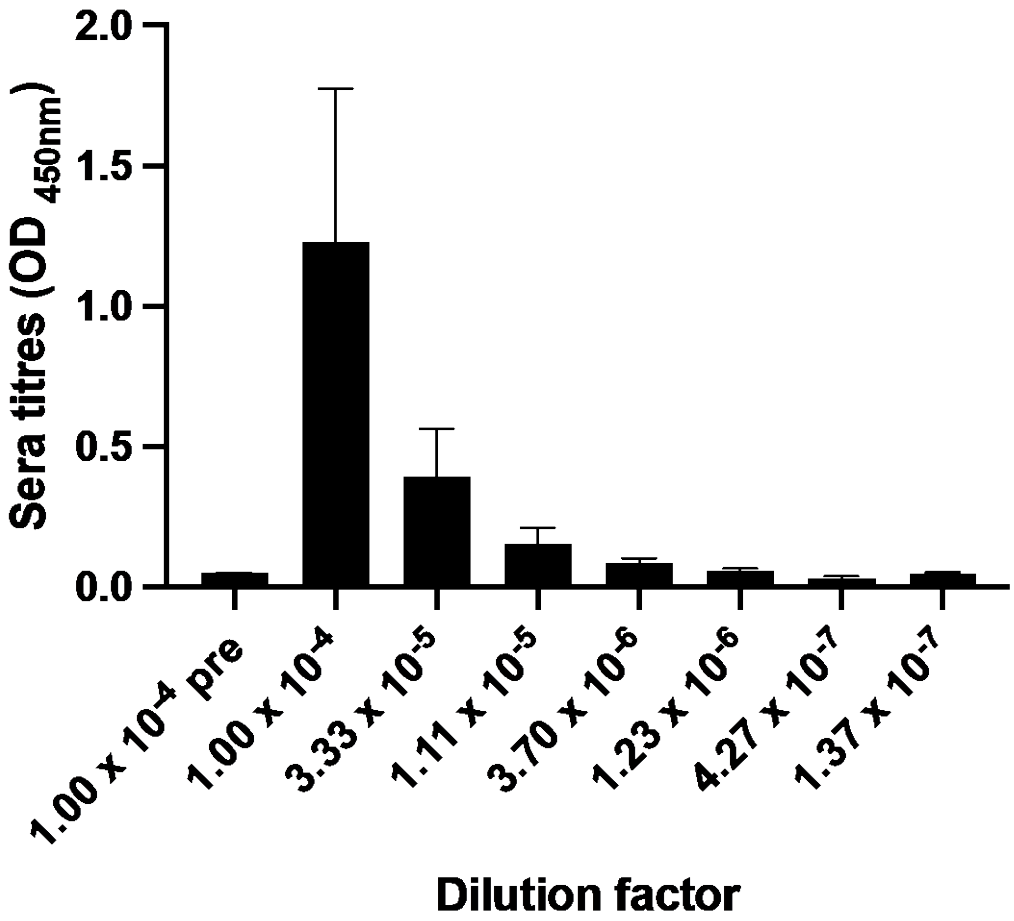

Figure 5.1: **Immune response of 14R1-immunized TgMHu2ME199K mice following prime-boost schedule.** Antibody titres of collected sera following the third and final boost of 14R1 and alum were determined via indirect ELISA by measurement of the OD at 450 nm. The pre-immune titre was measured at a 1.00 x 10^4 fold dilution while the post-immune serum was serial diluted from 1.00 x 10^4 to 1.37 x 10^7 fold.

5.2 Comparison of immune response to vaccine and scaffold between mouse lines

When human genetic prion disease mouse models were immunized with 14R1 and alum, TgP101L mice produced the largest antibody titre compared to TgMHu2ME199K and TgFFI (figure 5.2). The OD_{450nm} reading for the TgP101L mice reached the upper limit of detection at a 1 x 10^4 fold dilution with an average of 3.65 (n=7). The post-immune antibody titres for 14R1-immunized TgMHu2ME199K and TgFFI mice were similar with a mean OD_{450nm} of 1.24 (n=12) and 1.36 (n=5) at a 1.00 x 10^4 fold dilution, respectively (figure 5.2).

Mice immunized with the vaccine scaffold, HET-2s, had a large variation in immune response depending on the mouse background. TgP101L mice immunized with HET-2s and either alum or Freund's adjuvant produced a significant antibody titre which diluted out to 1.37 x 10^{-7} and 4.27 x 10^{-7}, respectively (figure 5.3). Conversely, TgFFI and TgMHu2ME199K mice produced nearly no immune response when immunized with HET-2s, regardless of co-immunization with either alum or Freund's adjuvant, even at a 1.00 x 10^4 fold dilution (figure 5.3). Figure 5.3 illustrates that mice on a C57BL/6J background (TgMHu2ME199K and TgFFI) produced almost no immune response to the vaccine

scaffold with either Freund's or alum adjuvant while mice on a FVB background (TgP101L) produced a significant immune response, regardless of adjuvant.

To further analyze the immune response to HET-2s in mice on a C57BL/6J background, a secondary antibody which detects IgM, rather than the IgG secondary antibody used in all other sera titre measurements, was used. HET-2s-immunized TgMHu2ME199K and TgFFI mice did not have a significantly higher IgM response than IgG (figure 5.4).

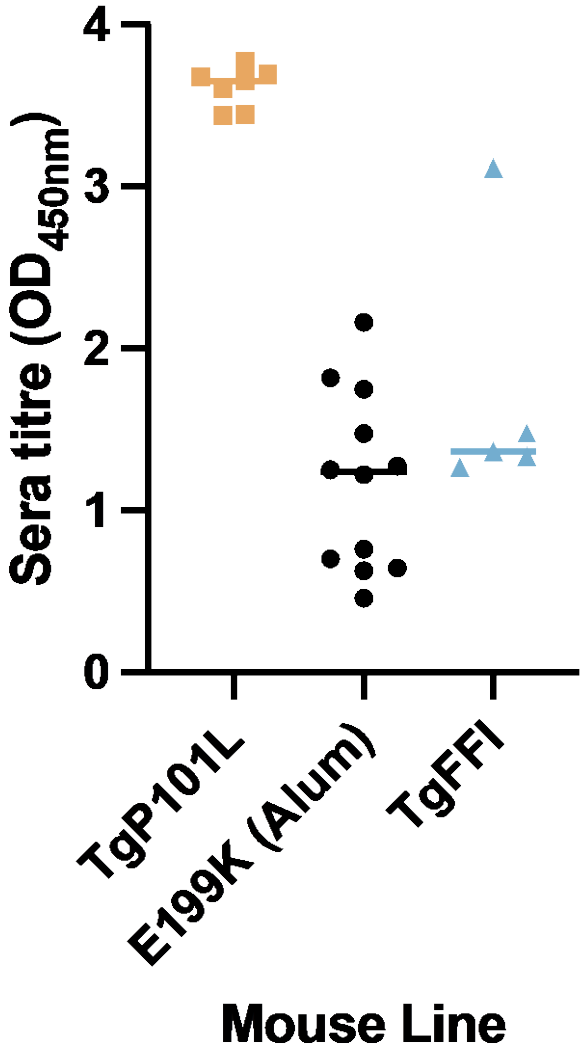

Figure 5.2: **Immune response to 14R1 in three different prion disease mouse models.** Antibody titres of collected post-immune sera were determined via indirect ELISA by measurement of the OD at 450 nm. E199K mice which received alum adjuvant (n=12) have a titre similar to that of the TgFFI mice which received Freund's adjuvant (n=5). Both E199K and TgFFI mice produce a lower antibody titre than that of the TgP101L mice which received alum adjuvant (n=7). All measurements were collected at a 1.00 x 10^4 fold dilution.

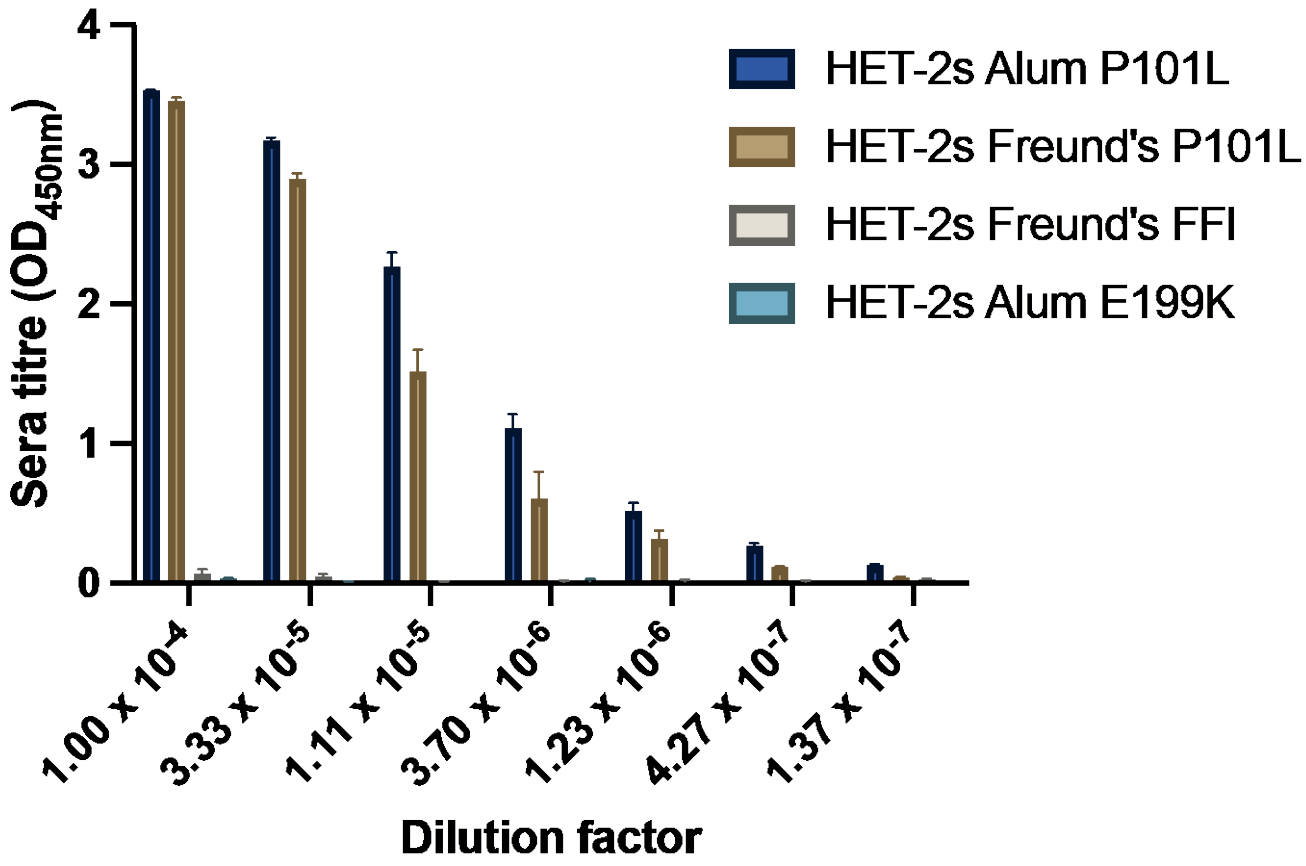

Figure 5.3: **Immune response to HET-2s in three different prion disease mouse models on different backgrounds with varying adjuvant.** Antibody titres of collected post-immune sera were determined via indirect ELISA by measurement of the OD at 450 nm. Mice on an FVB background (P101L), regardless of adjuvant, produce a large antibody titre to HET-2s whereas mice on a C57BL/6J background (E199K and FFI) produce nearly no immune response to HET-2s.

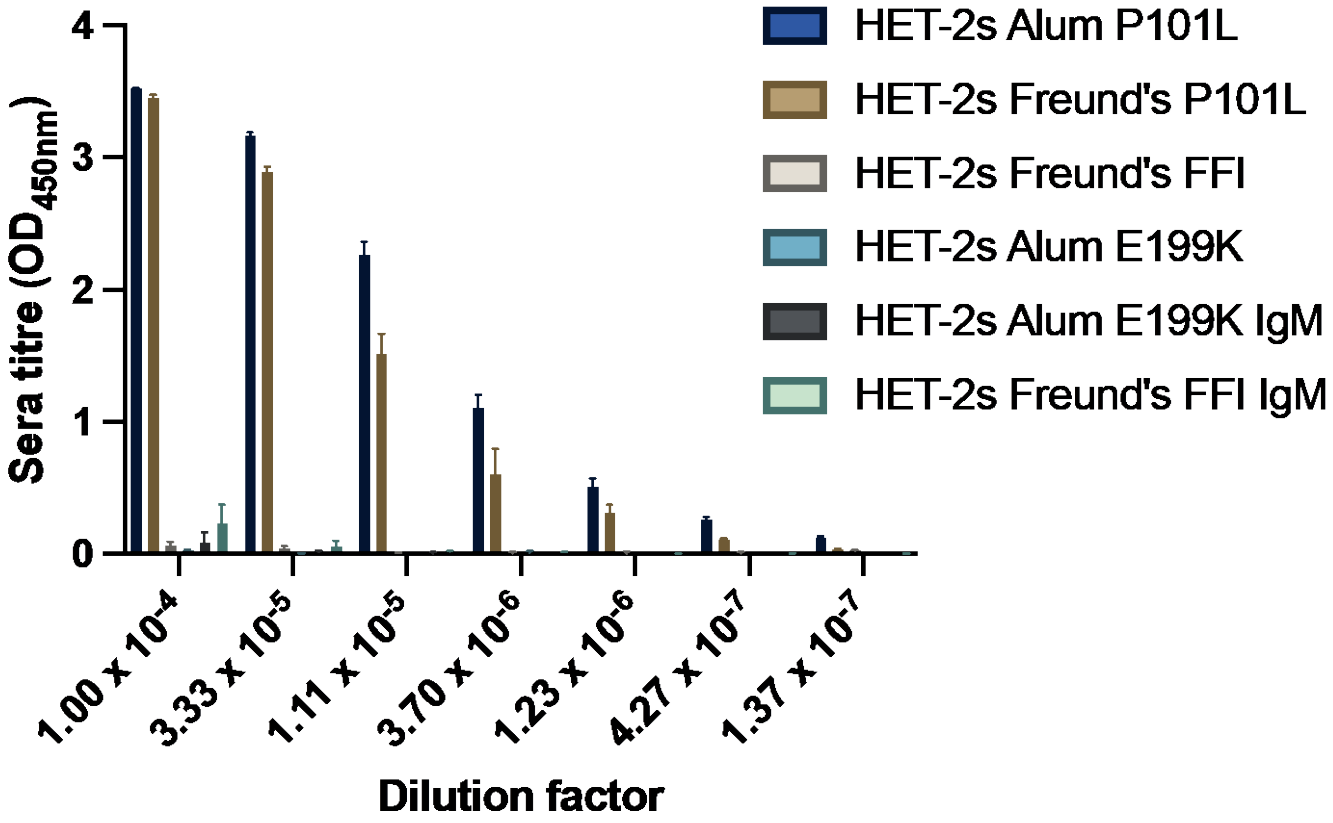

Figure 5.4: **Immune response to HET-2s in mouse models on a C57BL/6J background with varying adjuvant and antibody recognition.** Antibody titres of collected post-immune sera were determined via indirect ELISA by measurement of the OD at 450 nm. Mice on a C57BL/6J background produce almost no IgG immune response to HET-2s whereas mice on an FVB background produce a large IgG antibody titre. The immune response to HET-2s in mice on a C57BL/6J background (E199K and FFI) did not improve when measuring an IgM response compared to the usual IgG response.

5.3 Immune response to prion vaccine and scaffold with QS21 adjuvant

Following information that different mouse backgrounds have immunological biases which can affect immunopotentiation (Disis & Palucka, 2014; Schulte et al., 2008), I immunized TgMHu2ME199K mice with QS21 adjuvant and compared the results to immunization with alum. When co-immunized with antigen and QS21 adjuvant, TgMHu2ME199K mice produced a higher immune response than with alum adjuvant (figure 5.5). QS21 significantly improved the immune response over alum when co-immunized with 14R1 to the C57BL/6J mice (p-value = 0.03). As well, QS21 significantly improved the antibody titre of HET-2s-immunized mice compared to alum (p-value = 0.0001).

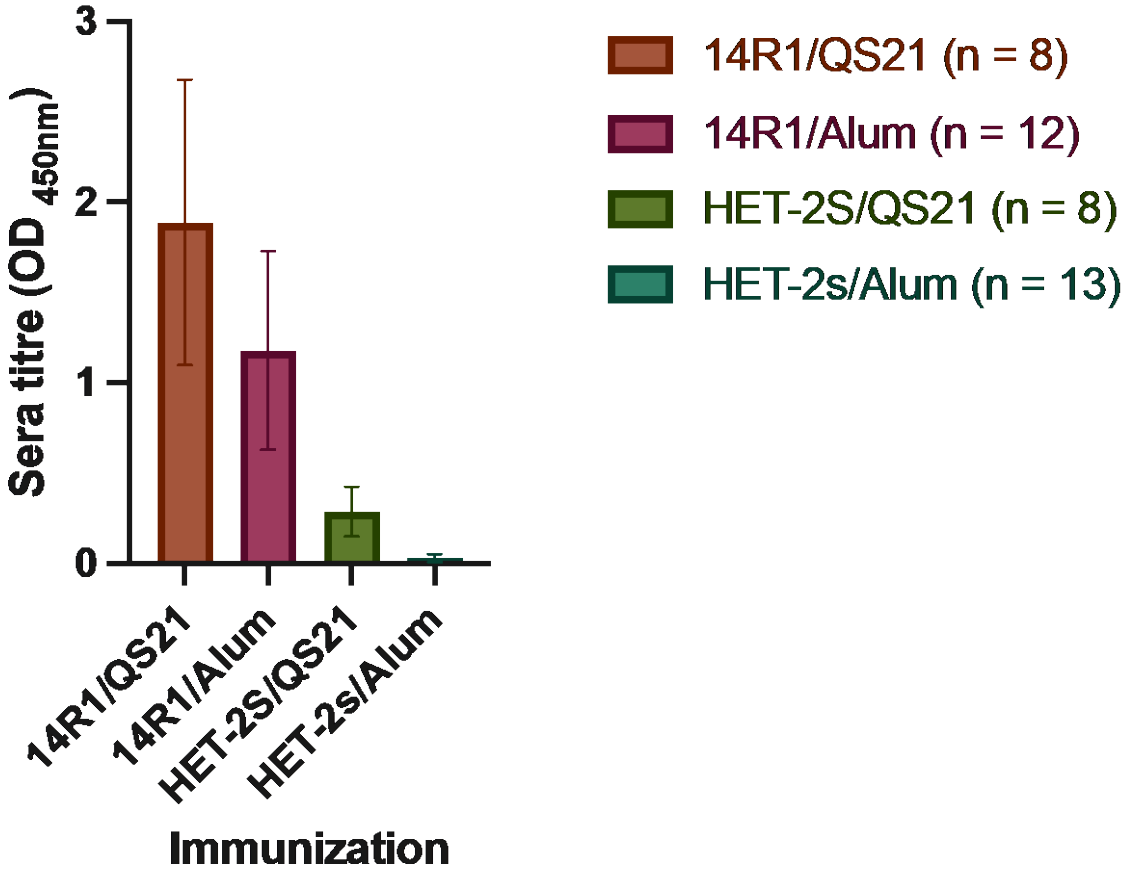

Figure 5.5: **Immune response to 14R1 and HET-2s with varying adjuvants in TgMHu2ME199K mice.** Antibody titres of collected post-immune serum were determined via indirect ELISA by measurement of the OD at 450 nm. QS21 produce a larger immune response than alum adjuvant when co-immunized with either 14R1 (p-value = 0.0284) or HET-2s (p-value = 0.0001).

5.4 Investigating the effect of cathepsin E deficiency on the immune response to vaccine and scaffold in C57BL/6J mice

When trying to understand the difference in immune response between mouse lines, I found that C57BL/6J mice have a tissue-specific deficiency in the antigen-processing aspartic protease, cathepsin E, which may prevent processing of 14R1 and HET-2s necessary to produce an immune response (Tulone et al., 2007). A western blot was used to confirm the cathepsin E deficiency in the lymphocytes of TgMHu2ME199K mice (figure 5.6). As predicted, the TgMHu2ME199K lymphocytes lacked the presence of a band at 42 kDa corresponding to cathepsin E, apart from A8804 in which the lymphocyte solution was contaminated with red blood cells. Red blood cells are not deficient in cathepsin E in the C57BL/6J mice. Importantly, the TgP101L mice had a distinct band corresponding to cathepsin E indicating a potential difference in antigen processing between the two mouse backgrounds.

Figure 5.7 shows that cathepsin E processes both the vaccine and scaffold antigens in a relatively similar manner. When comparing the digestion pattern of 14R1 to that of HET-2s by cathepsin E, there is no discernable difference between the two. 14R1 and HET-2s undergo minimal degradation in buffer conditions of low pH and high temperature

in the absence of cathepsin E (control). When exposed to cathepsin E for 1 hour, additional bands appear at lower MW compared to the undigested protein (~17 kDa). Following overnight digestion, both 14R1 and HET-2s have additional bands at lower MW, of which, three are most intense (~15, 13, and 9 kDa) in addition to a decreased signal in the band corresponding to undigested antigen. It appears that cathepsin E will digest both 14R1 and HET-2s at favourable processing conditions (pH 3.5, 37°C).

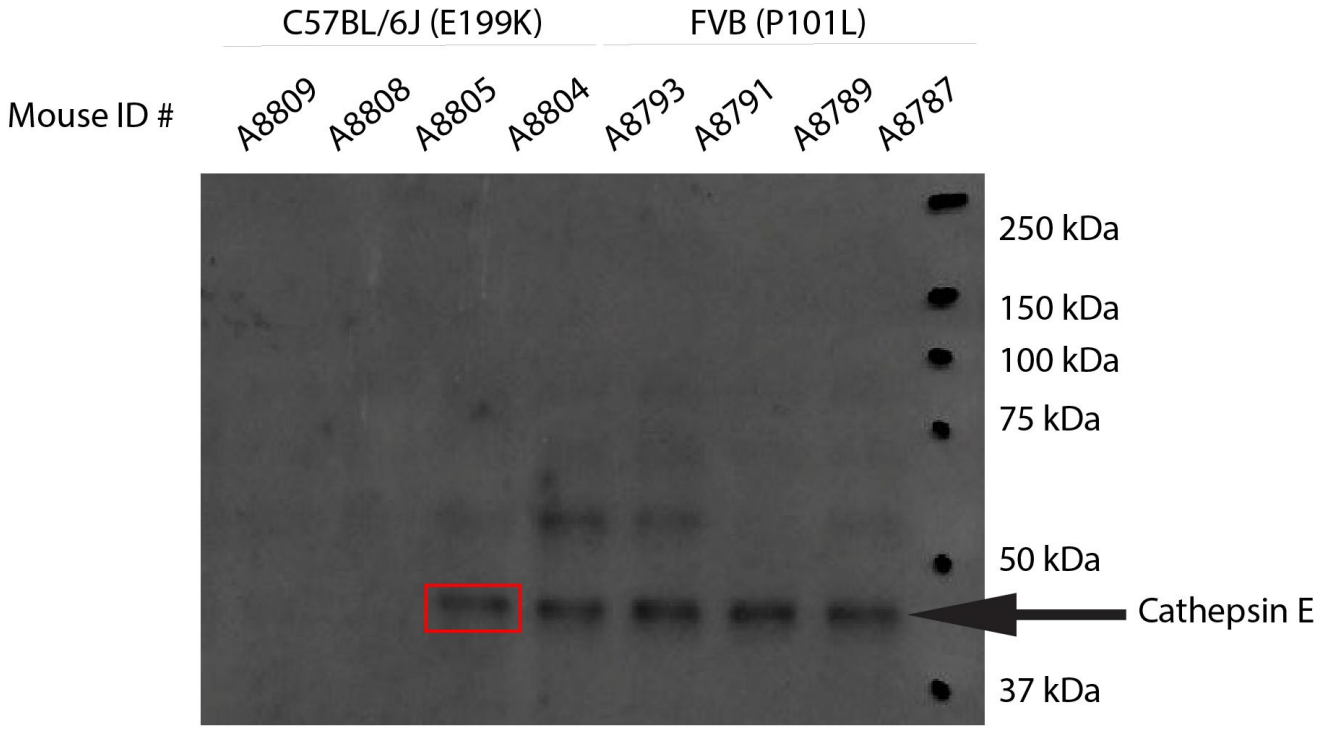

Figure 5.6: **Western blot to visualize presence of cathepsin E in FVB mice**. Cathepsin E present in FVB mice was detected with rat anti-mouse cathepsin E monoclonal antibody (R&D Systems, MAB1130). A single band at 42 kDa corresponds to cathepsin E in the lymphocytes of FVB mice. The band corresponding to cathepsin E in the E199K mouse, A8804, was due to contamination of the lymphocytes with red blood cells. The absence of a band at 42 kDa in the E199K mice supports the deficiency of cathepsin E in the lymphocytes of C57BL/6J mice.

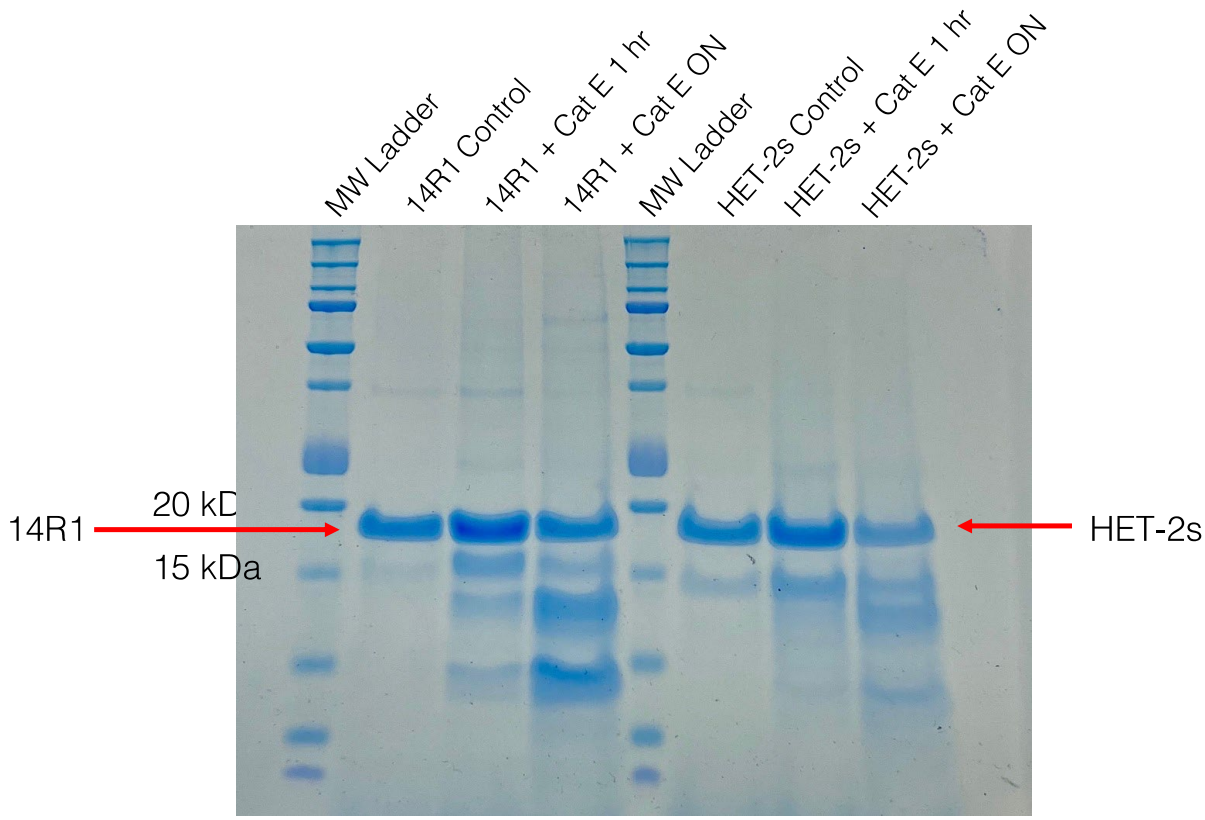

Figure 5.7: **SDS-PAGE to visualize processing of 14R1 and HET-2s by cathepsin E.** A band at ~17 kDa corresponds to undigested antigen. Bands below 17 kDa in the experimental lanes correspond to digestion products of antigen processing by cathepsin E. Cathepsin E processes both 14R1 and HET-2s to yield similar digestion patterns. Samples were separated by gel electrophoresis on a 12% Bis-Tris gel and stained with Coomassie Blue.

6 Development and analysis of a PIRIBS-based prion vaccine

6.1 Design of PIRIBS vaccine constructs

Prion vaccine constructs were created using the high-resolution 263K (Kraus et al., 2021) and RML (Manka et al., 2022) cryo-EM structures. I designed the vaccine constructs by replacing residues of HET-s with surface residues of PrP^{Sc}. PrP^{Sc} surface residues were considered for potential epitopes only if they were shown to be unobstructed by glycans and the GPI-anchor. Epitopes for the PIRIBS vaccine candidates were either 3 or 4 residues long. Residues were replaced on both rungs of the two-rung β-solenoid.

Figure 6.1 illustrates the surface amino acid residue replacements made on HET-s to create each PIRIBS vaccine candidate. PIRIBS 1 (P1) contains the 263K residues D147, R148, and Y150 from the middle β-arch. The epitope on PIRIBS 2 (P2) is composed of the N-terminal residues N97, W101, and K103. PIRIBS 3a (P3a) and PIRIBS 3b (P3b) are both replaced with residues 221, 223, and 225 near the C-terminus. However, PIRIBS 3b is optimized for the elk PrP sequence with a glutamate residue in position 223 whereas PIRIBS 3a is optimized for every other target species (mouse, human, hamster, deer, bovine, and ovine) with a glutamine in position 223. Residue replacement with E221 and

Y225 remain consistent between the two constructs. PIRIBS 4 (P4) construct contains the PrP^{Sc} residues V189, T191, T193, and K194. The PIRIBS 4 epitope was considered following the release of the 263K structure but was not created until the RML structure was released when residues 194 through 196 were more clearly resolved.

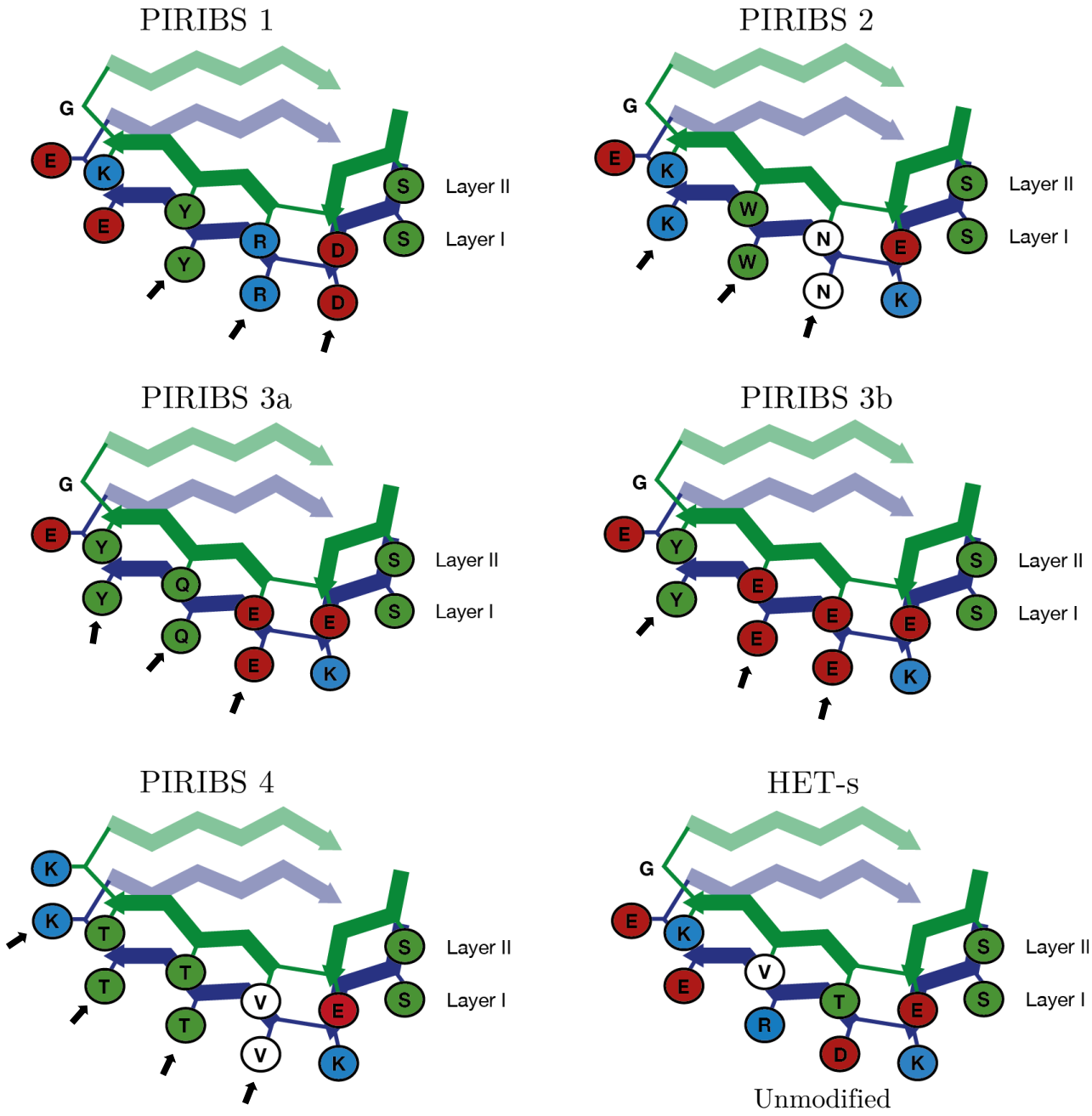

Figure 6.1: **PIRIBS vaccine construct design.** Illustration of two-rung β-solenoid surface scaffold, HET-s, modified to create PrP^{Sc} epitope. PIRIBS 1, 2, 3a, 3b, and 4 contain the residue replacements DRY, NWK, EQY, EEY, and VTTK respectively. Residues were replaced on both layers (rungs). Green represents polar, white represents hydrophobic, red represents negatively charged, and blue represents positively charged side chains.

6.2 Purification and quality control of PIRIBS vaccine candidates

The *E. coli*-optimized and sequence-verified vaccine construct plasmids were ordered, expressed, and purified as described (section 2.1).

The SDS-PAGE gel in figure 6.2 illustrates the successful purification of the PIRIBS constructs. The pure monomer appears at ~9 kDa and the dimer at ~18 kDa. Considering there is only a 6-8 amino acid variation, it is expected that all constructs have a similar MW to one another and to HET-s. Variations in binding to the detergent affect the mobility of the proteins through the gel matrix resulting in slightly different positions of the protein bands. PIRIBS 2V (P2V) was an accidental single point mutation of PIRIBS 2 which then served as a control.

Negative stain TEM micrographs of PIRIBS vaccine constructs show long, bundled fibrils similar to HET-s (figure 6.3). PIRIBS 3b did not form typical fibrils under the same conditions as HET-s and therefore, was not considered further.

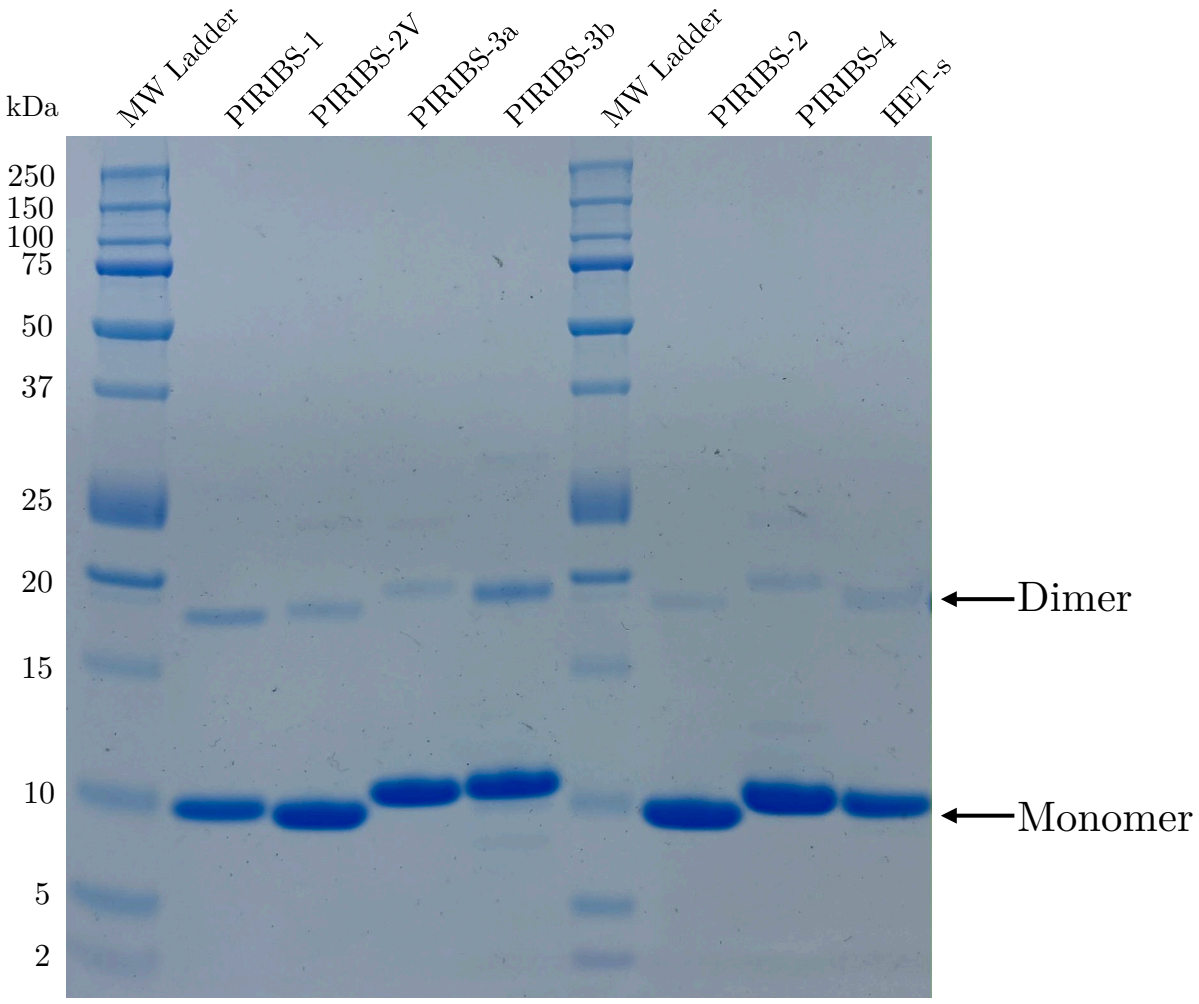

Figure 6.2: **SDS-PAGE of purified PIRIBS constructs.** A single, intense band at ~9 kDa corresponds to the pure PIRIBS construct monomer. A single, less intense band at ~18 kDa corresponds to the pure PIRIBS construct dimer. Samples were separated by gel electrophoresis on a 12% Bis-Tris gel and stained with Coomassie Blue.

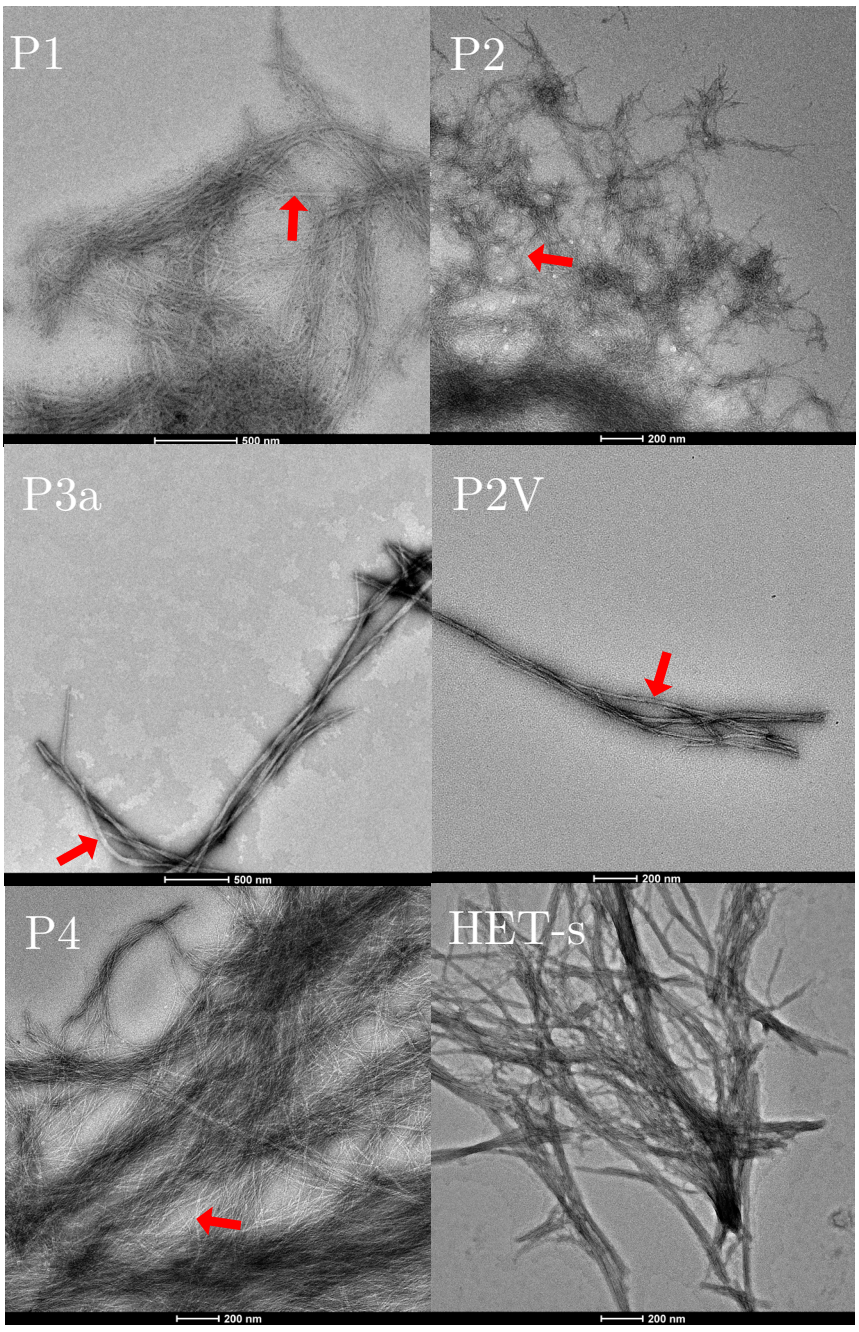

Figure 6.3: **TEM of PIRIBS-based vaccine construct fibrils.** Purified vaccine candidates (P1, P2, P3a, and P4) shows long, bundled fibrils similar to those of the HET-s control. Red arrow indicates typical bundled fibrils of 14R1. Fibrils were stained with 2% uranyl acetate and visualized at 19k magnification.

6.3 Immune response to PIRIBS vaccine candidates in FVB mice

I immunized FVB PrPKO mice with each PIRIBS vaccine antigen and alum adjuvant on a prime-boost schedule. Mice received an initial dose at ~8 weeks of age followed by three subsequent boosts at 2-week intervals. Figure 6.4 shows the immune response to the PIRIBS vaccine constructs at a 1.00 x 10^4 fold dilution. Mice which received P1 (n=4) had a large increase in antibody titre following the first boost which then levelled off with a maximum tire of 2.67 in the post-immune serum. The P2V control-immunized mice (n=2) had a maximum tire of 3.54 in the post-immune serum. P2-immunized mice (n=4) had an antibody titre which gradually increased throughout the prime-boost schedule before reaching a maximum of 2.70. Mice which received P3a (n=4) had a large immune response following the first boost which then reached a maximum of 2.84. P4-immunized mice had an immune response which increased most dramatically following the second boost which further increased to a maximum of 3.39 in the post-immune serum. Figure 6.5 illustrates that the immune response to the PIRIBS vaccine candidates is still detectable at a 4.27 x 10^7 fold dilution.

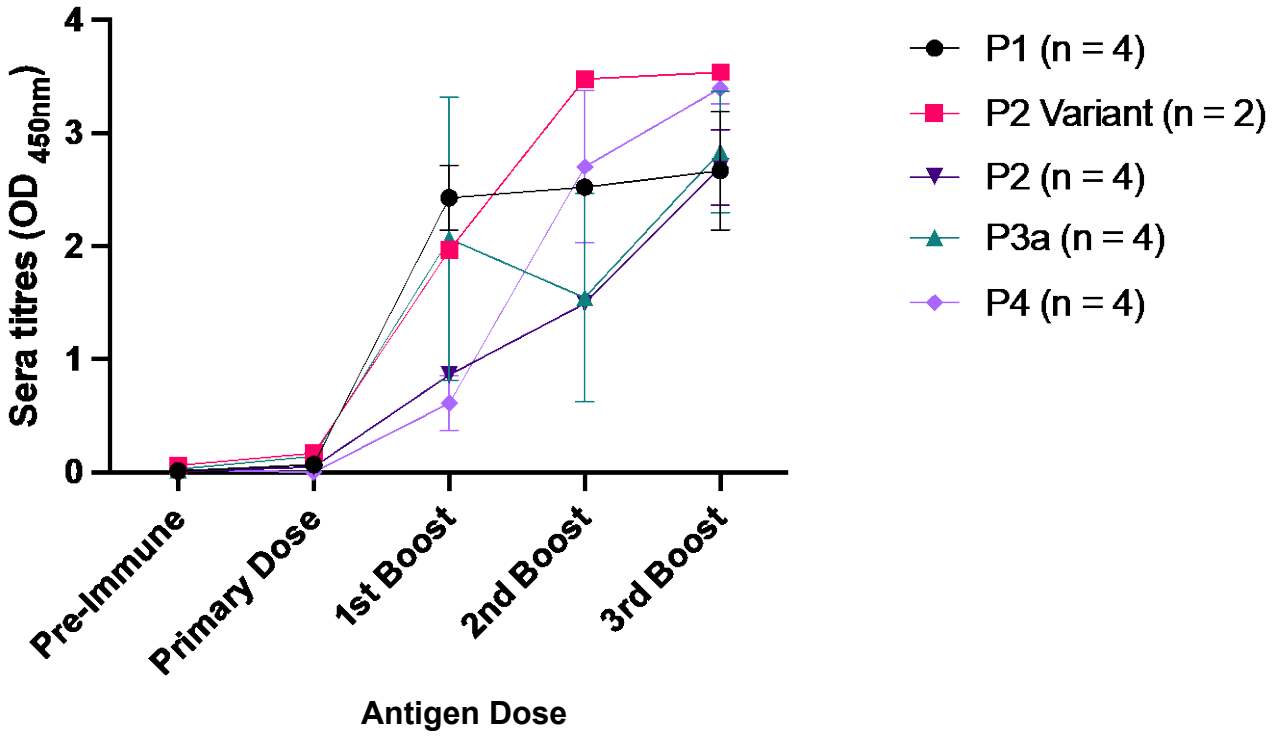

Figure 6.4: **Immune response of PIRIBS-immunized PrPKO mice.** Antibody titres of collected sera were determined via indirect ELISA by measurement of the OD at 450 nm. All PIRIBS vaccine candidates produced a high antibody titre following the prime-boost immunization trial. Pre-immune serum produced no immune response. Titres were measured at a 1.00 x 10^4 fold dilution.

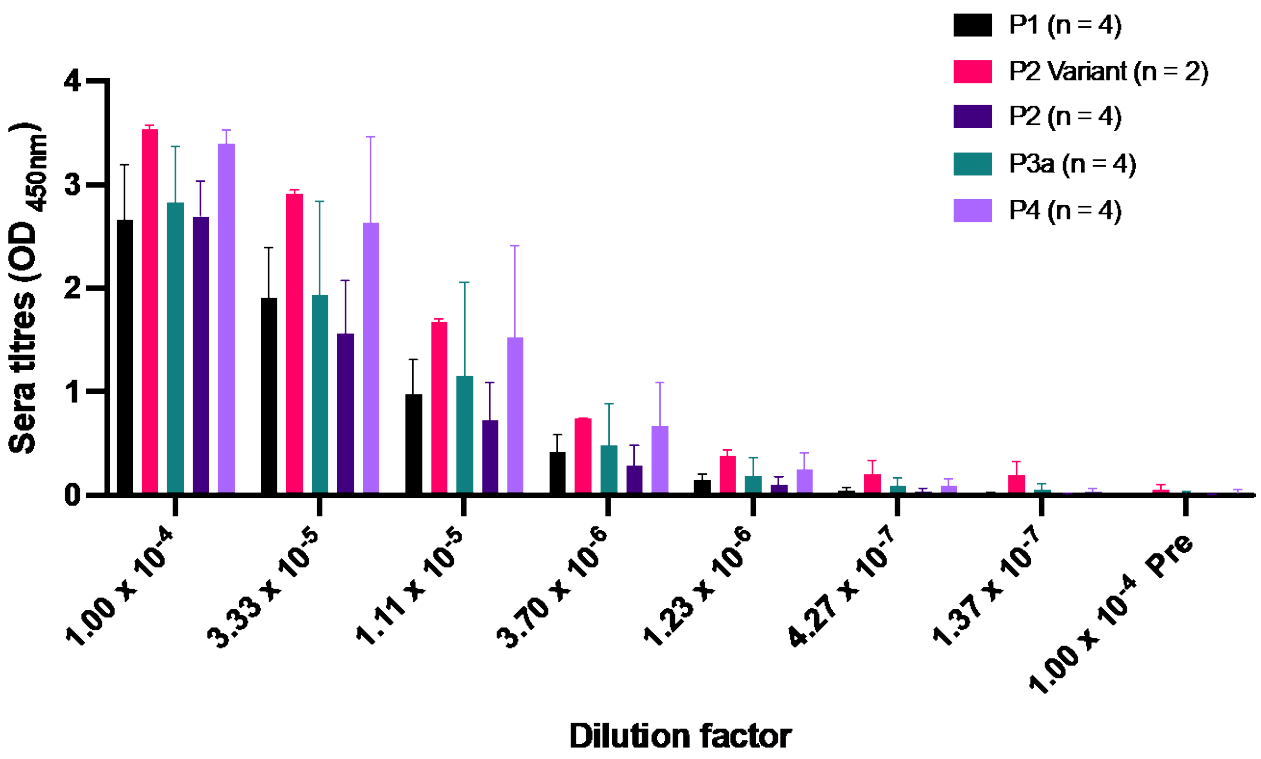

Figure 6.5: **Serially diluted immune response of PIRIBS-immunized PrPKO mice.** Antibody titres of collected sera were determined via indirect ELISA by measurement of the OD at 450 nm. All PIRIBS vaccine candidates produced a high antibody titre following the prime-boost immunization trial which diluted out to 4.27×10^{-7}. Pre-immune serum produced no immune response at a 1.00×10^{4} fold dilution.

6.4 PrP^{Sc}-specific immune response of PIRIBS-immunized mice

Following immunization trials with PIRIBS vaccine candidates in FVB mice, post-immune serum was analyzed for PrP^{Sc} specificity by bridge ELISA. This assay compared the antibody recognition of proteins in PK-digested RML brain homogenate to uninfected brain homogenate. Recognition of PrP^{Sc} is illustrated by an OD_{450nm} value above zero in the RML infected brain homogenate. As FVB uninfected brain homogenate contains no PrP^{Sc}, this value is expected to be negative for all animals tested. As there is no PrP^{Sc}-specific antibody for use as a positive control, 14R1-immunized mouse serum was used instead. 14R1 had a highly variable but average positive value in the RML infected brain homogenate (n=2) while HET-2s did not (n=1) (figure 6.6). For all animals immunized with P1, P2, or P3a (n=4), the value was above zero (figure 6.7a-c). This suggests a PrP^{Sc}-specific immune response following immunization with either P1, P2, or P3a. P4, on the other hand, had a value below zero for all animals (n=4) indicating no PrP^{Sc} recognition by antibodies in the post-immune serum (figure 6.7d). Although animal 2 of P3a had a much lower titre than the other P3a-immunized animals (figure 6.7c), it was significantly positive but not significantly different enough to be considered an outlier.

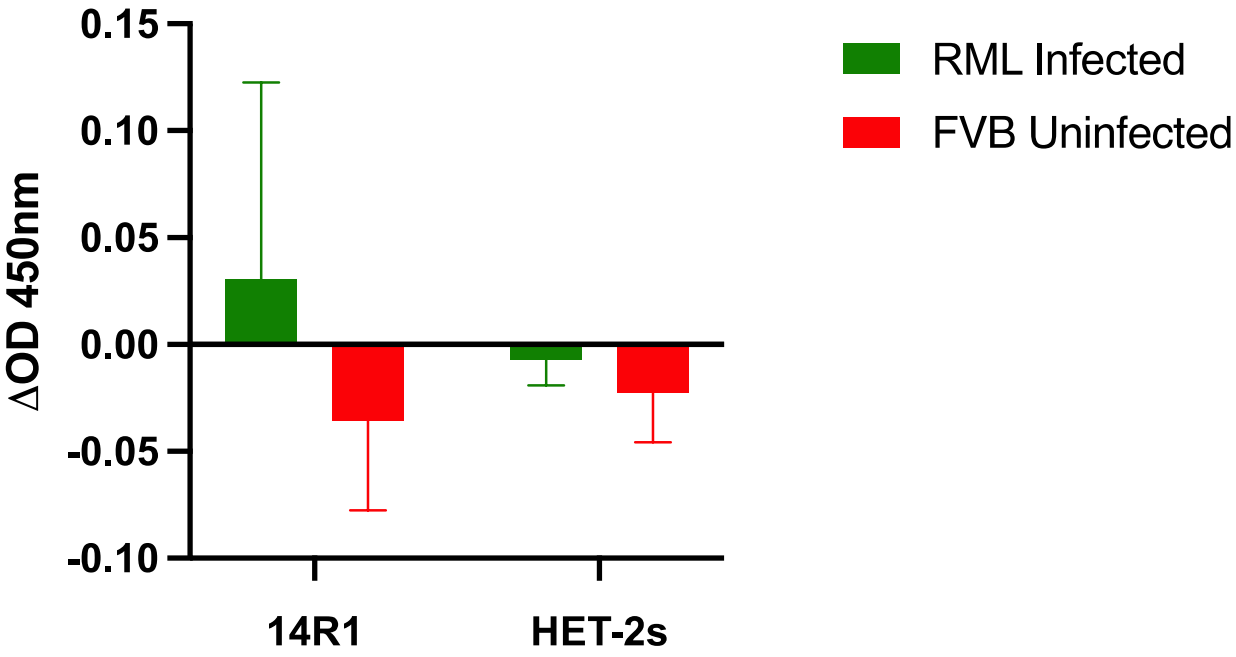

Figure 6.6: **Controls for measuring antibody recognition of PrP^{Sc} in RML infected brain homogenate**. OD_{450nm} was measured by bridge ELISA to compare antibody recognition of proteins in PK-digested RML brain homogenate and normal FVB brain homogenate. ΔOD_{450nm} was calculated by setting a cut-off value equal to the sum of the uninfected mean and the uninfected standard deviation. The ΔOD_{450nm} is then equal to the average of the measured OD_{450nm} minus the cut-off for each triplicate value. PrP^{Sc} recognition is indicated by a positive value in the RML infected brain homogenate (green) and a negative value in the FVB infected brain homogenate (red). 14R1 has a positive ΔOD_{450nm} in the RML infected BH while HET-2s has a negative ΔOD_{450nm}.

a.

P1

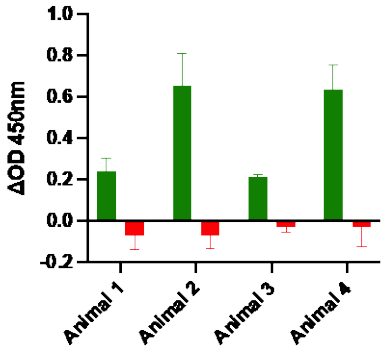

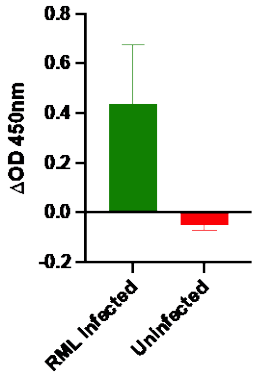

b.

P2

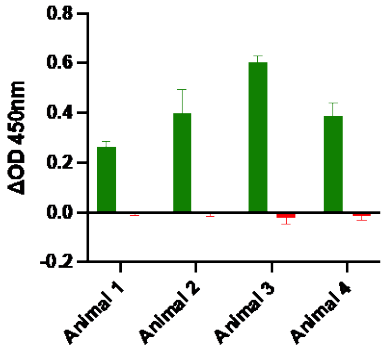

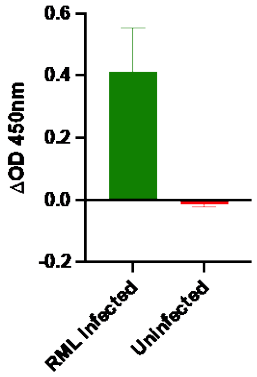

c.

P3a

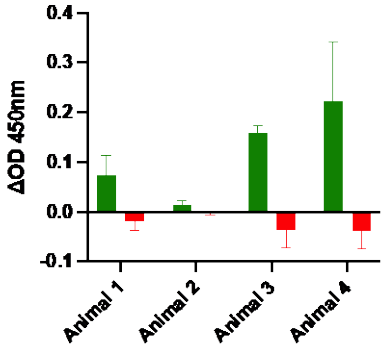

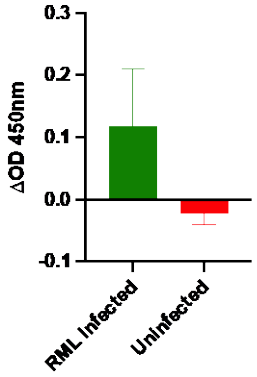

d.

P4

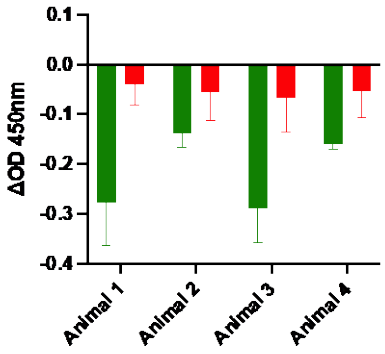

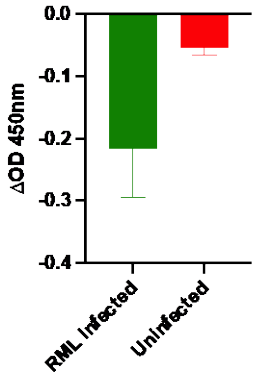

Figure 6.7: **PIRIBS vaccine derived antibody recognition of PrP^{Sc} in RML infected brain homogenate**. OD_{450nm} was measured by bridge ELISA to compare antibody recognition of proteins in PK-digested RML brain homogenate and normal FVB brain homogenate. ΔOD_{450nm} was calculated by setting a cut-off value equal to the sum of the uninfected mean and the uninfected standard deviation. The ΔOD_{450nm} is then equal to the average of the measured OD_{450nm} minus the cut-off for each triplicate value. PrP^{Sc} recognition is indicated by a positive value in the RML infected brain homogenate (green) and a negative value in the FVB infected brain homogenate (red). The graphs on the left show the ΔOD_{450nm} for each animal vaccinated. The graphs on the right show the average ΔOD_{450nm} for all four animals vaccinated with each PIRIBS candidate. a-c. P1, P2, and P3a post-immune sera have a positive ΔOD_{450nm} when in the RML infected brain homogenate. d. P4 post-immune serum has a negative ΔOD_{450nm} in both the RML infected and uninfected brain homogenate.

7 Discussion

7.1 Rationally Designed Structure-based prion vaccines

Throughout this thesis, I have demonstrated the potential and adaptability of rationally designed, structure-based prion vaccines through optimization and development. The four-rung β-solenoid-based vaccine, 14R1, created by Dr. Andrew Fang, showed potential as a prion vaccine due to its stable fibrillar structure and production of PrP^{Sc}-specific antibodies which are sufficient to delay symptom onset. In addition to its potential as a vaccine, 14R1 serves as a proof of concept for the use of HET-s as a scaffold for vaccines targeting misfolded proteins.

7.2 Adjuvant Comparison in P101L mice

The initial successful efficacy trials of 14R1 were performed with Freund's adjuvant which is too toxic for use in most animals and humans (Dubé et al., 2020) (section 1.10.5.1). Therefore, optimization of the vaccine delivery is essential for future trials in deer, elk, and potentially humans. Without adjuvant, the antibody titre is lower and more variable (figure 3.4). Therefore, two safer adjuvants, alum and QS21, were co-immunized with 14R1 and compared to the efficacy seen with FA. Alum and QS21 were chosen as

they are both approved for use in large animals and humans and they potentiate different immune responses (Isaacs et al., 2021; Sellers, 2017) (section 1.10.5). In the P101L mouse line, both adjuvants resulted in a comparable immune response to 14R1 and FA (figure 3.4). However, alum proved to be the best adjuvant with a significant delay in symptom onset over FA-immunized mice (figure 3.5). As well, alum has been a safe and reliable adjuvant for nearly a century (Kool et al., 2012). For these reasons, alum was used in all future prion disease vaccine trials.

7.3 Continued boosts with 14R1 decreases efficacy of the vaccine

The mechanism of the structure-based prion vaccine is the production of antibodies which recognize and target PrP^{Sc} for removal. Mice immunized with 14R1, regardless of adjuvant, have a significant delay in symptom onset and survival (figure 3.5 & figure 3.6). However, all immunized mice eventually succumb to prion disease. From previous experiments in the lab, it is known that the antibody titre of the mice decreases over time coinciding with an increase in PrP^{Sc} levels in the CNS. Thus, it was thought that to further delay clinical onset, ideally past the natural lifespan of the mice, the immune response needs to be maintained.

To prevent the decrease in sera titre, we added an additional boost of 14R1 and adjuvant every 14 weeks following the initial prime-boost schedule. Although the additional boosts did help to maintain the antibody titre (figure 3.7), the mice have a significantly decreased delay in symptom onset compared to mice immunized on the regular prime-boost schedule (figure 3.8). This could be due to the phenomenon of lymphocyte exhaustion. Lymphocyte exhaustion affects T-cells, B-cells, and NK-cells and has been an issue in cancer therapeutics (Roe, 2022). Persistent antigen stimulation, prolonged exposure to inflammatory cues, and general senescence can result in a decrease in immune response stimulating proteins, an increase in inhibitory receptors, and overall hyporesponsiveness of the immune system (Roe, 2022). Whether or not this immune cell dysfunction is responsible for the decreased efficacy of the vaccine while trying to maintain the antibody titre will require further analysis.

7.4 Comparison and optimization of 14R1 in human genetic prion disease mouse lines

The success of 14R1 vaccination in the GSS mouse line warranted efficacy trials in other human genetic prion disease transgenic mouse lines. Considering the rarity of human prion diseases, genetic prion diseases are an ideal target for a vaccine as there is a long

pre-symptomatic phase and no viable therapeutic options following symptom onset. To target the most common and invariably fatal human genetic prion diseases, efficacy trials were conducted in gCJD and FFI mouse lines in addition to the GSS mouse line.

Efficacy trials in the FFI mouse line were performed in Milan, Italy by Dr. Roberto Chiesa and his team. Following purification and quality control, 14R1 was sent to Italy and efficacy trials were performed as in the GSS mouse line. Upon analyzing the sera collected from the 14R1-immunized mice, the antibody titres were lower than in the GSS mouse line (figure 4.1). However, when subjected to motor coordination experiments on a rotarod, 14R1-immunized TgFFI mice performed better than HET-2s-immunized mice (figure 4.2). This suggests that the strength of the immune response does not necessarily correlate with the efficacy of the vaccine, as previously thought.

The E199K mouse line was chosen for efficacy trials as gCJD is the most common genetic human prion disease and E200K is the most common gCJD-associated mutation (Gambetti et al., 2003). The mouse line used, is currently the only available transgenic mouse model recapitulating gCJD with the E200K mutation (Friedman-Levi et al., 2011).

The immune response to 14R1 in the gCJD mouse line was comparable to that in the FFI mouse line, in that both had a much lower antibody titre than the GSS mouse line (figure 5.2).

When attempting to understand the difference in immune response between mouse lines, many factors were considered. For one, both the gCJD and FFI mice are on a C57BL/6J background while the GSS mice are on an FVB background (section 1.12). This initially did not present an issue but following literature search, it was discovered that C57BL/6J have a deficiency in cathepsin E, an aspartic protease responsible for antigen processing. This deficiency is tissue-specific, affecting only the T-cells, B-cells, and macrophages (Tulone et al., 2007). After confirming the lymphocytes of the E199K mice do not contain cathepsin E while lymphocytes of the P101L mice do (figure 5.6), it could be suggested that the antigen processing mechanism differs between the two mouse backgrounds.

In addition to a difference in immune response between mouse lines, we also observed a difference in the immune response between antigens. When immunized with HET-2s, the E199K mice and the FFI mice produced almost no immune response (figure 5.3). This was surprising for a few reasons. For one, 14R1 and HET-2s have a very similar

structure and sequence, with only 7 amino acid differences. As well, in the P101L mice, 14R1 and HET-2s had nearly identical antibody titres following immunization (figure 5.2 & figure 5.3).

It was thought that the cathepsin E deficiency in the E199K mice may also be responsible for the difference in immune response between the two antigens, 14R1 and HET-2s. Perhaps, the amino acid substitutions made to create 14R1 removed a cathepsin E cleavage site necessary for antigen processing. 14R1 and HET-2s were both digested by cathepsin E (figure 5.7) suggesting that a cathepsin E deficiency in the lymphocytes of these mice may be responsible for the decreased immune response. However, with no significant difference in the digestion pattern of 14R1 and HET-2s when treated with cathepsin E, this deficiency does not explain the lower immune response to HET-2s compared to 14R1 in E199K mice.

Another reason considered for the decreased antibody titre of HET-2s-immunized mice is that there may be a different type of immune response generated by the two antigens in the E199K mouse line. The secondary antibody used for the indirect ELISA when measuring the sera titres of immunized mice detects only the IgG antibodies (section 2.5.1). Immunoglobulin G (IgG) antibodies are the most abundant immunoglobulins in

the blood and are produced during the secondary immune response. IgG antibodies have a high affinity for their antigen and are long-lasting in the blood stream (Alberts et al., 2002). Another immunoglobulin, IgM, is the first to appear on the surface of the B-cell following immunization but has relatively low abundance in subsequent phases of the immune response (Janeway & Travers, 1994). Although IgM antibodies are likely to be in very low amounts when serum is collected (14 days post-immune), our lab has detected and isolated some effective IgM mAbs following the prime-boost immunization schedule. Therefore, reanalyzing the serum with a secondary antibody which detects IgM antibodies could help to determine whether there was an initial immune response to HET-2s that was, for some reason, unable to produce a secondary immune response. However, the IgM response, showed no significant improvement over the IgG titre (figure 5.4).

As neither the cathepsin E deficiency nor the IgM response provided us with a complete explanation for the difference in immune response between mice on a C57BL/6J background compared to FVB mice, further inquiry was required. It was discovered that different mouse backgrounds have certain immunological biases. One of which is a bias in the T-helper (Th)-type response. Th cells are essential for adaptive immunity as they activate B-cells which produce antibodies (Alberts et al., 2002). FVB mice have a Th2-type response bias which would better be potentiated by alum adjuvant whereas

C57BL/6J mice have Th1-type response bias that would better be potentiated by QS21 adjuvant (Disis & Palucka, 2014; Schulte et al., 2008; Sellers, 2017). Th2 cells stimulate a humoral response and antibody production via B cell proliferation. Th1 cells stimulate a cellular immune response and induce production of immunoglobulins via B-cells (Umetsu & DeKruyff, 1997). These findings align with our adjuvant comparison data in the P101L mouse line, where alum proved slightly more effective than QS21 (figure 3.5 & figure 3.6). After learning of this bias, we reperformed the efficacy trial in the E199K mouse line using QS21 adjuvant. While the antibody titre in the post-immune serum of these mice was still not as high as in the P101L mice, it was a significant improvement for both HET-2s and 14R1 over co-immunization with alum adjuvant (figure 5.5).

7.5 Design and development of a PIRIBS-based prion vaccine

Throughout this thesis, there has been much evidence provided to support the idea of a rationally designed, structure-based vaccine for prion diseases. Until recently, the debate of the structure of PrP^{Sc} centred around two potential models, four-rung β-solenoid and PIRIBS. With low-resolution structural data to support both models, 14R1 was created assuming a four-rung β-solenoid structure of PrP^{Sc}. In addition to the low-resolution structural evidence, the success of 14R1 and the PrP^{Sc}-specific mAb, G1,

isolated as a result complicate the story of relevant structures of misfolded PrP. However, there have now been five brain-derived, high-resolution structures of PrP^{Sc} published which all have a PIRIBS conformation. Data exists which cannot be explained by the PIRIBS PrP^{Sc} structures. For example, the success of 14R1 is dependent on an exposed epitope of H114 and D150 residues (based on deer PrP sequence) in proximity on PrP^{Sc} for antibody recognition. This epitope is not present in the PIRIBS model of PrP^{Sc} and therefore the vaccine should not work. All this conflicting data surrounding the structure of PrP^{Sc} could suggest there are multiple relevant structures of misfolded PrP which contribute to prion disease. When analyzing the folding of the GSS synthetic peptide using G1, it was found that a β-solenoid structure containing the HD epitope required for Ab binding formed first before drifting to an intermolecular β-rich structure like the PIRIBS fold. Considering the potential explanation of a beta-solenoid intermediate followed by formation of a PIRIBS structure, we decided to create new vaccine constructs based on the published PIRIBS PrP^{Sc} structures.

In our lab, we have used 14R1 as a blueprint to develop vaccine constructs targeting many neurodegenerative disease-associated misfolded proteins such as amyloid β, tau, and alpha synuclein. By using HET-s as a scaffold, we can mimic select surface residues of the target protein sufficient to produce antibodies which recognize and bind

the target protein. This method was applied to create four new vaccine candidates based on the 263K and RML PIRIBS structures (Kraus et al., 2021; Manka et al., 2022) using HET-s as a scaffold. HET-s is sufficient as a scaffold for the new constructs because, in the PIRIBS structure, each monomer is stacked directly on top of the other and therefore the same residues can be replaced on both rungs. HET-s also offers increased freedom in residue selection and placement due to greater stability than HET-2s. Like 14R1, the epitope of each PIRIBS vaccine construct is conformational. Conformational epitopes are non-linear in the primary structure of the protein but form the epitope upon protein folding, or in this case, misfolding (Forsström et al., 2015).

When selecting residues for the PIRIBS vaccine candidate epitopes, many factors had to be considered. To mimic the surface of PrP^{Sc}, selected residues had to be present at the surface and unobstructed by glycans or the GPI anchor. The placement of selected residues on HET-s was adjusted based on their position in PrP^{Sc}. Constructs P1, P2, P3a, and P3b, residues were chosen based on the 263K structure (Kraus et al., 2021) while P4 was created following the release of the RML structure (Manka et al., 2022). While 14R1 was designed using the deer PrP sequence, the PIRIBS constructs were designed to be applicable to a variety of prion diseases. For this reason, P3 has two variants. The residues which make up the P3a epitope are unchanged for all target species except for elk. As

there are currently vaccination trials with 14R1 in elk, it was important to create another vaccine construct mimicking the same region of PrP^{Sc} as P3a but optimized for the elk PrP sequence. Thus, P3b was designed and purified. However, when performing quality control measures on the purified constructs, P3b was the only vaccine candidate to not form typical HET-s-like fibrils. As the vaccines require the correct conformation to form their respective epitopes, confirmation of fibril formation with electron microscopy is an essential step in development. Although P3b was not considered further as a vaccine candidate, it could be revisited at a later point and optimized to improve fibril formation. When examining the sequence of the P3b epitope (EEY), it could be suggested that the stacking of multiple negatively charged glutamate residues both side-by-side and on top of one another prevents proper folding of the HET-s scaffold.

As P1, P2, P3a, and P4 were successfully purified (figure 6.2) and formed typical fibrils (figure 6.3), they were chosen for immunization trials in FVB mice. FVB PrPKO mice were immunized with one of the PIRIBS vaccine candidates and alum adjuvant on our usual prime-boost schedule. When delivered the same amount of antigen per dose, PIRIBS vaccine-immunized mice had an antibody titre comparable to that of 14R1 in the P101L mice. All PIRIBS vaccine candidates produced a high antibody titre which dilutes out to 4.27×10^{-7} (figure 6.4).

To determine whether the resultant immune response from PIRIBS vaccination is PrP^{Sc}-specific, a bridge ELISA was performed. This ELISA tested whether the post-immune polyclonal antibody serum contained antibodies which recognize a protein which is present in RML-infected brain homogenate but absent in the uninfected brain homogenate, arguably PrP^{Sc}. RML prions were chosen for the assay because they were easily accessible in our lab and the constructs were designed based on the published RML structure (Manka et al., 2022). However, the assay will need to be repeated with many other prion-infected brain homogenates as new high-resolution structures are released. This will allow for comparison of the potential of 14R1 and P1-P4 as prion vaccines for at-risk humans and animals. The results of the bridge ELISA suggests that three of four PIRIBS vaccine constructs resulted in production of PrP^{Sc}-specific antibodies. Results were consistent between both technical replicates and biological replicates for all constructs (figure 6.7). In other words, all animals immunized with P1, P2, or P3a showed PrP^{Sc} recognition whereas all P4-immunized animals did not (figure 6.7). Although we thought it possible that every construct could work because they were based on a verified structure, the VTTK epitope of P4 was the most questionable. This epitope was not fully resolved in the 263K structure (Kraus et al., 2021) and had the lowest local resolution in the RML structure (Manka et al., 2022). As well, this region is highly variable between the two structures. This suggests that this region is highly flexible compared to the regions

from which the other candidates were created and therefore may not be the best candidate for a structure-based prion vaccine.

For the bridge ELISA to work with RML brain homogenate, it had to be digested with proteinase K. Proteinase K digestion removes the N-terminus and induces folding of the PrP^{res} structure into its fibril form (Bolton et al., 1982; Cronier et al., 2008). Considering 14R1 antibodies may recognize an intermediate structure rather than the final fibril form of RML, it is expected that it would not be the perfect positive control in the PK-digested RML bridge ELISA. This is supported by the higher variability of 14R1 antibody recognition of PrP^{Sc} in the RML-infected brain homogenate (figure 6.6). However, as there are currently no PIRIBS-based PrP^{Sc}-specific antibodies, 14R1 antibodies are the best positive control available for this assay. As expected, serum from HET-2s-immunized mice did not recognize PrP^{Sc} because there is no epitope present at the surface of HET-2s which mimics PrP^{Sc}. Considering the promising results of the bridge ELISA, P1, P2, and P3a will move on to efficacy trials in the GSS mouse line.

8 Conclusion

The goal of this thesis was to optimize prion vaccination in mouse models recapitulating the most common human prion diseases. Differences in the immune response between immunized mouse lines can be partially explained by immunological deficiencies and biases. The low immune response to 14R1 and HET-2s in CJD mice can be partially overcome by matching the adjuvant with the Th-type response bias of the mouse line. While 14R1 greatly delays clinical onset in GSS mice, regardless of adjuvant, mice still succumb to prion disease. However, additional boosts of 14R1 do not further delay symptom onset. While optimizing the four-rung β-solenoid vaccine targeting PrP^{Sc}, new cryo-EM structures of PrP^{Sc} which all adopt a PIRIBS conformation were released. Therefore, PIRIBS vaccines targeting PrP^{Sc} were designed using the same methodology as 14R1. Four PIRIBS vaccine candidates formed typical fibrils and produced a large immune response in FVB mice. Three of the constructs produced antibodies which recognize PrP^{Sc} and will therefore go on to efficacy trials in GSS mice. As well, isolation of PrP^{Sc}-specific mAbs from the PIRIBS vaccine-immunized mice is in progress. Comparing the efficacy of the two types of structure-based vaccines will not only advance prion disease therapeutic options but also provide insight into the conformational changes of the prion protein and their relevance to prion disease.

Bibliography

Abdelaziz, D. H., Thapa, S., Brandon, J., Maybee, J., Vankuppeveld, L., McCorkell, R., & Schätzl, H. M. (2018). Recombinant prion protein vaccination of transgenic elk PrP mice and reindeer overcomes self-tolerance and protects mice against chronic wasting disease. *J Biol Chem*, *293*(51), 19812-19822. https://doi.org/10.1074/jbc.RA118.004810

Adjou, K. T., Privat, N., Demart, S., Deslys, J. P., Seman, M., Hauw, J. J., & Dormont, D. (2000). MS-8209, an amphotericin B analogue, delays the appearance of spongiosis, astrogliosis and PrPres accumulation in the brain of scrapie-infected hamsters. *J Comp Pathol*, *122*(1), 3-8. https://doi.org/10.1053/jcpa.1999.0338

Ahn, M., Bajsarowicz, K., Oehler, A., Lemus, A., Bankiewicz, K., & DeArmond, S. J. (2014). Convection-enhanced delivery of AAV2-PrPshRNA in prion-infected mice. *PLoS One*, *9*(5), e98496. https://doi.org/10.1371/journal.pone.0098496

Alberts, B., Johnson, A., Lewis, J., Walter, P., Raff, M., & Roberts, K. (2002). *Molecular Biology of the Cell 4th Edition: International Student Edition*. Routledge. https://books.google.ca/books?id=ozigkQEACAAJ

Alpers, M. (1968). The Central Nervous System. In.

Alpers, M. P. (2008). The epidemiology of kuru: monitoring the epidemic from its peak to its end. *Philosophical Transactions of the Royal Society B: Biological Sciences*, *363*(1510), 3707-3713. https://doi.org/doi:10.1098/rstb.2008.0071

Awate, S., Babiuk, L. A., & Mutwiri, G. (2013). Mechanisms of action of adjuvants. *Front Immunol*, *4*, 114. https://doi.org/10.3389/fimmu.2013.00114

Bachy, V., Ballerini, C., Gourdain, P., Prignon, A., Iken, S., Antoine, N., Rosset, M., & Carnaud, C. (2010). Mouse vaccination with dendritic cells loaded with prion protein peptides overcomes tolerance and delays scrapie. *J Gen Virol*, *91*(Pt 3), 809-820. https://doi.org/10.1099/vir.0.013417-0

Bade, S., Baier, M., Boetel, T., & Frey, A. (2006). Intranasal immunization of Balb/c mice against prion protein attenuates orally acquired transmissible spongiform encephalopathy. *Vaccine*, *24*(9), 1242-1253. https://doi.org/10.1016/j.vaccine.2005.12.051

Bade, S., & Frey, A. (2007). Potential of active and passive immunizations for the prevention and therapy of transmissible spongiform encephalopathies. *Expert Rev Vaccines*, *6*(2), 153-168. https://doi.org/10.1586/14760584.6.2.153

Balguerie, A., Dos Reis, S., Ritter, C., Chaignepain, S., Coulary-Salin, B., Forge, V., Bathany, K., Lascu, I., Schmitter, J. M., Riek, R., & Saupe, S. J. (2003). Domain organization and structure-function relationship of the HET-s prion protein of

Podospora anserina. *Embo j*, *22*(9), 2071-2081. https://doi.org/10.1093/emboj/cdg213

Baral, P. K., Swayampakula, M., Aguzzi, A., & James, M. N. (2015). X-ray structural and molecular dynamical studies of the globular domains of cow, deer, elk and Syrian hamster prion proteins. *J Struct Biol*, *192*(1), 37-47. https://doi.org/10.1016/j.jsb.2015.08.014

Baron, G. S., Hughson, A. G., Raymond, G. J., Offerdahl, D. K., Barton, K. A., Raymond, L. D., Dorward, D. W., & Caughey, B. (2011). Effect of glycans and the glycophosphatidylinositol anchor on strain dependent conformations of scrapie prion protein: improved purifications and infrared spectra. *Biochemistry*, *50*(21), 4479-4490. https://doi.org/10.1021/bi2003907

Baskakov, I. V., & Katorcha, E. (2016). Multifaceted Role of Sialylation in Prion Diseases. *Front Neurosci*, *10*, 358. https://doi.org/10.3389/fnins.2016.00358

Bayer, A. J., Bullock, R., Jones, R. W., Wilkinson, D., Paterson, K. R., Jenkins, L., Millais, S. B., & Donoghue, S. (2005). Evaluation of the safety and immunogenicity of synthetic Abeta42 (AN1792) in patients with AD. *Neurology*, *64*(1), 94-101. https://doi.org/10.1212/01.Wnl.0000148604.77591.67

Bloom, G. S. (2014). Amyloid-β and Tau: The Trigger and Bullet in Alzheimer Disease Pathogenesis. *JAMA Neurology*, *71*(4), 505-508. https://doi.org/10.1001/jamaneurol.2013.5847

Bolton, D. C., McKinley, M. P., & Prusiner, S. B. (1982). Identification of a protein that purifies with the scrapie prion. *Science*, *218*(4579), 1309-1311. https://doi.org/10.1126/science.6815801

Bounhar, Y., Zhang, Y., Goodyer, C. G., & LeBlanc, A. (2001). Prion protein protects human neurons against Bax-mediated apoptosis. *J Biol Chem*, *276*(42), 39145-39149. https://doi.org/10.1074/jbc.C100443200

Bouybayoune, I., Mantovani, S., Del Gallo, F., Bertani, I., Restelli, E., Comerio, L., Tapella, L., Baracchi, F., Fernández-Borges, N., Mangieri, M., Bisighini, C., Beznoussenko, G. V., Paladini, A., Balducci, C., Micotti, E., Forloni, G., Castilla, J., Fiordaliso, F., Tagliavini, F., . . . Chiesa, R. (2015). Transgenic fatal familial insomnia mice indicate prion infectivity-independent mechanisms of pathogenesis and phenotypic expression of disease. *PLoS Pathog*, *11*(4), e1004796. https://doi.org/10.1371/journal.ppat.1004796

Bremer, J., Baumann, F., Tiberi, C., Wessig, C., Fischer, H., Schwarz, P., Steele, A. D., Toyka, K. V., Nave, K. A., Weis, J., & Aguzzi, A. (2010). Axonal prion protein is required for peripheral myelin maintenance. *Nat Neurosci*, *13*(3), 310-318. https://doi.org/10.1038/nn.2483

Brown, K., & Mastrianni, J. A. (2010). The prion diseases. *J Geriatr Psychiatry Neurol*, *23*(4), 277-298. https://doi.org/10.1177/0891988710383576

Brown, P., Brandel, J. P., Sato, T., Nakamura, Y., MacKenzie, J., Will, R. G., Ladogana, A., Pocchiari, M., Leschek, E. W., & Schonberger, L. B. (2012). Iatrogenic Creutzfeldt-Jakob disease, final assessment. *Emerg Infect Dis*, *18*(6), 901-907. https://doi.org/10.3201/eid1806.120116

Browning, S. R., Mason, G. L., Seward, T., Green, M., Eliason, G. A. J., Mathiason, C., Miller, M. W., Williams, E. S., Hoover, E., & Telling, G. C. (2004). Transmission of Prions from Mule Deer and Elk with Chronic Wasting Disease to Transgenic Mice Expressing Cervid PrP. *Journal of Virology*, *78*(23), 13345-13350. https://doi.org/doi:10.1128/JVI.78.23.13345-13350.2004

Büeler, H., Aguzzi, A., Sailer, A., Greiner, R. A., Autenried, P., Aguet, M., & Weissmann, C. (1993). Mice devoid of PrP are resistant to scrapie. *Cell*, *73*(7), 1339-1347. https://doi.org/10.1016/0092-8674(93)90360-3

Büeler, H., Fischer, M., Lang, Y., Bluethmann, H., Lipp, H. P., DeArmond, S. J., Prusiner, S. B., Aguet, M., & Weissmann, C. (1992). Normal development and behaviour of mice lacking the neuronal cell-surface PrP protein. *Nature*, *356*(6370), 577-582. https://doi.org/10.1038/356577a0

Cagampang, F. R., Whatley, S. A., Mitchell, A. L., Powell, J. F., Campbell, I. C., & Coen, C. W. (1999). Circadian regulation of prion protein messenger RNA in the rat forebrain: a widespread and synchronous rhythm. *Neuroscience*, *91*(4), 1201-1204. https://doi.org/10.1016/s0306-4522(99)00092-5

Capobianco, R., Casalone, C., Suardi, S., Mangieri, M., Miccolo, C., Limido, L., Catania, M., Rossi, G., Di Fede, G., Giaccone, G., Bruzzone, M. G., Minati, L., Corona, C., Acutis, P., Gelmetti, D., Lombardi, G., Groschup, M. H., Buschmann, A., Zanusso, G., . . . Tagliavini, F. (2007). Conversion of the BASE prion strain into the BSE strain: the origin of BSE? *PLoS Pathog*, *3*(3), e31. https://doi.org/10.1371/journal.ppat.0030031

Castle, A. R., & Gill, A. C. (2017). Physiological Functions of the Cellular Prion Protein [Review]. *Frontiers in Molecular Biosciences*, *4*. https://doi.org/10.3389/fmolb.2017.00019

Chen, R. J., Chang, W. W., Lin, Y. C., Cheng, P. L., & Chen, Y. R. (2013). Alzheimer's amyloid-β oligomers rescue cellular prion protein induced tau reduction via the Fyn pathway. *ACS Chem Neurosci*, *4*(9), 1287-1296. https://doi.org/10.1021/cn400085q

Chiti, F., & Dobson, C. M. (2017). Protein Misfolding, Amyloid Formation, and Human Disease: A Summary of Progress Over the Last Decade. *Annual Review of*

Biochemistry, *86*(1), 27-68. https://doi.org/10.1146/annurev-biochem-061516-045115

Cobb, N. J., Sönnichsen, F. D., McHaourab, H., & Surewicz, W. K. (2007). Molecular architecture of human prion protein amyloid: a parallel, in-register beta-structure. *Proc Natl Acad Sci U S A*, *104*(48), 18946-18951. https://doi.org/10.1073/pnas.0706522104

Collinge, J., Gorham, M., Hudson, F., Kennedy, A., Keogh, G., Pal, S., Rossor, M., Rudge, P., Siddique, D., Spyer, M., Thomas, D., Walker, S., Webb, T., Wroe, S., & Darbyshire, J. (2009). Safety and efficacy of quinacrine in human prion disease (PRION-1 study): a patient-preference trial. *Lancet Neurol*, *8*(4), 334-344. https://doi.org/10.1016/s1474-4422(09)70049-3

Collinge, J., Sidle, K. C., Meads, J., Ironside, J., & Hill, A. F. (1996). Molecular analysis of prion strain variation and the aetiology of 'new variant' CJD. *Nature*, *383*(6602), 685-690. https://doi.org/10.1038/383685a0

Collinge, J., Whitfield, J., McKintosh, E., Frosh, A., Mead, S., Hill, A. F., Brandner, S., Thomas, D., & Alpers, M. P. (2008). A clinical study of kuru patients with long incubation periods at the end of the epidemic in Papua New Guinea. *Philos Trans R Soc Lond B Biol Sci*, *363*(1510), 3725-3739. https://doi.org/10.1098/rstb.2008.0068

Collins, S., McLean, C. A., & Masters, C. L. (2001). Gerstmann-Sträussler-Scheinker syndrome,fatal familial insomnia, and kuru: a review of these less common human transmissible spongiform encephalopathies. *J Clin Neurosci*, *8*(5), 387-397. https://doi.org/10.1054/jocn.2001.0919

Collins, S. J., Sanchez-Juan, P., Masters, C. L., Klug, G. M., van Duijn, C., Poleggi, A., Pocchiari, M., Almonti, S., Cuadrado-Corrales, N., de Pedro-Cuesta, J., Budka, H., Gelpi, E., Glatzel, M., Tolnay, M., Hewer, E., Zerr, I., Heinemann, U., Kretszchmar, H. A., Jansen, G. H., . . . Will, R. G. (2006). Determinants of diagnostic investigation sensitivities across the clinical spectrum of sporadic Creutzfeldt-Jakob disease. *Brain*, *129*(Pt 9), 2278-2287. https://doi.org/10.1093/brain/awl159

Colombo, R. (2000). Age and origin of the PRNP E200K mutation causing familial Creutzfeldt-Jacob disease in Libyan Jews. *Am J Hum Genet*, *67*(2), 528-531. https://doi.org/10.1086/303021

Corsaro, A., Bajetto, A., Thellung, S., Begani, G., Villa, V., Nizzari, M., Pattarozzi, A., Solari, A., Gatti, M., Pagano, A., Würth, R., Daga, A., Barbieri, F., & Florio, T. (2016). Cellular prion protein controls stem cell-like properties of human glioblastoma tumor-initiating cells. *Oncotarget*, *7*(25), 38638-38657. https://doi.org/10.18632/oncotarget.9575

Cortes, C. J., Qin, K., Cook, J., Solanki, A., & Mastrianni, J. A. (2012). Rapamycin delays disease onset and prevents PrP plaque deposition in a mouse model of Gerstmann-Sträussler-Scheinker disease. *J Neurosci*, *32*(36), 12396-12405. https://doi.org/10.1523/jneurosci.6189-11.2012

Cox, B. (1994). Cytoplasmic inheritance. Prion-like factors in yeast. *Curr Biol*, *4*(8), 744-748. https://doi.org/10.1016/s0960-9822(00)00167-6

Cracco, L., Appleby, B. S., & Gambetti, P. (2018). Fatal familial insomnia and sporadic fatal insomnia. *Handb Clin Neurol*, *153*, 271-299. https://doi.org/10.1016/b978-0-444-63945-5.00015-5

Cremades, N., & Dobson, C. M. (2018). The contribution of biophysical and structural studies of protein self-assembly to the design of therapeutic strategies for amyloid diseases. *Neurobiology of Disease*, *109*, 178-190. https://doi.org/https://doi.org/10.1016/j.nbd.2017.07.009

Creutzfeldt, H. G. (1920). Über eine eigenartige herdförmige erkrankung des zentralnervensystems (Vorläufige mitteilung). *Zeitschrift für die gesamte Neurologie und Psychiatrie*, *57*(1), 1-18. https://doi.org/10.1007/BF02866081

Crick, F. H. (1958). On protein synthesis. *Symp Soc Exp Biol*, *12*, 138-163.

Cronier, S., Gros, N., Tattum, M. H., Jackson, G. S., Clarke, A. R., Collinge, J., & Wadsworth, J. D. (2008). Detection and characterization of proteinase K-sensitive disease-related prion protein with thermolysin. *Biochem J*, *416*(2), 297-305. https://doi.org/10.1042/bj20081235

Cuillé, J., & Chelle, P. (1936). La maladie dite "tremblante du mouton" est-elle inoculable?[Is the disease known as "scrapie" inoculable?]. *CR Seances Acad Sci*, *203*, 1552-1554.

Cuillé, J., & Chelle, P.-L. (1938). Investigations of scrapie in sheep. *Vet Med*, *34*, 417-418.

Dalsgaard, K. (1974). Saponin adjuvants. 3. Isolation of a substance from Quillaja saponaria Molina with adjuvant activity in food-and-mouth disease vaccines. *Arch Gesamte Virusforsch*, *44*(3), 243-254.

Daude, N., Marella, M., & Chabry, J. (2003). Specific inhibition of pathological prion protein accumulation by small interfering RNAs. *J Cell Sci*, *116*(Pt 13), 2775-2779. https://doi.org/10.1242/jcs.00494

DeArmond, S. J., & Prusiner, S. B. (1995). Prion protein transgenes and the neuropathology in prion diseases. *Brain Pathol*, *5*(1), 77-89. https://doi.org/10.1111/j.1750-3639.1995.tb00579.x

del Río, J. A., & Gavín, R. (2016). Functions of the cellular prion protein, the end of Moore's law, and Ockham's razor theory. *Prion*, *10*(1), 25-40. https://doi.org/10.1080/19336896.2015.1126038

Disis, M. L., & Palucka, K. (2014). Evaluation of cancer immunity in mice. *Cold Spring Harbor protocols*, *2014*(3), 231-234. https://doi.org/10.1101/pdb.top078816

Dobson, C. M. (2003). Protein folding and misfolding. *Nature*, *426*(6968), 884-890. https://doi.org/10.1038/nature02261

Doh-ura, K., Ishikawa, K., Murakami-Kubo, I., Sasaki, K., Mohri, S., Race, R., & Iwaki, T. (2004). Treatment of transmissible spongiform encephalopathy by intraventricular drug infusion in animal models. *J Virol*, *78*(10), 4999-5006. https://doi.org/10.1128/jvi.78.10.4999-5006.2004

Doh-ura, K., Tateishi, J., Sasaki, H., Kitamoto, T., & Sakaki, Y. (1989). Pro----leu change at position 102 of prion protein is the most common but not the sole mutation related to Gerstmann-Sträussler syndrome. *Biochem Biophys Res Commun*, *163*(2), 974-979. https://doi.org/10.1016/0006-291x(89)92317-6

Dossena, S., Imeri, L., Mangieri, M., Garofoli, A., Ferrari, L., Senatore, A., Restelli, E., Balducci, C., Fiordaliso, F., Salio, M., Bianchi, S., Fioriti, L., Morbin, M., Pincherle, A., Marcon, G., Villani, F., Carli, M., Tagliavini, F., Forloni, G., & Chiesa, R. (2008). Mutant prion protein expression causes motor and memory deficits and abnormal sleep patterns in a transgenic mouse model. *Neuron*, *60*(4), 598-609. https://doi.org/10.1016/j.neuron.2008.09.008

Douet, J.-Y., Huor, A., Cassard, H., Lugan, S., Aron, N., Mesic, C., Vilette, D., Barrio, T., Streichenberger, N., Perret-Liaudet, A., Delisle, M.-B., Péran, P., Deslys, J.-P., Comoy, E., Vilotte, J.-L., Goudarzi, K., Béringue, V., Barria, M. A., Ritchie, D. L., . . . Andréoletti, O. (2021). Prion strains associated with iatrogenic CJD in French and UK human growth hormone recipients. *Acta Neuropathologica Communications*, *9*(1), 145. https://doi.org/10.1186/s40478-021-01247-x

Dubé, J.-Y., McIntosh, F., Zarruk, J. G., David, S., Nigou, J., & Behr, M. A. (2020). Synthetic mycobacterial molecular patterns partially complete Freund's adjuvant. *Scientific Reports*, *10*(1), 5874. https://doi.org/10.1038/s41598-020-62543-5

Duffy, P., Wolf, J., Collins, G., DeVoe, A. G., Streeten, B., & Cowen, D. (1974). Letter: Possible person-to-person transmission of Creutzfeldt-Jakob disease. *N Engl J Med*, *290*(12), 692-693.

Dvorak, A. M., & Dvorak, H. F. (1974). Structure of Freund's complete and incomplete adjuvants. Relation of adjuvanticity to structure. *Immunology*, *27*(1), 99-114.

Eiden, M., Gedvilaite, A., Leidel, F., Ulrich, R. G., & Groschup, M. H. (2021). Vaccination with Prion Peptide-Displaying Polyomavirus-Like Particles Prolongs Incubation Time in Scrapie-Infected Mice. *Viruses*, *13*(5). https://doi.org/10.3390/v13050811

Elbashir, S. M., Harborth, J., Lendeckel, W., Yalcin, A., Weber, K., & Tuschl, T. (2001). Duplexes of 21-nucleotide RNAs mediate RNA interference in cultured mammalian cells. *Nature*, *411*(6836), 494-498. https://doi.org/10.1038/35078107

Fainstein, N., Dori, D., Frid, K., Fritz, A. T., Shapiro, I., Gabizon, R., & Ben-Hur, T. (2016). Chronic Progressive Neurodegeneration in a Transgenic Mouse Model of Prion Disease [Original Research]. *Frontiers in Neuroscience*, *10*. https://doi.org/10.3389/fnins.2016.00510

Fernandez-Borges, N., Brun, A., Whitton, J. L., Parra, B., Diaz-San Segundo, F., Salguero, F. J., Torres, J. M., & Rodriguez, F. (2006). DNA vaccination can break immunological tolerance to PrP in wild-type mice and attenuates prion disease after intracerebral challenge. *J Virol*, *80*(20), 9970-9976. https://doi.org/10.1128/jvi.01210-06

Finkel, R. S., Mercuri, E., Darras, B. T., Connolly, A. M., Kuntz, N. L., Kirschner, J., Chiriboga, C. A., Saito, K., Servais, L., Tizzano, E., Topaloglu, H., Tulinius, M., Montes, J., Glanzman, A. M., Bishop, K., Zhong, Z. J., Gheuens, S., Bennett, C. F., Schneider, E., . . . De Vivo, D. C. (2017). Nusinersen versus Sham Control in Infantile-Onset Spinal Muscular Atrophy. *N Engl J Med*, *377*(18), 1723-1732. https://doi.org/10.1056/NEJMoa1702752

Forsström, B., Axnäs, B. B., Rockberg, J., Danielsson, H., Bohlin, A., & Uhlen, M. (2015). Dissecting antibodies with regards to linear and conformational epitopes. *PLoS One*, *10*(3), e0121673-e0121673. https://doi.org/10.1371/journal.pone.0121673

Freund, J., & McDermott, K. (1942). Sensitization to Horse Serum by Means of Adjuvants. *Proceedings of the Society for Experimental Biology and Medicine*, *49*(4), 548-553. https://doi.org/10.3181/00379727-49-13625

Friedman-Levi, Y., Meiner, Z., Canello, T., Frid, K., Kovacs, G. G., Budka, H., Avrahami, D., & Gabizon, R. (2011). Fatal prion disease in a mouse model of genetic E200K Creutzfeldt-Jakob disease. *PLoS Pathog*, *7*(11), e1002350. https://doi.org/10.1371/journal.ppat.1002350

Frontzek, K., & Aguzzi, A. (2020). Recent developments in antibody therapeutics against prion disease. *Emerg Top Life Sci*, *4*(2), 169-173. https://doi.org/10.1042/etls20200002

Gabizon, R., McKinley, M. P., Groth, D., & Prusiner, S. B. (1988). Immunoaffinity purification and neutralization of scrapie prion infectivity. *Proc Natl Acad Sci U S A*, *85*(18), 6617-6621. https://doi.org/10.1073/pnas.85.18.6617

Gajdusek, D. C., Gibbs, C. J., & Alpers, M. (1966). Experimental transmission of a Kuru-like syndrome to chimpanzees. *Nature*, *209*(5025), 794-796. https://doi.org/10.1038/209794a0

Gajdusek, D. C., & Zigas, V. (1957). Degenerative disease of the central nervous system in New Guinea; the endemic occurrence of kuru in the native population. *N Engl J Med*, *257*(20), 974-978. https://doi.org/10.1056/nejm195711142572005

Gajdusek, D. C., & Zigas, V. (1959). Kuru; clinical, pathological and epidemiological study of an acute progressive degenerative disease of the central nervous system among natives of the Eastern Highlands of New Guinea. *Am J Med*, *26*(3), 442-469. https://doi.org/10.1016/0002-9343(59)90251-7

Gambetti, P., Dong, Z., Yuan, J., Xiao, X., Zheng, M., Alshekhlee, A., Castellani, R., Cohen, M., Barria, M. A., Gonzalez-Romero, D., Belay, E. D., Schonberger, L. B., Marder, K., Harris, C., Burke, J. R., Montine, T., Wisniewski, T., Dickson, D. W., Soto, C., . . . Zou, W.-Q. (2008). A novel human disease with abnormal prion protein sensitive to protease. *Annals of Neurology*, *63*(6), 697-708. https://doi.org/https://doi.org/10.1002/ana.21420

Gambetti, P., Kong, Q., Zou, W., Parchi, P., & Chen, S. G. (2003). Sporadic and familial CJD: classification and characterisation. *Br Med Bull*, *66*, 213-239. https://doi.org/10.1093/bmb/66.1.213

Gendoo, D. M., & Harrison, P. M. (2011). Origins and evolution of the HET-s prion-forming protein: searching for other amyloid-forming solenoids. *PLoS One*, *6*(11), e27342. https://doi.org/10.1371/journal.pone.0027342

Gerstmann, J. (1928). Uber ein noch nicht beschriebenes Reflexphanomen bei einer Erkrankung des zerebellaren Systems. *Wein Medizin Wochenschr*, *78*, 906-908.

Gerstmann, J. (1936). Uber eine eigenartige hereditar-familiare Erkrankung des Zentralnervensystems. Zugleich ein Beitrag zur Frage des vorzeitigen lokalen Alterns. *Z Gesamte Neurol Psychiatr*, *154*, 736-762.

Geschwind, M. D., Kuo, A. L., Wong, K. S., Haman, A., Devereux, G., Raudabaugh, B. J., Johnson, D. Y., Torres-Chae, C. C., Finley, R., Garcia, P., Thai, J. N., Cheng, H. Q., Neuhaus, J. M., Forner, S. A., Duncan, J. L., Possin, K. L., Dearmond, S. J., Prusiner, S. B., & Miller, B. L. (2013). Quinacrine treatment trial for sporadic Creutzfeldt-Jakob disease. *Neurology*, *81*(23), 2015-2023. https://doi.org/10.1212/WNL.0b013e3182a9f3b4

Ghaemmaghami, S., Ahn, M., Lessard, P., Giles, K., Legname, G., DeArmond, S. J., & Prusiner, S. B. (2009). Continuous quinacrine treatment results in the formation of drug-resistant prions. *PLoS Pathog*, *5*(11), e1000673. https://doi.org/10.1371/journal.ppat.1000673

Gibbs, C. J., Jr., Gajdusek, D. C., Asher, D. M., Alpers, M. P., Beck, E., Daniel, P. M., & Matthews, W. B. (1968). Creutzfeldt-Jakob disease (spongiform encephalopathy): transmission to the chimpanzee. *Science*, *161*(3839), 388-389. https://doi.org/10.1126/science.161.3839.388

Giles, K., Berry, D. B., Condello, C., Hawley, R. C., Gallardo-Godoy, A., Bryant, C., Oehler, A., Elepano, M., Bhardwaj, S., Patel, S., Silber, B. M., Guan, S., DeArmond, S. J., Renslo, A. R., & Prusiner, S. B. (2015). Different 2-

Aminothiazole Therapeutics Produce Distinct Patterns of Scrapie Prion Neuropathology in Mouse Brains. *J Pharmacol Exp Ther*, *355*(1), 2-12. https://doi.org/10.1124/jpet.115.224659

Glenny, A. T. (1926). The antigenic value of toxoid precipitated by potassium alum. *J Pathol Bacteriol*, *29*, 38-40.

Goldfarb, L. G., Brown, P., Mitrovà, E., Cervenáková, L., Goldin, L., Korczyn, A. D., Chapman, J., Gálvez, S., Cartier, L., Rubenstein, R., & et al. (1991). Creutzfeldt-Jacob disease associated with the PRNP codon 200Lys mutation: an analysis of 45 families. *Eur J Epidemiol*, *7*(5), 477-486. https://doi.org/10.1007/bf00143125

Goldfarb, L. G., Petersen, R. B., Tabaton, M., Brown, P., LeBlanc, A. C., Montagna, P., Cortelli, P., Julien, J., Vital, C., Pendelbury, W. W., & et al. (1992). Fatal familial insomnia and familial Creutzfeldt-Jakob disease: disease phenotype determined by a DNA polymorphism. *Science*, *258*(5083), 806-808. https://doi.org/10.1126/science.1439789

Goldgaber, D., Goldfarb, L. G., Brown, P., Asher, D. M., Brown, W. T., Lin, S., Teener, J. W., Feinstone, S. M., Rubenstein, R., Kascsak, R. J., & et al. (1989). Mutations in familial Creutzfeldt-Jakob disease and Gerstmann-Sträussler-Scheinker's syndrome. *Exp Neurol*, *106*(2), 204-206. https://doi.org/10.1016/0014-4886(89)90095-2

Goldmann, W. (2008). PrP genetics in ruminant transmissible spongiform encephalopathies. *Veterinary research*, *39*(4), 1-14.

Goldmann, W., Hunter, N., Smith, G., Foster, J., & Hope, J. (1994). PrP genotype and agent effects in scrapie: change in allelic interaction with different isolates of agent in sheep, a natural host of scrapie. *Journal of General Virology*, *75*(5), 989-995.

Goñi, F., Knudsen, E., Schreiber, F., Scholtzova, H., Pankiewicz, J., Carp, R., Meeker, H. C., Rubenstein, R., Brown, D. R., Sy, M. S., Chabalgoity, J. A., Sigurdsson, E. M., & Wisniewski, T. (2005). Mucosal vaccination delays or prevents prion infection via an oral route. *Neuroscience*, *133*(2), 413-421. https://doi.org/https://doi.org/10.1016/j.neuroscience.2005.02.031

Goñi, F., Mathiason, C. K., Yim, L., Wong, K., Hayes-Klug, J., Nalls, A., Peyser, D., Estevez, V., Denkers, N., Xu, J., Osborn, D. A., Miller, K. V., Warren, R. J., Brown, D. R., Chabalgoity, J. A., Hoover, E. A., & Wisniewski, T. (2015). Mucosal immunization with an attenuated Salmonella vaccine partially protects white-tailed deer from chronic wasting disease. *Vaccine*, *33*(5), 726-733. https://doi.org/10.1016/j.vaccine.2014.11.035

Goñi, F., Prelli, F., Schreiber, F., Scholtzova, H., Chung, E., Kascsak, R., Brown, D. R., Sigurdsson, E. M., Chabalgoity, J. A., & Wisniewski, T. (2008). High titers of mucosal and systemic anti-PrP antibodies abrogate oral prion infection in mucosal-

vaccinated mice. *Neuroscience*, *153*(3), 679-686. https://doi.org/10.1016/j.neuroscience.2008.02.051

Griffith, J. S. (1967). Nature of the Scrapie Agent: Self-replication and Scrapie. *Nature*, *215*(5105), 1043-1044. https://doi.org/10.1038/2151043a0

Groveman, B. R., Dolan, M. A., Taubner, L. M., Kraus, A., Wickner, R. B., & Caughey, B. (2014). Parallel In-register Intermolecular β-Sheet Architectures for Prion-seeded Prion Protein (PrP) Amyloids*. *Journal of Biological Chemistry*, *289*(35), 24129-24142. https://doi.org/https://doi.org/10.1074/jbc.M114.578344

Guillot-Sestier, M. V., Sunyach, C., Druon, C., Scarzello, S., & Checler, F. (2009). The alpha-secretase-derived N-terminal product of cellular prion, N1, displays neuroprotective function in vitro and in vivo. *J Biol Chem*, *284*(51), 35973-35986. https://doi.org/10.1074/jbc.M109.051086

Guy, B. (2007). The perfect mix: recent progress in adjuvant research. *Nat Rev Microbiol*, *5*(7), 505-517. https://doi.org/10.1038/nrmicro1681

Hadlow, W. J. (1959). Scrapie and kuru. *Scrapie and Kuru.*, 289-290.

Haïk, S., Marcon, G., Mallet, A., Tettamanti, M., Welaratne, A., Giaccone, G., Azimi, S., Pietrini, V., Fabreguettes, J. R., Imperiale, D., Cesaro, P., Buffa, C., Aucan, C., Lucca, U., Peckeu, L., Suardi, S., Tranchant, C., Zerr, I., Houillier, C., . . . Tagliavini, F. (2014). Doxycycline in Creutzfeldt-Jakob disease: a phase 2, randomised, double-blind, placebo-controlled trial. *Lancet Neurol*, *13*(2), 150-158. https://doi.org/10.1016/s1474-4422(13)70307-7

Hallinan, G. I., Ozcan, K. A., Hoq, M. R., Cracco, L., Vago, F. S., Bharath, S. R., Li, D., Jacobsen, M., Doud, E. H., Mosley, A. L., Fernandez, A., Garringer, H. J., Jiang, W., Ghetti, B., & Vidal, R. (2022). Cryo-EM structures of prion protein filaments from Gerstmann-Sträussler-Scheinker disease. *Acta Neuropathol*, *144*(3), 509-520. https://doi.org/10.1007/s00401-022-02461-0

Hannaoui, S., Zemlyankina, I., Chang, S. C., Arifin, M. I., Béringue, V., McKenzie, D., Schatzl, H. M., & Gilch, S. (2022). Transmission of cervid prions to humanized mice demonstrates the zoonotic potential of CWD. *Acta Neuropathol*, *144*(4), 767-784. https://doi.org/10.1007/s00401-022-02482-9

Hara, H., & Sakaguchi, S. (2020). N-Terminal Regions of Prion Protein: Functions and Roles in Prion Diseases. *Int J Mol Sci*, *21*(17). https://doi.org/10.3390/ijms21176233

Hartl, F. U. (2017). Protein Misfolding Diseases. *Annual Review of Biochemistry*, *86*(1), 21-26. https://doi.org/10.1146/annurev-biochem-061516-044518

Heppner, F. L., & Aguzzi, A. (2003). Prion Diseases. In *eLS*. https://doi.org/https://doi.org/10.1038/npg.els.0000428

Herrmann, U. S., Sonati, T., Falsig, J., Reimann, R. R., Dametto, P., O'Connor, T., Li, B., Lau, A., Hornemann, S., Sorce, S., Wagner, U., Sanoudou, D., & Aguzzi, A. (2015). Prion infections and anti-PrP antibodies trigger converging neurotoxic pathways. *PLoS Pathog*, *11*(2), e1004662. https://doi.org/10.1371/journal.ppat.1004662

Hewitt, P. E., Llewelyn, C. A., Mackenzie, J., & Will, R. G. (2006). Creutzfeldt-Jakob disease and blood transfusion: results of the UK Transfusion Medicine Epidemiological Review study. *Vox Sang*, *91*(3), 221-230. https://doi.org/10.1111/j.1423-0410.2006.00833.x

Honda, H., Sasaki, K., Minaki, H., Masui, K., Suzuki, S. O., Doh-Ura, K., & Iwaki, T. (2012). Protease-resistant PrP and PrP oligomers in the brain in human prion diseases after intraventricular pentosan polysulfate infusion. *Neuropathology*, *32*(2), 124-132. https://doi.org/10.1111/j.1440-1789.2011.01245.x

Hoyt, F., Standke, H. G., Artikis, E., Schwartz, C. L., Hansen, B., Li, K., Hughson, A. G., Manca, M., Thomas, O. R., Raymond, G. J., Race, B., Baron, G. S., Caughey, B., & Kraus, A. (2022). Cryo-EM structure of anchorless RML prion reveals variations in shared motifs between distinct strains. *Nature Communications*, *13*(1), 4005. https://doi.org/10.1038/s41467-022-30458-6

Hsiao, K., Baker, H. F., Crow, T. J., Poulter, M., Owen, F., Terwilliger, J. D., Westaway, D., Ott, J., & Prusiner, S. B. (1989). Linkage of a prion protein missense variant to Gerstmann-Sträussler syndrome. *Nature*, *338*(6213), 342-345. https://doi.org/10.1038/338342a0

Hsiao, K. K., Scott, M., Foster, D., Groth, D. F., DeArmond, S. J., & Prusiner, S. B. (1990). Spontaneous Neurodegeneration in Transgenic Mice with Mutant Prion Protein. *Science*, *250*(4987), 1587-1590. http://www.jstor.org.login.ezproxy.library.ualberta.ca/stable/2878347

Huor, A., Espinosa, J. C., Vidal, E., Cassard, H., Douet, J. Y., Lugan, S., Aron, N., Marín-Moreno, A., Lorenzo, P., Aguilar-Calvo, P., Badiola, J., Bolea, R., Pumarola, M., Benestad, S. L., Orge, L., Thackray, A. M., Bujdoso, R., Torres, J. M., & Andreoletti, O. (2019). The emergence of classical BSE from atypical/Nor98 scrapie. *Proc Natl Acad Sci U S A*, *116*(52), 26853-26862. https://doi.org/10.1073/pnas.1915737116

Ingrosso, L., Ladogana, A., & Pocchiari, M. (1995). Congo red prolongs the incubation period in scrapie-infected hamsters. *J Virol*, *69*(1), 506-508. https://doi.org/10.1128/jvi.69.1.506-508.1995

Isaacs, A., Li, Z., Cheung, S. T. M., Wijesundara, D. K., McMillan, C. L. D., Modhiran, N., Young, P. R., Ranasinghe, C., Watterson, D., & Chappell, K. J. (2021).

Adjuvant Selection for Influenza and RSV Prefusion Subunit Vaccines. *Vaccines*, *9*(2), 71. https://www.mdpi.com/2076-393X/9/2/71

Ishibashi, D., Yamanaka, H., Mori, T., Yamaguchi, N., Yamaguchi, Y., Nishida, N., & Sakaguchi, S. (2011). Antigenic mimicry-mediated anti-prion effects induced by bacterial enzyme succinylarginine dihydrolase in mice. *Vaccine*, *29*(50), 9321-9328. https://doi.org/10.1016/j.vaccine.2011.10.017

Ishibashi, D., Yamanaka, H., Yamaguchi, N., Yoshikawa, D., Nakamura, R., Okimura, N., Yamaguchi, Y., Shigematsu, K., Katamine, S., & Sakaguchi, S. (2007). Immunization with recombinant bovine but not mouse prion protein delays the onset of disease in mice inoculated with a mouse-adapted prion. *Vaccine*, *25*(6), 985-992. https://doi.org/10.1016/j.vaccine.2006.09.078

Jakob, A. (1921). Über eigenartige erkrankungen des zentralnervensystems mit bemerkenswertem anatomischen befunde. *Zeitschrift für die gesamte Neurologie und Psychiatrie*, *64*(1), 147-228. https://doi.org/10.1007/BF02870932

Janeway, C., & Travers, P. (1994). *Immunobiology: The Immune System in Health and Disease*. Current Biology Limited. https://books.google.ca/books?id=fTJnQgAACAAJ

Jarius, C., Kovacs, G. G., Belay, G., Hainfellner, J. A., Mitrova, E., & Budka, H. (2003). Distinctive cerebellar immunoreactivity for the prion protein in familial (E200K) Creutzfeldt-Jakob disease. *Acta Neuropathol*, *105*(5), 449-454. https://doi.org/10.1007/s00401-002-0664-z

Jenner, E. (1799). History of the Inoculation of the Cow-Pox: Further Observations on the Variolæ Vaccinæ, or Cow-Pox. *Med Phys J*, *1*(4), 313-318.

Jones, E. M., Wu, B., Surewicz, K., Nadaud, P. S., Helmus, J. J., Chen, S., Jaroniec, C. P., & Surewicz, W. K. (2011). Structural polymorphism in amyloids: new insights from studies with Y145Stop prion protein fibrils. *J Biol Chem*, *286*(49), 42777-42784. https://doi.org/10.1074/jbc.M111.302539

Jucker, M., & Walker, L. C. (2013). Self-propagation of pathogenic protein aggregates in neurodegenerative diseases. *Nature*, *501*(7465), 45-51. https://doi.org/10.1038/nature12481

Karapetyan, Y. E., Sferrazza, G. F., Zhou, M., Ottenberg, G., Spicer, T., Chase, P., Fallahi, M., Hodder, P., Weissmann, C., & Lasmézas, C. I. (2013). Unique drug screening approach for prion diseases identifies tacrolimus and astemizole as antiprion agents. *Proc Natl Acad Sci U S A*, *110*(17), 7044-7049. https://doi.org/10.1073/pnas.1303510110

Kensil, C. R., Patel, U., Lennick, M., & Marciani, D. (1991). Separation and characterization of saponins with adjuvant activity from Quillaja saponaria Molina cortex. *J Immunol*, *146*(2), 431-437.

Kocisko, D. A., Caughey, W. S., Race, R. E., Roper, G., Caughey, B., & Morrey, J. D. (2006). A porphyrin increases survival time of mice after intracerebral prion infection. *Antimicrob Agents Chemother*, *50*(2), 759-761. https://doi.org/10.1128/aac.50.2.759-761.2006

Kool, M., Fierens, K., & Lambrecht, B. N. (2012). Alum adjuvant: some of the tricks of the oldest adjuvant. *J Med Microbiol*, *61*(Pt 7), 927-934. https://doi.org/10.1099/jmm.0.038943-0

Kossel, H. (1893). Ueber die Behandlung diphtheriekranker Kinder mit „Diphtherieheilserum". *DMW-Deutsche Medizinische Wochenschrift*, *19*(17), 392-393.

Kraus, A., Hoyt, F., Schwartz, C. L., Hansen, B., Artikis, E., Hughson, A. G., Raymond, G. J., Race, B., Baron, G. S., & Caughey, B. (2021). High-resolution structure and strain comparison of infectious mammalian prions. *Mol Cell*, *81*(21), 4540-4551.e4546. https://doi.org/10.1016/j.molcel.2021.08.011

Küffer, A., Lakkaraju, A. K., Mogha, A., Petersen, S. C., Airich, K., Doucerain, C., Marpakwar, R., Bakirci, P., Senatore, A., Monnard, A., Schiavi, C., Nuvolone, M., Grosshans, B., Hornemann, S., Bassilana, F., Monk, K. R., & Aguzzi, A. (2016). The prion protein is an agonistic ligand of the G protein-coupled receptor Adgrg6. *Nature*, *536*(7617), 464-468. https://doi.org/10.1038/nature19312

Kurt, T. D., Jiang, L., Fernández-Borges, N., Bett, C., Liu, J., Yang, T., Spraker, T. R., Castilla, J., Eisenberg, D., Kong, Q., & Sigurdson, C. J. (2015). Human prion protein sequence elements impede cross-species chronic wasting disease transmission. *J Clin Invest*, *125*(4), 1485-1496. https://doi.org/10.1172/jci79408

Lancaster, E., & Dalmau, J. (2012). Neuronal autoantigens--pathogenesis, associated disorders and antibody testing. *Nat Rev Neurol*, *8*(7), 380-390. https://doi.org/10.1038/nrneurol.2012.99

Lee, W. S., Wheatley, A. K., Kent, S. J., & DeKosky, B. J. (2020). Antibody-dependent enhancement and SARS-CoV-2 vaccines and therapies. *Nature Microbiology*, *5*(10), 1185-1191. https://doi.org/10.1038/s41564-020-00789-5

Lee, Y. J., & Baskakov, I. V. (2014). The cellular form of the prion protein guides the differentiation of human embryonic stem cells into neuron-, oligodendrocyte-, and astrocyte-committed lineages. *Prion*, *8*(3), 266-275. https://doi.org/10.4161/pri.32079

Lefebvre-Roque, M., Kremmer, E., Gilch, S., Zou, W. Q., Féraudet, C., Gilles, C. M., Salès, N., Grassi, J., Gambetti, P., Baron, T., Schätzl, H., & Lasmézas, C. I. (2007). Toxic effects of intracerebral PrP antibody administration during the course of BSE infection in mice. *Prion*, *1*(3), 198-206. https://doi.org/10.4161/pri.1.3.4870

Lisle, E. (1757). *Observations in husbandry* (Vol. 1). J. Hughes.

Llewelyn, C. A., Hewitt, P. E., Knight, R. S., Amar, K., Cousens, S., Mackenzie, J., & Will, R. G. (2004). Possible transmission of variant Creutzfeldt-Jakob disease by blood transfusion. *Lancet*, *363*(9407), 417-421. https://doi.org/10.1016/s0140-6736(04)15486-x

Llorens, F., Carulla, P., Villa, A., Torres, J. M., Fortes, P., Ferrer, I., & del Río, J. A. (2013). PrP(C) regulates epidermal growth factor receptor function and cell shape dynamics in Neuro2a cells. *J Neurochem*, *127*(1), 124-138. https://doi.org/10.1111/jnc.12283

Lotze, M. T., Robinson, B. W. S., June, C. H., & Whiteside, T. L. (2013). 77 - Tumor immunotherapy. In R. R. Rich, T. A. Fleisher, W. T. Shearer, H. W. Schroeder, A. J. Frew, & C. M. Weyand (Eds.), *Clinical Immunology (Fourth Edition)* (pp. 935-945). Elsevier. https://doi.org/https://doi.org/10.1016/B978-0-7234-3691-1.00091-X

Loubet, D., Dakowski, C., Pietri, M., Pradines, E., Bernard, S., Callebert, J., Ardila-Osorio, H., Mouillet-Richard, S., Launay, J. M., Kellermann, O., & Schneider, B. (2012). Neuritogenesis: the prion protein controls β1 integrin signaling activity. *Faseb j*, *26*(2), 678-690. https://doi.org/10.1096/fj.11-185579

Lugaresi, E., Medori, R., Montagna, P., Baruzzi, A., Cortelli, P., Lugaresi, A., Tinuper, P., Zucconi, M., & Gambetti, P. (1986). Fatal familial insomnia and dysautonomia with selective degeneration of thalamic nuclei. *N Engl J Med*, *315*(16), 997-1003. https://doi.org/10.1056/nejm198610163151605

Maddelein, M. L., Dos Reis, S., Duvezin-Caubet, S., Coulary-Salin, B., & Saupe, S. J. (2002). Amyloid aggregates of the HET-s prion protein are infectious. *Proc Natl Acad Sci U S A*, *99*(11), 7402-7407. https://doi.org/10.1073/pnas.072199199

Magri, G., Clerici, M., Dall'Ara, P., Biasin, M., Caramelli, M., Casalone, C., Giannino, M. L., Longhi, R., Piacentini, L., Della Bella, S., Gazzuola, P., Martino, P. A., Della Bella, S., Pollera, C., Puricelli, M., Servida, F., Crescio, I., Boasso, A., Ponti, W., & Poli, G. (2005). Decrease in pathology and progression of scrapie after immunisation with synthetic prion protein peptides in hamsters. *Vaccine*, *23*(22), 2862-2868. https://doi.org/10.1016/j.vaccine.2004.11.067

Mallucci, G., Dickinson, A., Linehan, J., Klöhn, P. C., Brandner, S., & Collinge, J. (2003). Depleting neuronal PrP in prion infection prevents disease and reverses spongiosis. *Science*, *302*(5646), 871-874. https://doi.org/10.1126/science.1090187

Manetto, V., Medori, R., Cortelli, P., Montagna, P., Tinuper, P., Baruzzi, A., Rancurel, G., Hauw, J. J., Vanderhaeghen, J. J., Mailleux, P., & et al. (1992). Fatal familial insomnia: clinical and pathologic study of five new cases. *Neurology*, *42*(2), 312-319. https://doi.org/10.1212/wnl.42.2.312

Manka, S. W., Zhang, W., Wenborn, A., Betts, J., Joiner, S., Saibil, H. R., Collinge, J., & Wadsworth, J. D. F. (2022). 2.7 Å cryo-EM structure of ex vivo RML prion fibrils. *Nat Commun*, *13*(1), 4004. https://doi.org/10.1038/s41467-022-30457-7

Marín-Moreno, A., Espinosa, J. C., & Torres, J. M. (2020). Transgenic mouse models for the study of prion diseases. *Prog Mol Biol Transl Sci*, *175*, 147-177. https://doi.org/10.1016/bs.pmbts.2020.08.007

Marsh, R. F., Kincaid, A. E., Bessen, R. A., & Bartz, J. C. (2005). Interspecies transmission of chronic wasting disease prions to squirrel monkeys (Saimiri sciureus). *J Virol*, *79*(21), 13794-13796. https://doi.org/10.1128/jvi.79.21.13794-13796.2005

Masters, C. L., Gajdusek, D. C., & Gibbs, C. J., Jr. (1981). Creutzfeldt-Jakob disease virus isolations from the Gerstmann-Sträussler syndrome with an analysis of the various forms of amyloid plaque deposition in the virus-induced spongiform encephalopathies. *Brain*, *104*(3), 559-588. https://doi.org/10.1093/brain/104.3.559

Mathews, J., Glasse, R., & Lindenbaum, S. (1968). KURU AND CANNIBALISM. *The Lancet*, *292*(7565), 449-452. https://doi.org/https://doi.org/10.1016/S0140-6736(68)90482-0

Mathiason, C. K. (2017). Chapter Twelve - Scrapie, CWD, and Transmissible Mink Encephalopathy. In G. Legname & S. Vanni (Eds.), *Progress in Molecular Biology and Translational Science* (Vol. 150, pp. 267-292). Academic Press. https://doi.org/https://doi.org/10.1016/bs.pmbts.2017.07.009

Mawhinney, S., Pape, W. J., Forster, J. E., Anderson, C. A., Bosque, P., & Miller, M. W. (2006). Human prion disease and relative risk associated with chronic wasting disease. *Emerg Infect Dis*, *12*(10), 1527-1535. https://doi.org/10.3201/eid1210.060019

Mead, S., Khalili-Shirazi, A., Potter, C., Mok, T., Nihat, A., Hyare, H., Canning, S., Schmidt, C., Campbell, T., Darwent, L., Muirhead, N., Ebsworth, N., Hextall, P., Wakeling, M., Linehan, J., Libri, V., Williams, B., Jaunmuktane, Z., Brandner, S., . . . Collinge, J. (2022). Prion protein monoclonal antibody (PRN100) therapy for Creutzfeldt-Jakob disease: evaluation of a first-in-human treatment programme. *Lancet Neurol*, *21*(4), 342-354. https://doi.org/10.1016/s1474-4422(22)00082-5

Medori, R., Tritschler, H. J., LeBlanc, A., Villare, F., Manetto, V., Chen, H. Y., Xue, R., Leal, S., Montagna, P., Cortelli, P., & et al. (1992). Fatal familial insomnia, a prion disease with a mutation at codon 178 of the prion protein gene. *N Engl J Med*, *326*(7), 444-449. https://doi.org/10.1056/nejm199202133260704

Michaels, T. C. T., Šarić, A., Habchi, J., Chia, S., Meisl, G., Vendruscolo, M., Dobson, C. M., & Knowles, T. P. J. (2018). Chemical Kinetics for Bridging Molecular Mechanisms and Macroscopic Measurements of Amyloid Fibril Formation. *Annual*

Review of Physical Chemistry, *69*(1), 273-298. https://doi.org/10.1146/annurev-physchem-050317-021322

Minikel, E. V., Zhao, H. T., Le, J., O'Moore, J., Pitstick, R., Graffam, S., Carlson, G. A., Kavanaugh, M. P., Kriz, J., Kim, J. B., Ma, J., Wille, H., Aiken, J., McKenzie, D., Doh-Ura, K., Beck, M., O'Keefe, R., Stathopoulos, J., Caron, T., . . . Vallabh, S. M. (2020). Prion protein lowering is a disease-modifying therapy across prion disease stages, strains and endpoints. *Nucleic Acids Res*, *48*(19), 10615-10631. https://doi.org/10.1093/nar/gkaa616

Moda, F., Vimercati, C., Campagnani, I., Ruggerone, M., Giaccone, G., Morbin, M., Zentilin, L., Giacca, M., Zucca, I., Legname, G., & Tagliavini, F. (2012). Brain delivery of AAV9 expressing an anti-PrP monovalent antibody delays prion disease in mice. *Prion*, *6*(4), 383-390. https://doi.org/10.4161/pri.20197

Moore, C. B., Guthrie, E. H., Huang, M. T., & Taxman, D. J. (2010). Short hairpin RNA (shRNA): design, delivery, and assessment of gene knockdown. *Methods Mol Biol*, *629*, 141-158. https://doi.org/10.1007/978-1-60761-657-3_10

Moreno, J. A., Halliday, M., Molloy, C., Radford, H., Verity, N., Axten, J. M., Ortori, C. A., Willis, A. E., Fischer, P. M., Barrett, D. A., & Mallucci, G. R. (2013). Oral treatment targeting the unfolded protein response prevents neurodegeneration and clinical disease in prion-infected mice. *Sci Transl Med*, *5*(206), 206ra138. https://doi.org/10.1126/scitranslmed.3006767

Müller, S., Kehm, R., Handermann, M., Jakob, N. J., Bahr, U., Schröder, B., & Darai, G. (2005). Testing the possibility to protect bovine PrPC transgenic Swiss mice against bovine PrPSc infection by DNA vaccination using recombinant plasmid vectors harboring and expressing the complete or partial cDNA sequences of bovine PrPC. *Virus Genes*, *30*(2), 279-296. https://doi.org/10.1007/s11262-004-5634-1

Nazor, K. E., Kuhn, F., Seward, T., Green, M., Zwald, D., Pürro, M., Schmid, J., Biffiger, K., Power, A. M., Oesch, B., Raeber, A. J., & Telling, G. C. (2005). Immunodetection of disease-associated mutant PrP, which accelerates disease in GSS transgenic mice. *The EMBO Journal*, *24*(13), 2472-2480. https://doi.org/10.1038/sj.emboj.7600717

Ness, A., Aiken, J., & McKenzie, D. (2023). Sheep scrapie and deer rabies in England prior to 1800. *Prion*, *17*(1), 7-15. https://doi.org/10.1080/19336896.2023.2166749

Nitschke, C., Flechsig, E., van den Brandt, J., Lindner, N., Lührs, T., Dittmer, U., & Klein, M. A. (2007). Immunisation strategies against prion diseases: prime-boost immunisation with a PrP DNA vaccine containing foreign helper T-cell epitopes does not prevent mouse scrapie. *Vet Microbiol*, *123*(4), 367-376. https://doi.org/10.1016/j.vetmic.2007.03.032

Notari, S., Appleby, B. S., & Gambetti, P. (2018). Chapter 10 - Variably protease-sensitive prionopathy. In M. Pocchiari & J. Manson (Eds.), *Handbook of Clinical Neurology* (Vol. 153, pp. 175-190). Elsevier. https://doi.org/https://doi.org/10.1016/B978-0-444-63945-5.00010-6

Ohsawa, N., Song, C. H., Suzuki, A., Furuoka, H., Hasebe, R., & Horiuchi, M. (2013). Therapeutic effect of peripheral administration of an anti-prion protein antibody on mice infected with prions. *Microbiol Immunol*, *57*(4), 288-297. https://doi.org/10.1111/1348-0421.12037

Otero, A., Velásquez, C. D., Aiken, J., & McKenzie, D. (2021). Chronic wasting disease: a cervid prion infection looming to spillover. *Vet Res*, *52*(1), 115. https://doi.org/10.1186/s13567-021-00986-y

Otto, M., Cepek, L., Ratzka, P., Doehlinger, S., Boekhoff, I., Wiltfang, J., Irle, E., Pergande, G., Ellers-Lenz, B., Windl, O., Kretzschmar, H. A., Poser, S., & Prange, H. (2004). Efficacy of flupirtine on cognitive function in patients with CJD: A double-blind study. *Neurology*, *62*(5), 714-718. https://doi.org/10.1212/01.wnl.0000113764.35026.ef

Palmer, M. S., Dryden, A. J., Hughes, J. T., & Collinge, J. (1991). Homozygous prion protein genotype predisposes to sporadic Creutzfeldt-Jakob disease. *Nature*, *352*(6333), 340-342. https://doi.org/10.1038/352340a0

Parchi, P., Castellani, R., Capellari, S., Ghetti, B., Young, K., Chen, S. G., Farlow, M., Dickson, D. W., Sima, A. A., Trojanowski, J. Q., Petersen, R. B., & Gambetti, P. (1996). Molecular basis of phenotypic variability in sporadic Creutzfeldt-Jakob disease. *Ann Neurol*, *39*(6), 767-778. https://doi.org/10.1002/ana.410390613

Parchi, P., Giese, A., Capellari, S., Brown, P., Schulz-Schaeffer, W., Windl, O., Zerr, I., Budka, H., Kopp, N., Piccardo, P., Poser, S., Rojiani, A., Streichemberger, N., Julien, J., Vital, C., Ghetti, B., Gambetti, P., & Kretzschmar, H. (1999). Classification of sporadic Creutzfeldt-Jakob disease based on molecular and phenotypic analysis of 300 subjects. *Ann Neurol*, *46*(2), 224-233.

Parchi, P., Strammiello, R., Giese, A., & Kretzschmar, H. (2011). Phenotypic variability of sporadic human prion disease and its molecular basis: past, present, and future. *Acta Neuropathol*, *121*(1), 91-112. https://doi.org/10.1007/s00401-010-0779-6

Parchi, P., Strammiello, R., Notari, S., Giese, A., Langeveld, J. P., Ladogana, A., Zerr, I., Roncaroli, F., Cras, P., Ghetti, B., Pocchiari, M., Kretzschmar, H., & Capellari, S. (2009). Incidence and spectrum of sporadic Creutzfeldt-Jakob disease variants with mixed phenotype and co-occurrence of PrPSc types: an updated classification. *Acta Neuropathol*, *118*(5), 659-671. https://doi.org/10.1007/s00401-009-0585-1

Parkin, E. T., Watt, N. T., Hussain, I., Eckman, E. A., Eckman, C. B., Manson, J. C., Baybutt, H. N., Turner, A. J., & Hooper, N. M. (2007). Cellular prion protein

regulates beta-secretase cleavage of the Alzheimer's amyloid precursor protein. *Proc Natl Acad Sci U S A*, *104*(26), 11062-11067. https://doi.org/10.1073/pnas.0609621104

Pasquier, F., Sadowsky, C., Holstein, A., Leterme Gle, P., Peng, Y., Jackson, N., Fox, N. C., Ketter, N., Liu, E., & Ryan, J. M. (2016). Two Phase 2 Multiple Ascending-Dose Studies of Vanutide Cridificar (ACC-001) and QS-21 Adjuvant in Mild-to-Moderate Alzheimer's Disease. *J Alzheimers Dis*, *51*(4), 1131-1143. https://doi.org/10.3233/jad-150376

Peckeu, L., Brandel, J. P., Welaratne, A., Amar, E., Costagliola, D., & Haïk, S. (2020). Factors Influencing the Incubation of an Infectious Form of Creutzfeldt-Jakob Disease. *Clin Infect Dis*, *70*(7), 1487-1490. https://doi.org/10.1093/cid/ciz692

Pilon, J., Loiacono, C., Okeson, D., Lund, S., Vercauteren, K., Rhyan, J., & Miller, L. (2007). Anti-prion activity generated by a novel vaccine formulation. *Neurosci Lett*, *429*(2-3), 161-164. https://doi.org/10.1016/j.neulet.2007.10.015

Pilon, J. L., Rhyan, J. C., Wolfe, L. L., Davis, T. R., McCollum, M. P., O'Rourke, K. I., Spraker, T. R., VerCauteren, K. C., Miller, M. W., Gidlewski, T., Nichols, T. A., Miller, L. A., & Nol, P. (2013). Immunization with a synthetic peptide vaccine fails to protect mule deer (Odocoileus hemionus) from chronic wasting disease. *J Wildl Dis*, *49*(3), 694-698. https://doi.org/10.7589/2012-07-200

Pocchiari, M., Schmittinger, S., & Masullo, C. (1987). Amphotericin B delays the incubation period of scrapie in intracerebrally inoculated hamsters. *J Gen Virol*, *68 (Pt 1)*, 219-223. https://doi.org/10.1099/0022-1317-68-1-219

Poli, G., Martino, P. A., Villa, S., Carcassola, G., Giannino, M. L., Dall'Ara, P., Pollera, C., Iussich, S., Tranquillo, V. M., Bareggi, S., Mantegazza, P., & Ponti, W. (2004). Evaluation of anti-prion activity of congo red and its derivatives in experimentally infected hamsters. *Arzneimittelforschung*, *54*(7), 406-415. https://doi.org/10.1055/s-0031-1296992

Pollera, C., Caramelli, M., Giannino, M. L., Martino, P. A., Puricelli, M., Casalone, C., Gazzuola, P., & Poli, G. (2004). Transmissible Spongiform Encephalopathy (TSE): vaccinal approach using the hamster model. *Vet Res Commun*, *28 Suppl 1*, 303-306. https://doi.org/10.1023/b:verc.0000045432.41774.57

Polymenidou, M., Heppner, F. L., Pellicioli, E. C., Urich, E., Miele, G., Braun, N., Wopfner, F., Schätzl, H. M., Becher, B., & Aguzzi, A. (2004). Humoral immune response to native eukaryotic prion protein correlates with anti-prion protection. *Proc Natl Acad Sci U S A*, *101 Suppl 2*(Suppl 2), 14670-14676. https://doi.org/10.1073/pnas.0404772101

Prusiner, S. B. (1982). Novel proteinaceous infectious particles cause scrapie. *Science*, *216*(4542), 136. https://doi.org/10.1126/science.6801762

Puoti, G., Rossi, G., Giaccone, G., Awan, T., Lievens, P. M., Defanti, C. A., Tagliavini, F., & Bugiani, O. (2000). Polymorphism at codon 129 of PRNP affects the phenotypic expression of Creutzfeldt-Jakob disease linked to E200K mutation. *Ann Neurol*, *48*(2), 269-270.

Race, B., Meade-White, K. D., Miller, M. W., Barbian, K. D., Rubenstein, R., LaFauci, G., Cervenakova, L., Favara, C., Gardner, D., Long, D., Parnell, M., Striebel, J., Priola, S. A., Ward, A., Williams, E. S., Race, R., & Chesebro, B. (2009). Susceptibilities of nonhuman primates to chronic wasting disease. *Emerg Infect Dis*, *15*(9), 1366-1376. https://doi.org/10.3201/eid1509.090253

Race, B., Williams, K., Orrú, C. D., Hughson, A. G., Lubke, L., & Chesebro, B. (2018). Lack of Transmission of Chronic Wasting Disease to Cynomolgus Macaques. *J Virol*, *92*(14). https://doi.org/10.1128/jvi.00550-18

Ramon, G. (1924). Sur la toxine et sur l'anatoxine diphtheriques. *Ann. Inst. Pasteur*, *38*(1), 13.

Raymond, G. J., Bossers, A., Raymond, L. D., O'Rourke, K. I., McHolland, L. E., Bryant, P. K., 3rd, Miller, M. W., Williams, E. S., Smits, M., & Caughey, B. (2000). Evidence of a molecular barrier limiting susceptibility of humans, cattle and sheep to chronic wasting disease. *Embo j*, *19*(17), 4425-4430. https://doi.org/10.1093/emboj/19.17.4425

Reder, A. T., Mednick, A. S., Brown, P., Spire, J. P., Van Cauter, E., Wollmann, R. L., Cervenàkovà, L., Goldfarb, L. G., Garay, A., Ovsiew, F., & et al. (1995). Clinical and genetic studies of fatal familial insomnia. *Neurology*, *45*(6), 1068-1075. https://doi.org/10.1212/wnl.45.6.1068

Reimann, R. R., Sonati, T., Hornemann, S., Herrmann, U. S., Arand, M., Hawke, S., & Aguzzi, A. (2016). Differential Toxicity of Antibodies to the Prion Protein. *PLoS Pathog*, *12*(1), e1005401. https://doi.org/10.1371/journal.ppat.1005401

Requena, J. R., Kristensson, K., Korth, C., Zurzolo, C., Simmons, M., Aguilar-Calvo, P., Aguzzi, A., Andreoletti, O., Benestad, S. L., Böhm, R., Brown, K., Calgua, B., del Río, J. A., Espinosa, J. C., Girones, R., Godsave, S., Hoelzle, L. E., Knittler, M. R., Kuhn, F., . . . Zerr, I. (2016). The Priority position paper: Protecting Europe's food chain from prions. *Prion*, *10*(3), 165-181. https://doi.org/10.1080/19336896.2016.1175801

Requena, J. R., & Wille, H. (2014). The structure of the infectious prion protein. *Prion*, *8*(1), 60-66. https://doi.org/10.4161/pri.28368

Requena, J. R., & Wille, H. (2014). The structure of the infectious prion protein: experimental data and molecular models. *Prion*, *8*(1), 60-66. https://doi.org/10.4161/pri.28368

Riek, R., Hornemann, S., Wider, G., Billeter, M., Glockshuber, R., & Wüthrich, K. (1996). NMR structure of the mouse prion protein domain PrP(121–231). *Nature*, *382*(6587), 180-182. https://doi.org/10.1038/382180a0

Ritchie, D. L., Peden, A. H., & Barria, M. A. (2021). Variant CJD: Reflections a Quarter of a Century on. *Pathogens*, *10*(11), 1413. https://www.mdpi.com/2076-0817/10/11/1413

Roe, K. (2022). NK-cell exhaustion, B-cell exhaustion and T-cell exhaustion-the differences and similarities. *Immunology*, *166*(2), 155-168. https://doi.org/10.1111/imm.13464

Sacquin, A., Bergot, A. S., Aucouturier, P., & Bruley-Rosset, M. (2008). Contribution of antibody and T cell-specific responses to the progression of 139A-scrapie in C57BL/6 mice immunized with prion protein peptides. *J Immunol*, *181*(1), 768-775. https://doi.org/10.4049/jimmunol.181.1.768

Saupe, S. J. (2000). Molecular genetics of heterokaryon incompatibility in filamentous ascomycetes. *Microbiol Mol Biol Rev*, *64*(3), 489-502. https://doi.org/10.1128/mmbr.64.3.489-502.2000

Schenk, D., Barbour, R., Dunn, W., Gordon, G., Grajeda, H., Guido, T., Hu, K., Huang, J., Johnson-Wood, K., Khan, K., Kholodenko, D., Lee, M., Liao, Z., Lieberburg, I., Motter, R., Mutter, L., Soriano, F., Shopp, G., Vasquez, N., . . . Seubert, P. (1999). Immunization with amyloid-beta attenuates Alzheimer-disease-like pathology in the PDAPP mouse. *Nature*, *400*(6740), 173-177. https://doi.org/10.1038/22124

Schmitz, M., Dittmar, K., Llorens, F., Gelpi, E., Ferrer, I., Schulz-Schaeffer, W. J., & Zerr, I. (2017). Hereditary Human Prion Diseases: an Update. *Molecular Neurobiology*, *54*(6), 4138-4149. https://doi.org/10.1007/s12035-016-9918-y

Schulte, S., Sukhova, G. K., & Libby, P. (2008). Genetically programmed biases in Th1 and Th2 immune responses modulate atherogenesis. *The American journal of pathology*, *172*(6), 1500-1508. https://doi.org/10.2353/ajpath.2008.070776

Schwarz, A., Krätke, O., Burwinkel, M., Riemer, C., Schultz, J., Henklein, P., Bamme, T., & Baier, M. (2003). Immunisation with a synthetic prion protein-derived peptide prolongs survival times of mice orally exposed to the scrapie agent. *Neurosci Lett*, *350*(3), 187-189. https://doi.org/10.1016/s0304-3940(03)00907-8

Sellers, R. S. (2017). Translating Mouse Models. *Toxicol Pathol*, *45*(1), 134-145. https://doi.org/10.1177/0192623316675767

Sethi, S., Lipford, G., Wagner, H., & Kretzschmar, H. (2002). Postexposure prophylaxis against prion disease with a stimulator of innate immunity. *Lancet*, *360*(9328), 229-230. https://doi.org/10.1016/s0140-6736(02)09513-2

Seuring, C., Greenwald, J., Wasmer, C., Wepf, R., Saupe, S. J., Meier, B. H., & Riek, R. (2012). The mechanism of toxicity in HET-S/HET-s prion incompatibility. *PLoS Biol*, *10*(12), e1001451. https://doi.org/10.1371/journal.pbio.1001451

Sigurdsson, B. (1954). RIDA, A Chronic Encephalitis of Sheep: With General Remarks on Infections Which Develop Slowly and Some of Their Special Characteristics. *British Veterinary Journal*, *110*(9), 341-354. https://doi.org/https://doi.org/10.1016/S0007-1935(17)50172-4

Sigurdsson, E. M., Brown, D. R., Daniels, M., Kascsak, R. J., Kascsak, R., Carp, R., Meeker, H. C., Frangione, B., & Wisniewski, T. (2002). Immunization delays the onset of prion disease in mice. *Am J Pathol*, *161*(1), 13-17. https://doi.org/10.1016/s0002-9440(10)64151-x

Sigurdsson, E. M., Sy, M. S., Li, R., Scholtzova, H., Kascsak, R. J., Kascsak, R., Carp, R., Meeker, H. C., Frangione, B., & Wisniewski, T. (2003). Anti-prion antibodies for prophylaxis following prion exposure in mice. *Neurosci Lett*, *336*(3), 185-187. https://doi.org/10.1016/s0304-3940(02)01192-8

Slifka, M. K., & Amanna, I. J. (2018). Passive Immunization. *Plotkin's Vaccines*, 84-95.e10. https://doi.org/10.1016/B978-0-323-35761-6.00008-0

Smirnovas, V., Baron, G. S., Offerdahl, D. K., Raymond, G. J., Caughey, B., & Surewicz, W. K. (2011). Structural organization of brain-derived mammalian prions examined by hydrogen-deuterium exchange. *Nat Struct Mol Biol*, *18*(4), 504-506. https://doi.org/10.1038/nsmb.2035

Solassol, J., Crozet, C., Perrier, V., Leclaire, J., Béranger, F., Caminade, A. M., Meunier, B., Dormont, D., Majoral, J. P., & Lehmann, S. (2004). Cationic phosphorus-containing dendrimers reduce prion replication both in cell culture and in mice infected with scrapie. *J Gen Virol*, *85*(Pt 6), 1791-1799. https://doi.org/10.1099/vir.0.19726-0

Sonati, T., Reimann, R. R., Falsig, J., Baral, P. K., O'Connor, T., Hornemann, S., Yaganoglu, S., Li, B., Herrmann, U. S., Wieland, B., Swayampakula, M., Rahman, M. H., Das, D., Kav, N., Riek, R., Liberski, P. P., James, M. N., & Aguzzi, A. (2013). The toxicity of antiprion antibodies is mediated by the flexible tail of the prion protein. *Nature*, *501*(7465), 102-106. https://doi.org/10.1038/nature12402

Song, C. H., Furuoka, H., Kim, C. L., Ogino, M., Suzuki, A., Hasebe, R., & Horiuchi, M. (2008). Effect of intraventricular infusion of anti-prion protein monoclonal antibodies on disease progression in prion-infected mice. *J Gen Virol*, *89*(Pt 6), 1533-1544. https://doi.org/10.1099/vir.0.83578-0

Soto, C., & Estrada, L. D. (2008). Protein Misfolding and Neurodegeneration. *Archives of Neurology*, *65*(2), 184-189. https://doi.org/10.1001/archneurol.2007.56

Spagnolli, G., Rigoli, M., Orioli, S., Sevillano, A. M., Faccioli, P., Wille, H., Biasini, E., & Requena, J. R. (2019). Full atomistic model of prion structure and conversion. *PLoS Pathog*, *15*(7), e1007864. https://doi.org/10.1371/journal.ppat.1007864

Spraker, T. R., Zink, R. R., Cummings, B. A., Wild, M. A., Miller, M. W., & O'Rourke, K. I. (2002). Comparison of histological lesions and immunohistochemical staining of proteinase-resistant prion protein in a naturally occurring spongiform encephalopathy of free-ranging mule deer (Odocoileus hemionus) with those of chronic wasting disease of captive mule deer. *Vet Pathol*, *39*(1), 110-119. https://doi.org/10.1354/vp.39-1-110

Spudich, S., Mastrianni, J. A., Wrensch, M., Gabizon, R., Meiner, Z., Kahana, I., Rosenmann, H., Kahana, E., & Prusiner, S. B. (1995). Complete penetrance of Creutzfeldt-Jakob disease in Libyan Jews carrying the E200K mutation in the prion protein gene. *Mol Med*, *1*(6), 607-613.

Stahl, N., Borchelt, D. R., Hsiao, K., & Prusiner, S. B. (1987). Scrapie prion protein contains a phosphatidylinositol glycolipid. *Cell*, *51*(2), 229-240. https://doi.org/https://doi.org/10.1016/0092-8674(87)90150-4

Staniforth, G. L., & Tuite, M. F. (2012). Chapter 12 - Fungal Prions. In D. B. Teplow (Ed.), *Progress in Molecular Biology and Translational Science* (Vol. 107, pp. 417-456). Academic Press. https://doi.org/https://doi.org/10.1016/B978-0-12-385883-2.00007-2

Striebel, J. F., Race, B., & Chesebro, B. (2013). Prion protein and susceptibility to kainate-induced seizures: genetic pitfalls in the use of PrP knockout mice. *Prion*, *7*(4), 280-285. https://doi.org/10.4161/pri.25738

Strom, A., Wang, G. S., & Scott, F. W. (2011). Impaired glucose tolerance in mice lacking cellular prion protein. *Pancreas*, *40*(2), 229-232. https://doi.org/10.1097/mpa.0b013e3181f7e547

Swerdlow, A. J., Higgins, C. D., Adlard, P., Jones, M. E., & Preece, M. A. (2003). Creutzfeldt-Jakob disease in United Kingdom patients treated with human pituitary growth hormone. *Neurology*, *61*(6), 783-791. https://doi.org/10.1212/01.wnl.0000084000.27403.15

Tabrizi, S. J., Leavitt, B. R., Landwehrmeyer, G. B., Wild, E. J., Saft, C., Barker, R. A., Blair, N. F., Craufurd, D., Priller, J., Rickards, H., Rosser, A., Kordasiewicz, H. B., Czech, C., Swayze, E. E., Norris, D. A., Baumann, T., Gerlach, I., Schobel, S. A., Paz, E., . . . Lane, R. M. (2019). Targeting Huntingtin Expression in Patients with Huntington's Disease. *N Engl J Med*, *380*(24), 2307-2316. https://doi.org/10.1056/NEJMoa1900907

Terzano, M. G., Montanari, E., Calzetti, S., Mancia, D., & Lechi, A. (1983). The effect of amantadine on arousal and EEG patterns in Creutzfeldt-Jakob disease. *Arch Neurol*, *40*(9), 555-559. https://doi.org/10.1001/archneur.1983.04050080055010

Tobler, I., Gaus, S. E., Deboer, T., Achermann, P., Fischer, M., Rülicke, T., Moser, M., Oesch, B., McBride, P. A., & Manson, J. C. (1996). Altered circadian activity rhythms and sleep in mice devoid of prion protein. *Nature*, *380*(6575), 639-642. https://doi.org/10.1038/380639a0

Tulone, C., Tsang, J., Prokopowicz, Z., Grosvenor, N., & Chain, B. (2007). Natural cathepsin E deficiency in the immune system of C57BL/6J mice. *Immunogenetics*, *59*(12), 927-935. https://doi.org/10.1007/s00251-007-0256-0

Tycko, R., Savtchenko, R., Ostapchenko, V. G., Makarava, N., & Baskakov, I. V. (2010). The α-helical C-terminal domain of full-length recombinant PrP converts to an in-register parallel β-sheet structure in PrP fibrils: evidence from solid state nuclear magnetic resonance. *Biochemistry*, *49*(44), 9488-9497. https://doi.org/10.1021/bi1013134

Umetsu, D. T., & DeKruyff, R. H. (1997). Th1 and Th2 CD4+ cells in human allergic diseases. *Journal of Allergy and Clinical Immunology*, *100*(1), 1-6. https://doi.org/https://doi.org/10.1016/S0091-6749(97)70186-6

Vallabh, S. M., Minikel, E. V., Schreiber, S. L., & Lander, E. S. (2020). Towards a treatment for genetic prion disease: trials and biomarkers. *The Lancet Neurology*, *19*(4), 361-368. https://doi.org/https://doi.org/10.1016/S1474-4422(19)30403-X

Vázquez-Fernández, E., Alonso, J., Pastrana, M. A., Ramos, A., Stitz, L., Vidal, E., Dynin, I., Petsch, B., Silva, C. J., & Requena, J. R. (2012). Structural organization of mammalian prions as probed by limited proteolysis. *PLoS One*, *7*(11), e50111. https://doi.org/10.1371/journal.pone.0050111

Vázquez-Fernández, E., Vos, M. R., Afanasyev, P., Cebey, L., Sevillano, A. M., Vidal, E., Rosa, I., Renault, L., Ramos, A., Peters, P. J., Fernández, J. J., van Heel, M., Young, H. S., Requena, J. R., & Wille, H. (2016). The Structural Architecture of an Infectious Mammalian Prion Using Electron Cryomicroscopy. *PLoS Pathog*, *12*(9), e1005835. https://doi.org/10.1371/journal.ppat.1005835

Waddell, L., Greig, J., Mascarenhas, M., Otten, A., Corrin, T., & Hierlihy, K. (2018). Current evidence on the transmissibility of chronic wasting disease prions to humans-A systematic review. *Transbound Emerg Dis*, *65*(1), 37-49. https://doi.org/10.1111/tbed.12612

Wadsworth, J. D., Asante, E. A., & Collinge, J. (2010). Review: contribution of transgenic models to understanding human prion disease. *Neuropathol Appl Neurobiol*, *36*(7), 576-597. https://doi.org/10.1111/j.1365-2990.2010.01129.x

Wasmer, C., Lange, A., Van Melckebeke, H., Siemer, A. B., Riek, R., & Meier, B. H. (2008). Amyloid Fibrils of the HET-s(218–289) Prion Form a β Solenoid with a Triangular Hydrophobic Core. *Science*, *319*(5869), 1523. https://doi.org/10.1126/science.1151839

Watts, J. C., Bourkas, M. E. C., & Arshad, H. (2018). The function of the cellular prion protein in health and disease. *Acta Neuropathol*, *135*(2), 159-178. https://doi.org/10.1007/s00401-017-1790-y

Weissmann, C., & Aguzzi, A. (1997). Bovine spongiform encephalopathy and early onset variant Creutzfeldt-Jakob disease. *Curr Opin Neurobiol*, *7*(5), 695-700. https://doi.org/10.1016/s0959-4388(97)80091-8

Welker, E., Raymond, L. D., Scheraga, H. A., & Caughey, B. (2002). Intramolecular versus intermolecular disulfide bonds in prion proteins. *J Biol Chem*, *277*(36), 33477-33481. https://doi.org/10.1074/jbc.M204273200

Wessel, D., & Flügge, U. I. (1984). A method for the quantitative recovery of protein in dilute solution in the presence of detergents and lipids. *Analytical Biochemistry*, *138*(1), 141-143. https://doi.org/https://doi.org/10.1016/0003-2697(84)90782-6

Westaway, D., DeArmond, S. J., Cayetano-Canlas, J., Groth, D., Foster, D., Yang, S.-L., Torchia, M., Carlson, G. A., & Prusiner, S. B. (1994). Degeneration of skeletal muscle, peripheral nerves, and the central nervous system in transgenic mice overexpressing wild-type prion proteins. *Cell*, *76*(1), 117-129. https://doi.org/https://doi.org/10.1016/0092-8674(94)90177-5

White, A. R., Enever, P., Tayebi, M., Mushens, R., Linehan, J., Brandner, S., Anstee, D., Collinge, J., & Hawke, S. (2003). Monoclonal antibodies inhibit prion replication and delay the development of prion disease. *Nature*, *422*(6927), 80-83. https://doi.org/10.1038/nature01457

Whitehouse, I. J., Miners, J. S., Glennon, E. B., Kehoe, P. G., Love, S., Kellett, K. A., & Hooper, N. M. (2013). Prion protein is decreased in Alzheimer's brain and inversely correlates with BACE1 activity, amyloid-β levels and Braak stage. *PLoS One*, *8*(4), e59554. https://doi.org/10.1371/journal.pone.0059554

Wickner, R. B. (1994). [URE3] as an altered URE2 protein: evidence for a prion analog in Saccharomyces cerevisiae. *Science*, *264*(5158), 566-569. https://doi.org/10.1126/science.7909170

Will, R. G., Ironside, J. W., Zeidler, M., Cousens, S. N., Estibeiro, K., Alperovitch, A., Poser, S., Pocchiari, M., Hofman, A., & Smith, P. G. (1996). A new variant of Creutzfeldt-Jakob disease in the UK. *Lancet*, *347*(9006), 921-925. https://doi.org/10.1016/s0140-6736(96)91412-9

Wille, H., Bian, W., McDonald, M., Kendall, A., Colby, D. W., Bloch, L., Ollesch, J., Borovinskiy, A. L., Cohen, F. E., Prusiner, S. B., & Stubbs, G. (2009). Natural

and synthetic prion structure from X-ray fiber diffraction. *Proc Natl Acad Sci U S A*, *106*(40), 16990-16995. https://doi.org/10.1073/pnas.0909006106

Williams, E. S. (2005). Chronic Wasting Disease. *Veterinary Pathology*, *42*(5), 530-549. https://doi.org/10.1354/vp.42-5-530

Williams, E. S., & Young, S. (1980). Chronic wasting disease of captive mule deer: a spongiform encephalopathy. *J Wildl Dis*, *16*(1), 89-98. https://doi.org/10.7589/0090-3558-16.1.89

Wood, M. E., Griebel, P., Huizenga, M. L., Lockwood, S., Hansen, C., Potter, A., Cashman, N., Mapletoft, J. W., & Napper, S. (2018). Accelerated onset of chronic wasting disease in elk (Cervus canadensis) vaccinated with a PrP(Sc)-specific vaccine and housed in a prion contaminated environment. *Vaccine*, *36*(50), 7737-7743. https://doi.org/10.1016/j.vaccine.2018.10.057

Wroe, S. J., Pal, S., Siddique, D., Hyare, H., Macfarlane, R., Joiner, S., Linehan, J. M., Brandner, S., Wadsworth, J. D., Hewitt, P., & Collinge, J. (2006). Clinical presentation and pre-mortem diagnosis of variant Creutzfeldt-Jakob disease associated with blood transfusion: a case report. *Lancet*, *368*(9552), 2061-2067. https://doi.org/10.1016/s0140-6736(06)69835-8

Xanthopoulos, K., Lagoudaki, R., Kontana, A., Kyratsous, C., Panagiotidis, C., Grigoriadis, N., Yiangou, M., & Sklaviadis, T. (2013). Immunization with recombinant prion protein leads to partial protection in a murine model of TSEs through a novel mechanism. *PLoS One*, *8*(3), e59143. https://doi.org/10.1371/journal.pone.0059143

Yu, G., Jiang, L., Xu, Y., Guo, H., Liu, H., Zhang, Y., Yang, H., Yuan, C., & Ma, J. (2012). Silencing prion protein in MDA-MB-435 breast cancer cells leads to pleiotropic cellular responses to cytotoxic stimuli. *PLoS One*, *7*(11), e48146. https://doi.org/10.1371/journal.pone.0048146

Zabel, M. D., & Reid, C. (2015). A brief history of prions. *Pathogens and disease*, *73*(9), ftv087-ftv087. https://doi.org/10.1093/femspd/ftv087

Zahn, R., Liu, A., Lührs, T., Riek, R., von Schroetter, C., López García, F., Billeter, M., Calzolai, L., Wider, G., & Wüthrich, K. (2000). NMR solution structure of the human prion protein. *Proceedings of the National Academy of Sciences*, *97*(1), 145-150. https://doi.org/doi:10.1073/pnas.97.1.145

Zerr, I., Giese, A., Windl, O., Kropp, S., Schulz-Schaeffer, W., Riedemann, C., Skworc, K., Bodemer, M., Kretzschmar, H. A., & Poser, S. (1998). Phenotypic variability in fatal familial insomnia (D178N-129M) genotype. *Neurology*, *51*(5), 1398-1405. https://doi.org/10.1212/wnl.51.5.1398

Zerr, I., Kallenberg, K., Summers, D. M., Romero, C., Taratuto, A., Heinemann, U., Breithaupt, M., Varges, D., Meissner, B., Ladogana, A., Schuur, M., Haik, S.,

Collins, S. J., Jansen, G. H., Stokin, G. B., Pimentel, J., Hewer, E., Collie, D., Smith, P., . . . Sanchez-Juan, P. (2009). Updated clinical diagnostic criteria for sporadic Creutzfeldt-Jakob disease. *Brain*, *132*(Pt 10), 2659-2668. https://doi.org/10.1093/brain/awp191

Zhu, C., & Aguzzi, A. (2021). Prion protein and prion disease at a glance. *Journal of Cell Science*, *134*(17). https://doi.org/10.1242/jcs.245605